UNIVERSITY OF PALERMO
PHD JOINT PROGRAM:
UNIVERSITY OF CATANIA - UNIVERSITY OF MESSINA
XXXVI CYCLE

DOCTORAL THESIS

Analysis of Pattern Selection in Reaction-Diffusion Systems: From Toxic Zooplankton Dynamics to Tumor Growth Modelling

Author:
FARHAN KHAN

Supervisor:
Prof. MARIA CARMELA LOMBARDO

Co-Supervisor:
Prof. GAETANA GAMBINO

A thesis submitted in fulfillment of the requirements for the degree of Doctor of Philosophy

in

Mathematics and Computational Sciences

November 4, 2024

Signed:

Date:

"The beauty of mathematics only shows itself to more patient followers."

Maryam Mirzakhani

UNIVERSITY OF PALERMO

Abstract

Department of Mathematics and Computer Sciences

Doctor of Philosophy

Analysis of Pattern Selection in Reaction-Diffusion Systems: From Toxic Zooplankton Dynamics to Tumor Growth Modelling

by FARHAN KHAN

In this thesis, we developed a model to study how patterns form and evolve over time due to the interaction between toxic phytoplankton and zooplankton. Our analysis revealed that nonlinear cross-diffusion plays a crucial role in shaping spatial patterns. We derived amplitude equations to describe the dynamics under nonlinear cross-diffusion, which helped us to understand the transitions and stability of various Turing patterns. Our numerical simulations confirmed the validity of our theoretical results. We found that in the absence of cross-diffusion, the distribution of plankton is homogeneous. However, when cross-diffusivity exceeds a critical value, the spatial distribution of all plankton species becomes inhomogeneous in space, leading to different patterns. This thesis also presents a mathematical model of acid-mediated tumor growth using reaction-diffusion equations in spherical coordinates. Tumor invasion is a complex process involving cell migration and proliferation. Mathematical modelling can aid in understanding the mechanisms by which primary and secondary (metastatic) tumors invade and damage normal cells. A numerical study of acid-mediated tumor growth may provide a better understanding of how to design new experiments or cures for the future. Cancer cells use anaerobic glycolysis, which increases the production of lactic acid. This acidic environment is favourable for tumor growth, and if it persists, normal cells cannot survive and begin to die, thereby facilitating tumor invasion. The results show that the method of lines is a powerful numerical scheme for solving the proposed model, and MATLAB is used to analyze the computed results graphically.

Acknowledgements

All praise is due to **Allah Almighty (SWT)**, whose countless blessings and guidance have enabled me to complete this journey of knowledge and discovery. His mercy and benevolence have been my constant source of strength and inspiration throughout this endeavor. I also send uncountable Drood-O-Salam and blessings upon the **Holy Prophet Muhammad (PBUH)**, whose life serves as a guiding light for us in the darkness of life.

I would like to express my deepest gratitude to the **University of Palermo, Italy** for awarding me the PhD scholarship that made this achievement possible. The opportunity to pursue my doctoral studies at such a prestigious institution has been a profound honor and a transformative experience in my academic career.

My heartfelt thanks go to my supervisor, **Prof. Maria Carmela Lombardo**, and my co-supervisor, **Prof. Gaetana Gambino**. Their unwavering support, insightful guidance, and invaluable expertise have been instrumental in the completion of this thesis. Their patience, encouragement, and confidence in my abilities have inspired me to overcome challenges and strive for excellence.

I am immensely grateful to my parents, **Mr. and Mrs. Muhammad Afzal Khan**, whose love, prayers, and sacrifices have been the foundation of my success. Their belief in me has been a constant source of motivation, and I owe all my achievements to their unwavering support. To my siblings, whose encouragement and understanding have been a pillar of strength, I extend my deepest appreciation.

Lastly, I would like to thank all my friends for their companionship and support throughout this journey. Their kindness, laughter, and encouragement have enriched my life and made this experience truly memorable.

Farhan Khan

Contents

List of Figures

List of Tables

List of Abbreviations

ATP	**Adenosine triphosphate**
MOL	**Method of lines**
TPP	**Toxic Phytoplankton**
WNL	**Weakly nonlinear Analysis**
ODE	**Ordinary differential equations**
PDE	**Partial differential equations**

For/Dedicated /To
My Loving Parents for their continuous moral support and love.

Chapter 1

Introduction

Theoretical approaches to delineate the dynamics of pattern formation have advanced significantly over the past few decades because of their prime importance in understanding natural phenomena. In his seminal work, Turing ([97]) gave an idea of pattern formation and how reaction and diffusion parts of the system play an essential role in developing a pattern. He stated that a homogenous steady state of the system becomes unstable by adding diffusion, which leads to spatially inhomogeneous patterns, the so-called Turing instability. In many areas, including biology, chemistry, physics, ecology, geology, and many more, self-regulated pattern development can be explained by reaction-diffusion models ([18], [19], [68]). The interactions between species and their evolution are essential processes in biology and ecology; the mathematical model plays a vital role in understanding the interaction of species and their development; numerous models have been examined in the past ([76], [77], [85], [92], [93]).
In recent years, one interesting topic has been studying how cross-diffusion plays a crucial role in developing a pattern. Cross-diffusion is a phenomenon in which the gradient of one species' concentration affects the flux of another species. In biological modelling, it plays a crucial role in various processes such as chemotaxis, cancer progression, cell migration, and ecological interactions. For instance, in chemotaxis, cells move in response to chemical gradients, which can be modelled using cross-diffusion terms ([49], [94], [39]). In cancer modelling, cross-diffusion can represent the complex interactions between tumour cells and their microenvironment, influencing invasion and metastasis ([59]; [3],[35], [37], [56]). In ecological systems, cross-diffusion can describe predator-prey dynamics or competition between species ([86],[58]). Regarding Turing pattern formation, cross-diffusion can significantly impact the conditions for pattern emergence and the resulting spatial structures. It can destabilize homogeneous steady states and lead to the formation of more complex patterns than those observed in classical reaction-diffusion systems ([62], [33]; [11]). The inclusion of cross-diffusion terms in Turing-type models has expanded our understanding of pattern formation mechanisms in biological systems, offering new insights into morphogenesis and self-organization processes ([60]). Recent advancements in mathematical analysis have further elucidated the behaviour of cross-diffusion systems ([26]), contributing to more accurate and comprehensive biological models across various scales and applications.
In this thesis, our focus is on the study of plankton ecosystems, with particular attention to the dynamics between toxic phytoplankton and zooplankton. Phytoplankton are tiny organisms that live in the top sunlit layers of almost all water bodies, including oceans and freshwater. These drifting, photosynthetic organisms consist of various types of microalgae, cyanobacteria, and others that are able to convert inorganic nutrients and carbon dioxide into organic compounds through photosynthesis. Phytoplankton are at the base of the food chain in water ecosystems and are responsible

for producing about half of Earth's atmospheric oxygen. They play a crucial role in supporting marine life and regulating the planet's climate system ([25]).
While most phytoplankton species are harmless and essential food sources for organisms ranging from zooplankton to whales, a small fraction of phytoplankton varieties produce potent natural toxins. When environmental conditions are favourable, these toxic varieties can undergo rapid population increases known as harmful algal blooms (HABs) or "red tides" when high concentrations discolour the water ([4]).
Blooms of toxic phytoplankton have occurred throughout history, sometimes causing mass mortality events in marine life, human illness from contaminated seafood, and substantial economic impacts. Factors like excessive nutrient inputs, warming ocean temperatures, changes in water chemistry, and introduction of invasive species via shipping can create conditions that allow certain toxic phytoplankton to outcompete other varieties and reach high densities ([103]). Blooms have increased in geographic extent, frequency, and intensity in recent decades ([44]).
The impacts are severe and widespread. Toxic blooms have caused large-scale fish kills, mammal deaths, human poisoning or memory impairment from consuming contaminated seafood, and risks from inhaling toxic aerosols at beaches ([10]). Significant economic losses result from beach and fishery closures, damage to aquaculture operations, and human illness. Desalination and power plants can experience disruptions when intake pipes become clogged ([5]).
While most phytoplankton plays a vital role in supporting marine food webs, the threat from HABs created by toxic varieties demands increased scientific monitoring, controls on nutrient pollution sources, research into bloom dynamics, and other preventative measures ([40]). Understanding and mitigating toxic phytoplankton blooms is crucial for protecting marine ecosystems, seafood safety, coastal economies, and human health.
Zooplankton are a vital link in the marine food web, serving as the primary grazers of phytoplankton and transferring energy to higher trophic levels like fish, seabirds, and whales. However, the increasing prevalence of toxic algal blooms poses a significant threat to these microscopic animal drifters. When certain phytoplankton species produce biotoxins and undergo population explosions known as harmful algal blooms (HABs), zooplankton face dire consequences.
Some zooplankton that ingest toxic phytoplankton accumulate the toxins in their body tissues, passing the toxicity up the food chain to their predators with potentially fatal effects ([89]). Other zooplankton avoids ingesting toxic algae but face nutritional deficiencies or starvation during severe HABs when non-toxic food sources are depleted ([53]). Prolonged exposure to HABs toxins can impair zooplankton reproduction and development, negatively impacting growth, fecundity, hatching success, and larval survival ([9]).
The effects of HABs on zooplankton can ripple through entire marine ecosystems. If toxic blooms cause zooplankton populations to crash, it can reduce food availability and negatively impact organisms ranging from forage fish to whales that depend on zooplankton as a dietary source ([42]). Shifts in zooplankton community composition during HABs, as sensitive species decline and toxin-resistant species proliferate, can disrupt ecological dynamics and energy flows ([104]).
Furthermore, as climate change promotes the expansion of warm-water HAB species into new geographic regions, zooplankton communities unaccustomed to these invasive toxic algae may be particularly vulnerable ([95]). Range expansions of toxic blooms, combined with the synergistic effects of warming temperatures, ocean acidification, and other climate stressors, pose a growing threat to zooplankton.

Given the critical role of zooplankton in marine ecosystems and fisheries productivity, understanding and mitigating the adverse impacts of HABs on these grazers is crucial ([27]). Through monitoring programs, research into bloom dynamics and toxicity mechanisms, control strategies for nutrient pollution, and enhanced ability to predict bloom patterns, we can work to protect zooplankton from the increasingly pervasive global problem of harmful algal blooms.
A fascinating area of research in recent decades has been exploring how toxic substances released by phytoplankton reduce zooplankton grazing pressure ([12, 13, 16, 81, 15]). ([17]) proposed a mathematical model demonstrating how this phenomenon, termed TTP (toxic phytoplankton protection), acts as a biocontrol mechanism to mitigate planktonic blooms. Furthermore, ([80]) developed a mathematical model elucidating the interaction between toxin-producing phytoplankton and zooplankton, exploring Hopf-bifurcation and providing numerical simulations to comprehend the underlying dynamics.
In the second half of the thesis, we proposed a reaction-diffusion model of tumour growth based on glycolysis. Glycolysis has two types: aerobic and anaerobic. Aerobic glycolysis occurs in the presence of oxygen, whereas anaerobic glycolysis occurs in the absence of oxygen. Cellular respiration is the process by which a cell breaks down glucose molecules to obtain the energy required by the human body to function properly. This process involves three main steps in healthy cells: glycolysis, the Krebs cycle, and oxidative phosphorylation. Cellular respiration utilizes one glucose molecule and produces 36 adenosine triphosphate (ATP) molecules. In cancer cells, glucose molecules are broken down using anaerobic respiration, and they do not complete the other respiration steps. As a result, cancer cells produce only two molecules of ATP, which means they need to consume a lot more sugar molecules to obtain enough energy to survive. This concept was initially suggested by German scientists ([102]), who received the Nobel Prize in 1931 for their groundbreaking research.
([35]), were the first to propose a mathematical model for acid-mediated tumour invasion, building on the concept introduced by [102]. Experimental works have since supported this model, underscoring the crucial role of anaerobic glycolysis in cancer cells. This metabolic process leads to the production of H^+ ions ([35], [36], [37], [75]) which causes local acidification and destruction of normal cells, thereby facilitating the invasion of cancer cells. The reaction-diffusion model ([35]) further elucidates how the number of normal cells, tumor cells, and concentration of H^+ ions evolve due to interactions between these populations.
Another aspect of cancer invasion is that the microenvironment of particular interest to cancer researchers is the low pH ([20]). The anaerobic glycolysis of cancer cells produces H^+ ions, and these ions lower the pH of the surrounding environment of the primary tumour, which helps us to form a secondary tumour apart from the primary tumour; this process is also called metastatic. This high level of the metabolic process gives a large amount of lactic acid, leading to an excess concentration of H^+ ions, and due to this lactic acid, the surrounding environment of the tumour affects the normal cells. This lactic acid lowers the pH level of the surrounding tumour environment. This environment helps tumors to grow, and normal cells die due to low pH ([14], [74], [88]). The pH level of blood in which normal cells live is about 7.1-7.4; otherwise, tumour cell pH is 6.5-7 ([48], [83], [79]).
In 2013, ([64]) extended the primary model gave ([35]). They used logistic growth of normal and tumour cells and also discussed the competition of tumour cells on normal, i.e. the effect of tumour cells on normal cells. In this article, they find the

unique solution to a mathematical model of tumour growth and use different non-standard finite difference schemes to solve the model.
([43]) gave a model by adding time-carrying capacities, which depend on tumour cells' capacities. He numerically solved this model using the Dual Reciprocity Boundary Element Method (DRBEM). [7] also examines a model of acid-mediated tumour growth by adding some noticeable changes in the model given by [35]; they discuss fast and slow-motion travelling waves of tumour and normal.

([65]) generalized the mathematical model of the tumor as first given by ([35]); all the previous articles published about tumor growth tell that tumor cells can be grown in an acidic environment and normal cells will die in this environment, but this mathematical model tells that tumor cells will also be affected in too much acidic environment also they a add competition term of both normal and tumor cells, i.e. how normal and tumor both effects on each other by using Lotka–Volterra competition model ([105]) when both are proximity. In our article, we make a noticeable approach in the model given by ([65]); this approach we do in the model provides precise numerical results of the tumour, normal cells, the concentration of H^+ ions and how pH varies in this whole process. We convert the model ([35]) in spherical coordinates as ([82]); due to the geometry of the tumour and previous numerical work done on the model in dimensionless, we make a new approach to balance our mathematical system and then solve the numerical.

The thesis is organized as follows: "In Chapter (2), we provide the theoretical background for the current work. We present a detailed description of the reaction-diffusion system. First, we discuss the reaction terms, offering a comprehensive analysis of the Lotka-Volterra competition model, including its two types of competition: intraspecific and interspecific. We also briefly describe the different types of Holling-type functional responses. Additionally, we explore the linearization of the system around an equilibrium point and the general condition for Turing instability in reaction-diffusion systems with self- and cross-diffusion."
In Chapter (3), we present the main mathematical model of our thesis, which focuses on the interaction between toxic phytoplankton and zooplankton, formulated as a reaction-diffusion system with self-diffusion and nonlinear cross-diffusion. The novelty of our model lies in the introduction of nonlinear cross-diffusion, which captures the phenomenon of mutual avoidance between species, a concept proposed by ([47]) in his experimental work. This cross-diffusion term accounts for how individuals of one species tend to avoid areas where the other species are present. Additionally, we simplify the model by applying nondimensionalization, a mathematical technique that reduces the complexity of the system by scaling the variables, making it easier to analyze and interpret. Chapter (4) presents the first main contribution of the thesis, which is finding the equilibrium solution of the system's kinetics and discussing the system's stability analysis without diffusion. We also linearize the complete PDE system and prove that the cross-diffusion coefficient is crucial in obtaining Turing instability.
In Chapter (5), we give a second main contribution of our work, performing weakly nonlinear analysis near the bifurcation point to predict the amplitude and form of the patterns and develop Stuart-Landau amplitude equations that help to understand supercritical and subcritical bifurcation and numerical results performed using Matlab. Also, we perform WNL in the 2D domain and develop an amplitude equation to help understand different patterns: spot, stripe, and the mixture of spot and stripe, as we discuss in upcoming work ([54]). In Chapter 6, the first section

briefly describes the mathematical modelling of tumor growth in spherical coordinates using a reaction-diffusion system. We also provide an analysis explaining why the mathematical model of the tumor is discussed in spherical coordinates. Furthermore, we present the numerical results of the tumor growth model, obtained using the method of lines in Matlab, as discussed in our work ([56]).

Chapter 2

A Overview of Reaction Diffusion Systems

This chapter provides a comprehensive overview of reaction-diffusion systems, which are mathematical models used to describe the spatial and temporal dynamics of interacting substances. Reaction-diffusion systems are mathematical models that describe show how the concentration of one or more substances distributed in space changes under the influence of two processes: local chemical reactions and diffusion. These systems are widely used to model various phenomena in biology, chemistry, physics, and ecology. The chapter begins with an introduction to reaction terms, focusing on the Lotka-Volterra competition model, which is used to study interactions between species, including both intraspecific and interspecific competition. The discussion then extends to the concept of functional responses, particularly Holling's types, which describe the relationship between a consumer's consumption rate and prey density (see section 2.1). The chapter also delves into the mathematical analysis of these systems, covering key concepts like steady states, stability analysis through linearization and Jacobian matrices, and bifurcation points such as Hopf bifurcation, which marks transitions to oscillatory behaviour (see section 2.2). The diffusion term, critical for describing the spatial spread of substances, is explored alongside cross-diffusion, which leads to complex pattern formation. Finally, the chapter discusses the implications of cross-diffusion-driven instability, emphasizing its role in creating patterns in natural systems (see section 2.3). Through these discussions, the chapter lays the groundwork for understanding the dynamics and stability of reaction-diffusion systems in various scientific fields.

2.1 The Reaction

The reaction term in a reaction-diffusion system represents the local interactions between substances or species. It describes how the concentrations of substances change over time due to chemical reactions or other interactions independent of spatial effects. Different types of reaction terms are used, such as Michaelis-Menten kinetics, Hill function, Fisher-KPP (Kolmogorov-Petrovsky-Piskunov) equation, and Lotka-Volterra equations; here, we provide a brief description of the Lotka-Volterra Competition Model. Here, we will focus on the Lotka-Volterra model with logistic growth.

Lotka-Volterra model with competition

Species coexisting in a shared habitat inevitably interact and compete for limited resources such as food, mates, or space. These interactions can take various forms,

including competition, cooperation, exclusion, or predation. The more adept competitor often negatively impacts the other species, potentially reducing its population size or growth rate.

The Lotka-Volterra model is commonly used to better understand the various aspects and outcomes of competitive interactions. This mathematical model describes interactions between two species, typically representing one as the predator and the other as the prey. The interaction known as predation involves the predator killing and consuming the prey. The Lotka-Volterra model provides a valuable framework for predicting the outcomes of such competitive dynamics.

The Lotka-Volterra model comes in two forms: one for predation and one for competition. In the case of predation, often referred to as the predator-prey model, the model is based on exponential growth. In contrast, the competition model is based on logistic growth. Both exponential and logistic growth describe increasing population sizes, but they differ in key ways. Exponential growth applies to populations with no upper limit, where resources are unlimited, and the growth rate is proportional to the current population size. Logistic growth, however, includes a maximum limit, known as the carrying capacity, accounting for limited resources and competition with other species. As a result, logistic growth is more realistic than exponential growth in representing natural population dynamics.

Lotka-Volterra competition model

In the competition model, we take two types of competition,

(1) Intraspecific competition.
(2) Interspecific competition.

Intraspecific competition

Intraspecific competition occurs when members of the same species compete for limited resources. Individuals within the same population share similar needs and resource requirements, making intraspecific competition more intense than interspecific competition. As population density increases, the competition for these limited resources intensifies, leading to a decrease in the population's growth rate. As a result, the rate of change in the number of individuals is directly affected by this competition.

$$\frac{dN}{dt} = rN\left(\frac{K-N}{K}\right) \tag{2.1}$$

Here,
N is a population density,
r is the growth rate,
t is time,
K is the carrying capacity for the population density.

The logistic growth equation is well-suited for modeling intraspecific competition because it offers a simple yet realistic representation of biological systems.

If we isolate the term rN on the right-hand side of the equation, it represents population growth in the absence of competition, known as exponential growth. The second term, $\frac{K-N}{K}$, accounts for intraspecific competition or density dependence based on the carrying capacity. As the population size approaches the carrying capacity, this term $\frac{K-N}{K}$ becomes smaller, reducing the population growth rate. Conversely, when the population size is below the carrying capacity, the growth rate is higher than before. This illustrates that the growth rate is influenced by population density.

Interspecific competition

Interspecific competition occurs when individuals from different species vie for the same resources. For instance, lions and spotted hyenas, which share a common diet and occupy overlapping niches, compete for food and other resources. This competition can have negative effects on one species, as the presence of the competing species reduces the availability of food. In a model that integrates the effects of each species on the other, the impact of interspecific competition between these two populations can be used to predict their interactions and outcomes.

$$\begin{aligned} \frac{dN}{dt} &= r_{1.1}N\left(\frac{K_n - N - a_{12}T}{K_n}\right), \\ \frac{dT}{dt} &= r_{2.1}T\left(\frac{K_t - T - a_{21}N}{K_t}\right). \end{aligned} \tag{2.2}$$

Equation (2.2) represents the interspecific competition for species N and T respectively.

Where,
N is the population density for species 1,
T is the population density for species 2,
$r_{1.1}$ is the growth rate for population 1,
$r_{2.1}$ is the growth rate for population 2,
t is time,
K_n is the carrying capacity for population 1,
K_t is the carrying capacity for population 2.

The primary distinction between the interspecific and intraspecific competition models lies in the inclusion of terms involving a. In this context, a_{12} represents the impact of species T on the population of species N, while a_{21} denotes the effect of species N on the population of species T. When $a_{12} < 1$, it indicates that the influence of species T on species N is less significant compared to its effect on its own members. Conversely, when $a_{12} > 1$, it means that species T has a greater impact on species N than on its own population, and the same interpretation applies to a_{21}.

Holling type functional response

Holling-type functional response refers to a concept in ecology that describes the relationship between a consumer's consumption rate and its resources or prey availability. This relationship is often represented using mathematical models, and several types of functional responses are proposed by C.S. Holling in his seminal work ([51]).

Type I functional response (Linear)

The consumption rate of the consumer increases linearly with the prey density until it reaches a saturation point. This type of response is often observed in filter feeders or organisms that consume non-renewing resources. The equation for Type I functional response is:

$$F = a \times N. \tag{2.3}$$

Where F is the consumption rate, a is the attack rate (a constant), and N is the prey density.

Type II functional response (Hyperbolic)

The consumption rate increases with prey density but eventually reaches an asymptote or maximum value, known as the saturation level. This type of response is commonly observed in many predator-prey systems, where the predator spends more time handling and consuming prey as density increases. The equation for Type II functional response is:

$$F = \frac{a \times N}{1 + a \times N \times T_h}. \tag{2.4}$$

Where F is the consumption rate, a is the attack rate, N is the prey density, and T_h is the handling time (the time required to consume and digest a prey item).

Type III functional response (Sigmoid)

At low prey densities, the consumption rate increases slowly, but as prey density increases, it accelerates until it reaches a plateau. This type of response is often observed in generalist predators that switch to more profitable prey types as their density increases. The equation for Type III functional response is:

$$F = \frac{a \times N^2}{1 + a \times T_h \times N^2}. \tag{2.5}$$

F is the consumption rate, a is the attack rate, N is the prey density, and T_h is the handling time. These functional response models have been widely used in ecological studies to understand predator-prey dynamics, population regulation, and the stability of ecosystems. They provide a theoretical framework for predicting the consumption rates of consumers under different resources or prey densities and have been supported by numerous empirical studies across various ecosystems and organisms.

To understand complex kinetic systems, we apply quantitative approaches to understand the behaviour of the system, which will be discussed in the next section.

2.2 Qualitative Analysis of Reaction Term

A steady state (or equilibrium point) is a point in the phase space where the system remains at rest or exhibits a constant behaviour over time ([90]). Mathematically, a steady state is a solution to the system's governing equations where the time derivatives of the state variables are zero ([55]).

2.2.1 Linear analysis of a steady state

- To analyze the stability of the steady state, we need to linearize the system's governing equations around the steady state ([41]).
- This involves taking the partial derivatives of the system's equations with respect to the state variables and evaluating them at the steady state ([78]).
- The resulting linear system approximates the original nonlinear system near the steady state ([72]).

Analyze the eigenvalues of the Jacobian matrix

- The Jacobian matrix is the matrix of partial derivatives obtained in the linearization step ([87]).
- The eigenvalues of the Jacobian matrix determine the stability of the steady state ([55]).
- If all the eigenvalues have negative real parts, the steady state is stable ([90]).
- If any eigenvalue has a positive real part, the steady state is unstable ([41]).
- If some eigenvalues have zero real parts, the steady state is neutrally stable or marginally stable ([78]).

Classify the type of stability

- Stable node: All eigenvalues have negative real parts, and the trajectories approach the equilibrium without oscillations. This indicates that the equilibrium is asymptotically stable, and the system will settle to this point after a disturbance ([90]).
- Unstable node: At least one eigenvalue has a positive real part. Trajectories move away from the equilibrium, showing that the system is unstable and small disturbances will cause the system to diverge from this point ([55]).
- Saddle point: Eigenvalues have both positive and negative real parts. The equilibrium is unstable as trajectories approach along some directions (corresponding to negative eigenvalues) and diverge along others (corresponding to positive eigenvalues) ([41]).
- Stable focus (Spiral): Eigenvalues are complex with negative real parts, causing the trajectories to spiral towards the equilibrium. This is also asymptotically stable, with oscillatory behavior as the system returns to equilibrium ([78]).
- Unstable focus (Spiral): Complex eigenvalues with positive real parts cause trajectories to spiral outward from the equilibrium, making it unstable with oscillatory divergence ([87]).
- Center (Neutral stability): Eigenvalues are purely imaginary (zero real parts), leading to closed trajectories around the equilibrium. The equilibrium is neutrally stable, and trajectories neither approach nor diverge from it but instead form periodic orbits ([90]).

Determine the stability region

- The stability region is the initial condition for which the system converges to the stable, steady state ([90]).
- The stability region can be determined by analyzing the phase portrait or using Lyapunov's direct method ([55]).

2.2.2 Bifurcation Point

A bifurcation point is a parameter value at which the qualitative structure of the flow of a dynamical system changes. In other words, it is the point where the system undergoes a qualitative change in its dynamics, such as the creation or destruction of fixed points, or a change in the stability of existing fixed points.

Types of bifurcations

Saddle-Node bifurcation

In a saddle-node bifurcation, a pair of fixed points (stable and unstable) are created or annihilated as a parameter is varied. The collision and annihilation of a stable and unstable fixed point characterizes this bifurcation. The canonical form of a saddle-node bifurcation is:

$$\frac{dx}{dt} = \mu - x^2$$

where μ is the bifurcation parameter.

Transcritical bifurcation

In a transcritical bifurcation, a stable fixed point and an unstable fixed point collide and exchange stability as a parameter is varied. One fixed point persists on both sides of the bifurcation point, but its stability changes. The canonical form of a transcritical bifurcation is:

$$\frac{dx}{dt} = \mu x - x^2$$

where μ is the bifurcation parameter.

Pitchfork bifurcation

Pitchfork bifurcation is a type of bifurcation that occurs in dynamical systems when the stability of a fixed point changes, leading to the appearance of new equilibria. It's called a "pitchfork" because the bifurcation diagram resembles the shape of a pitchfork. There are two types of Pitchfork bifurcation.

Supercritical pitchfork bifurcation

In a supercritical pitchfork bifurcation, as the bifurcation parameter μ passes through a critical value (usually $\mu = 0$), a single stable equilibrium (fixed point) becomes unstable, and two new stable equilibria emerge symmetrically on either side of the unstable equilibrium for $\mu > 0$. The transition is smooth and continuous, and this type of bifurcation typically occurs in systems with symmetry.

The canonical form for a supercritical pitchfork bifurcation is:

$$\frac{dx}{dt} = \mu x - x^3$$

where:

- μ is the bifurcation parameter.
- $x = 0$ is the equilibrium point for $\mu = 0$.
- For $\mu > 0$, two new stable equilibrium points $x = \pm\sqrt{\mu}$ emerge, while $x = 0$ becomes unstable.

Subcritical pitchfork bifurcation

In a subcritical pitchfork bifurcation, as the bifurcation parameter μ approaches the critical value from below (typically $\mu = 0$), a single unstable equilibrium point becomes stable, and two unstable fixed points appear. For $\mu < 0$, the system typically displays bistability, meaning that both stable and unstable equilibria coexist. The transition is abrupt, leading to jumps in the system's behavior (hysteresis).

The canonical form for a subcritical pitchfork bifurcation is:

$$\frac{dx}{dt} = \mu x + x^3$$

where:

- μ is the bifurcation parameter.
- $x = 0$ is the equilibrium point for $\mu = 0$.
- For $\mu < 0$, the equilibrium at $x = 0$ is stable, and two unstable equilibrium points appear at $x = \pm\sqrt{-\mu}$

Hopf bifurcation

A Hopf bifurcation is a type of bifurcation in the dynamics of a dynamic system where a stable equilibrium point loses its stability as a system parameter is varied, giving rise to periodic or oscillatory behaviour. At the Hopf bifurcation point, eigenvalues of the system's Jacobian matrix cross the imaginary axis, creating stable limit cycles or periodic orbits. Hopf bifurcations are crucial in understanding the transition from steady-state behaviour to sustained oscillations in various physical, biological, and engineering systems.

2.3 Spatial Effect: Reaction Diffusion Systems

Diffusion is the process by which particles or substances spread out over time from areas of high concentration to areas of low concentration. In reaction-diffusion systems, the diffusion term describes this spatial movement of substances.

Types of diffusion

1. **Simple diffusion**: Described by Fick's laws of diffusion. The rate of diffusion is proportional to the concentration gradient.

2. **Cross-diffusion**: This occurs when the gradient in the concentration of one substance induces a flux of another substance. It's particularly important in systems with multiple interacting species.

2.3.1 General form of reaction-diffusion systems

The general mathematical form of a reaction-diffusion system for multiple interacting species can be written as:

$$\frac{\partial u_i}{\partial t} = D_i \nabla^2 u_i + f_i(u_1, u_2, \ldots, u_n)$$

where:

- u_i is the concentration of the i-th species,
- t is time,
- D_i is the diffusion coefficient of the i-th species,
- ∇^2 is the Laplacian operator (sum of second partial derivatives with respect to spatial coordinates),
- f_i is the reaction term for the i-th species, which may depend on the concentrations of all species.

For a system with cross-diffusion, the equation becomes:

$$\frac{\partial u_i}{\partial t} = \nabla \cdot \left(\sum_j D_{ij}(u_1, u_2, \ldots, u_n) \nabla u_j \right) + f_i(u_1, u_2, \ldots, u_n)$$

where D_{ij} represents the cross-diffusion coefficients.

Importance in pattern formation

Reaction-diffusion systems, particularly those involving cross-diffusion, are vital in explaining complex pattern formation in various natural systems. Turing's theory of morphogenesis demonstrated how reaction-diffusion mechanisms could lead to stable, spatially periodic patterns, a foundational concept for understanding biological and chemical pattern formation ([96, 57, 31, 30]).

Applications

- **Biological Systems:** Reaction-diffusion models explain animal coat patterns, cellular differentiation, and embryonic development ([57, 67]).
- **Chemical Systems:** Patterns like waves and spirals in the Belousov-Zhabotinsky reaction are classic examples of reaction-diffusion systems in chemistry ([23]).
- **Ecological Systems:** These models describe the spatial distribution of species in an ecosystem, taking into account both self and cross-diffusion to capture interactions between species ([73]).

2.3.2 Qualitative analysis of reaction-diffusion system

A reaction-diffusion system describes how chemical substances, or reactants, interact through local chemical reactions and diffuse through space. These systems are governed by partial differential equations that couple reaction kinetics with diffusion processes. Due to the complexity of reaction-diffusion systems, solving them analytically is challenging. Therefore, in this section, we present a quantitative approach to solve these systems. Specifically, we consider the reaction-diffusion system for two interacting species, u and v, with linear self- and cross-diffusion, which is given by:

$$\begin{aligned} \frac{\partial u}{\partial t} &= D_u \nabla^2 u + D_{uv} \nabla^2 v + f(u,v), \\ \frac{\partial v}{\partial t} &= D_v \nabla^2 v + D_{vu} \nabla^2 u + g(u,v). \end{aligned} \tag{2.6}$$

where u and v represent the concentrations of the chemical species, D_u and D_v are the diffusion coefficients, D_{uv} and D_{vu} are cross-diffusion coefficients, reflecting how the concentration gradients of v and u affect the diffusion of u and v, respectively, and f and g denote the reaction terms ([96, 63]). Cross-diffusion involves the influence of one species on the diffusion of another. This means that the diffusion of one species can be affected by the concentration gradients of other species in the system. For instance, the diffusion equation in (2.6) for species u include a term like $D_{uv}\nabla^2 v$, indicating that the diffusion of u is influenced by the concentration gradient of v ([71, 99]).

The non-dimensional reaction-diffusion system with cross-diffusion of the general form can be written as:

$$\begin{aligned} \frac{\partial u}{\partial t} &= \nabla^2 u + d_v \nabla^2 v + f(u,v), \\ \frac{\partial v}{\partial t} &= d\nabla^2 v + d_u \nabla^2 u + g(u,v). \end{aligned} \tag{2.7}$$

Here, d is the ratio of the diffusion coefficients only (without cross-diffusion), and d_u and d_v are the ratios of the cross-diffusion and the diffusion coefficients, respectively.

Cross-diffusion-driven instability

Cross-diffusion-induced diffusion-driven instability arises when a uniform steady state becomes unstable due to cross-diffusion and regular diffusion despite being linearly stable in the absence of cross-diffusion. The definition above can be further clarified and made more rigorous by following the definition for standard diffusion-driven instability given by ([21]).

Undertaking an investigation to explore the potential for cross-diffusion, we initiate our inquiry by expanding the solution $u(\boldsymbol{x},t)$ around the spatially independent uniform steady state $(u_s, v_s)^T$. To do this, we substitute

$$\begin{cases} u(\boldsymbol{x},t) = u^* + \epsilon u_1(\boldsymbol{x},t), \\ v(\boldsymbol{x},t) = v^* + \epsilon v_1(\boldsymbol{x},t), \end{cases} \quad \text{with} \quad \epsilon \ll 1 \tag{2.8}$$

By ignoring $O\left(\epsilon^2\right)$ and higher-order terms in the system (2.7), we arrive at the following linearized reaction-diffusion system with cross-diffusion, which can be succinctly expressed in vector form.

$$\boldsymbol{X}_t = \gamma J \boldsymbol{X} + D\nabla^2 \boldsymbol{X}, \tag{2.9}$$

with

$$J = \begin{pmatrix} \frac{\partial f}{\partial u} & \frac{\partial f}{\partial v} \\ \frac{\partial g}{\partial u} & \frac{\partial g}{\partial v} \end{pmatrix} \equiv \begin{pmatrix} f_u & f_v \\ g_u & g_v \end{pmatrix}\Bigg|_{(u^*,v^*)},$$

$$D = \begin{pmatrix} 1 & d_v \\ d_u & d \end{pmatrix} \text{ and } \boldsymbol{X} = \begin{pmatrix} u_1 \\ v_1 \end{pmatrix}.$$

Given that J represents the Jacobian matrix evaluated at (u^*, v^*), D is a matrix containing the ratios of the regular diffusion and cross-diffusion coefficients, and $\boldsymbol{X}$ is the vector of solutions to the linear system of partial differential equations, we can analytically solve the linear system (2.9) by applying the method of separation of variables. This approach yields a power series solution of the general form.

$$\boldsymbol{X}(\boldsymbol{x}, t) = \sum_k b_k e^{\lambda\left(k^2\right)t} \Phi_k(\boldsymbol{x}), \tag{2.10}$$

where for each k, Φ_k is the eigenfunction of the Laplace operator that satisfies the Helmholtz equation,

$$\begin{cases} \nabla^2 \Phi_k + k^2 \Phi_k = 0 & \text{on } \Omega, \\ (\boldsymbol{n} \cdot \nabla)\Phi_k = 0 & \text{on } \partial\Omega. \end{cases}$$

For each wavenumber k, we substitute the expression $b_k e^{\lambda\left(k^2\right)t}\Phi_k$ into equation (2.9) to obtain the following.

$$\left(\lambda I - \gamma J + k^2 D\right) \Phi_k b_k = \boldsymbol{0}, \tag{2.11}$$

Given that $\mathbf{I}$ is an identity matrix, and since we are seeking non-zero solutions, both b_k and Φ_k must be non-zero. Consequently, the matrix multiplying these variables must be singular. Therefore, this implies that

$$\left|\lambda I - \gamma J + k^2 D\right| = \begin{vmatrix} \lambda - \gamma f_u + k^2 & -\gamma f_v + d_v k^2 \\ -\gamma g_u + d_u k^2 & \lambda - \gamma g_v + d k^2 \end{vmatrix} = 0,$$

Thus $\lambda\left(k^2\right)$ satisfies the dispersion relation

$$\lambda^2 + b\left(k^2\right)\lambda + c\left(k^2\right) = 0, \tag{2.12}$$

where

$$\begin{aligned} b\left(k^2\right) &= k^2(1+d) - \gamma\left(f_u + g_v\right), \\ c\left(k^2\right) &= \left(d - d_u d_v\right)k^4 - \gamma k^2\left(d f_u + g_v - d_u f_v - d_v g_u\right) + \gamma^2\left(f_u g_v - f_v g_u\right). \end{aligned}$$

Given scalar variables u, v, and kinetic functions $f(u, v)$, $g(u, v)$ in Equation (2.7), the partial derivatives are computed with respect to the uniform steady state (u^*, v^*).

The solutions to the dispersion relation (2.12) are then provided by:

$$2\lambda\left(k^2\right) = -b\left(k^2\right) \pm \sqrt{b^2\left(k^2\right) - 4c\left(k^2\right)}.$$

Taking $k = 0$ indicates the absence of diffusion and cross-diffusion, leading to spatial homogeneity. To ensure that (u^*, v^*) is stable for the $k = 0$ spatially homogeneous mode, we must require that:

$$\mathrm{Re}[\lambda(0)] = \mathrm{Re}\left[-b(0) \pm \sqrt{b^2(0) - 4c(0)}\right] < 0. \tag{2.13}$$

This is assured given that $b(0) > 0$ and $c(0) > 0$ if and only if the following conditions are satisfied

$$\mathrm{Trace}\,(J) := f_u + g_v < 0, \tag{2.14}$$
$$\mathrm{Det}\,(J) := f_u g_v - f_v g_u > 0. \tag{2.15}$$

These two conditions are unaffected by cross-diffusion, making them the same as those without it. The following three conditions, however, emphasize the distinctions between traditional diffusion-driven scenarios without cross-diffusion and those where it is involved.

In the context of diffusion and cross-diffusion, where $k^2 > 0$, we have the following situation:

$$b\left(k^2\right) = k^2(1 + d) + b(0) > 0, \tag{2.16}$$

since $b(0) > 0$. For (u^*, v^*) to become unstable, we require that

$$\mathrm{Re}\left[\lambda\left(k^2\right)\right] > 0 \text{ for some } k^2 \text{ non-zero.} \tag{2.17}$$

Therefore, it is essential that $c(k^2)$ be negative for some non-zero value of k^2. Given the definition of $c(k^2)$, we can rewrite this as a quadratic polynomial in k^2 in the following manner:

$$c\left(k^2\right) = P_2 k^4 + P_1 k^2 + c(0), \tag{2.18}$$

where

$$\begin{aligned} P_2 &= d - d_u d_v := \mathrm{Det}(D), \\ P_1 &= \gamma\left(d_u f_v + d_v g_u - (d f_u + g_v)\right), \\ c(0) &= \gamma^2\left(f_u g_v - f_v g_u\right) > 0. \end{aligned}$$

To ensure that we have an upward-opening parabola (i.e., $c(k^2) < 0$ for some non-zero $k > 0$), it is necessary that a specific condition be met concerning the relationship between the diffusion and cross-diffusion coefficients.

$$\mathrm{Det}(D) = d - d_u d_v > 0, \tag{2.19}$$

It should be noted that if the parabola defined by $c(k^2)$ is downward opening, meaning the determinant $\mathrm{Det}(D) = d - d_u d_v$ is negative ($\mathrm{Det}(D) < 0$), then the cross-diffusion system is ill-posed.

Condition (2.19) represents the first of three necessary conditions for cross-diffusion-induced instability. To ensure that $c(k^2) < 0$ for some non-zero k^2, it is required that

$P_1 < 0$. Thus, this requirement gives the second condition for diffusion-driven instability in the context of cross-diffusion.

$$df_u + g_v - d_u f_v - d_v g_u > 0,$$

For diffusively-driven instability to occur, it is also necessary that there exist real values $k_{\pm}^2$ for which $c\left(k_{\pm}^2\right) = 0$. These values can be readily demonstrated as follows:

$$k_{\pm}^2 = \frac{-P_1 \pm \sqrt{P_1^2 - 4c(0)\left(d - d_u d_v\right)}}{2\left(d - d_u dv\right)}. \tag{2.20}$$

Thus, the requirement that $c(k^2) < 0$ leads to the condition $P_1^2 - 4c(0)(d - d_u d_v) > 0$. This establishes the third and final condition necessary for cross-diffusion-driven instability

$$\left(df_u + g_v - d_u f_v - d_v g_u\right)^2 - 4\left(d - d_u d_v\right)\left(f_u g_v - f_v g_u\right) > 0. \tag{2.21}$$

We can now present the following theorem, whose proof is given above:

Theorem 1 : ***Turing Instability for Reaction-Diffusion Systems with Cross-Diffusion*** *Let a reaction-diffusion system one as defined in (2.7) with cross-diffusion exhibit a Turing instability if the following conditions hold:*

$$f_u + g_v < 0, \tag{2.22}$$
$$f_u g_v - f_v g_u > 0, \tag{2.23}$$
$$d - d_u d_v > 0, \tag{2.24}$$
$$df_u + g_v - d_u f_v - d_v g_u > 0, \tag{2.25}$$
$$\left(df_u + g_v - d_u f_v - d_v g_u\right)^2 - 4\left(d - d_v d_u\right)\left(f_u g_v - f_v g_u\right) > 0. \tag{2.26}$$

In the above, the subscripts u and v represent partial derivatives, with the Jacobian components f_u, f_v, g_u, and g_v being evaluated at the point (u_s, v_s). The conditions ((2.22)-(2.26)) describe a parameter space for cross-diffusion-driven instability, within which the uniform steady state (u_s, v_s) becomes linearly unstable.

Chapter 3

Mathematical Formulation: Phytoplankton and Zooplankton with Toxicity

This chapter introduces a mathematical modelling framework that describes the interactions between toxic phytoplankton and zooplankton in aquatic ecosystems, with a particular emphasis on the dynamics influenced by toxin-producing phytoplankton (TPP). It begins with an introduction to the ecological roles of phytoplankton and zooplankton, emphasizing the harmful effects of certain phytoplankton species that produce toxins which can impact the entire food web. The chapter then details the development of a system of partial differential equations (PDE) to describe the spatiotemporal dynamics of these interactions. The proposed model incorporates diffusion processes, reaction terms, and nonlinear cross-diffusion to capture the mutual avoidance between toxic phytoplankton and zooplankton, a concept proposed by ([47]) in his experimental work. The model is designed to explore the emergent patterns, stability properties, and potential for TPP to act as a natural biocontrol mechanism against harmful algal blooms, as we will discuss in our forthcoming work ([54]). By integrating insights from existing literature, the chapter highlights the importance of understanding the complex, often chaotic, interactions within planktonic ecosystems, providing a foundation for further exploration of the role of TPP in maintaining ecological balance (see section 3.1).

3.1 Toxic Phytoplankton and Zooplankton Model with Cross Diffusion

Phytoplankton and zooplankton are microscopic organisms that play crucial roles in aquatic ecosystems. While most species are beneficial, some phytoplankton can produce toxins that have far-reaching impacts on marine life, including their zooplankton predators. These toxic phytoplankton, often referred to as harmful algal blooms (HABs), have become increasingly prevalent in recent years due to factors such as climate change and anthropogenic nutrient inputs ([6]).

Toxic phytoplankton species, such as those belonging to the genera *Alexandrium*, *Karenia*, and *Pseudo-nitzschia*, can produce a variety of potent neurotoxins and hepatotoxins. These toxins serve as a defense mechanism against predation and can accumulate in the food web, affecting not only zooplankton but also fish, marine mammals, and even humans ([45]). The production of these toxins is often triggered by environmental stressors or competitive pressures, highlighting the complex interplay between phytoplankton and their environment ([103]).

Zooplankton, as primary consumers of phytoplankton, plays a critical role in controlling phytoplankton populations and transferring energy up the food chain. However, toxic phytoplankton pose significant challenges to zooplankton grazers. Some zooplankton species have developed mechanisms to detect and avoid toxic prey, while others have evolved tolerance or resistance to certain phytoplankton toxins (Ger et al., 2016). This selective grazing pressure can lead to changes in phytoplankton community composition, potentially favouring the growth of toxic species and altering ecosystem dynamics ([98]).

The interactions between toxic phytoplankton and zooplankton are bidirectional and complex. While toxic phytoplankton can negatively impact zooplankton through direct toxicity, reduced feeding efficiency, or decreased reproductive success, zooplankton grazing can also influence the growth and toxin production of phytoplankton. Some studies have shown that zooplankton grazing can induce increased toxin production in certain phytoplankton species, suggesting a chemical arms race between predator and prey ([84]).

Moreover, the presence of toxic phytoplankton can lead to cascading effects throughout the food web. When zooplankton avoid toxic prey, they may overgraze on non-toxic phytoplankton species, potentially leading to shifts in phytoplankton community structure and biogeochemical cycling ([91]). Additionally, the bioaccumulation of phytoplankton toxins in zooplankton can result in the transfer of these toxins to higher trophic levels, affecting fish populations and potentially posing risks to human health through seafood consumption ([8]).

The impact of toxic phytoplankton on zooplankton populations can vary depending on factors such as toxin type, concentration, and exposure duration. Some zooplankton species may experience acute toxicity effects, leading to increased mortality rates, while others may suffer from chronic, sublethal effects that impact growth, reproduction, or behaviour ([52]). These effects can have long-term consequences for zooplankton population dynamics and community structure, ultimately influencing the stability and resilience of aquatic ecosystems.

The study of [47] focused on the toxic phytoplankton species Heterosigma akashiwo and its responses to the presence of a ciliate predator, Favella sp. The researchers found that the phytoplankton exhibited significant fleeing behaviours, including increased swimming speed and upward vertical migration when exposed to predators or predator-derived cues. These behaviours effectively reduced predation pressure by decreasing encounters with predators, resulting in a three-fold increase in the net algal population growth rate. The study also incorporated these behaviours into a spatially explicit population model, which predicted rapid bloom formation under conditions where fleeing behaviours were present. This novel finding suggests that predator-induced behaviours in phytoplankton can be a critical factor in HAB dynamics, highlighting the importance of behavioural responses in ecological modelling and management of marine environments.

The authors [66] proposed a reaction-diffusion model for phytoplankton and zooplankton populations with self-diffusion, described by:

$$\begin{aligned} \frac{\partial \tilde{u}}{\partial \tilde{t}} &= r\tilde{u}\left(1-\frac{\tilde{u}}{b}\right) - \alpha_1 f(\tilde{u})\tilde{v} + D_1\frac{\partial^2 \tilde{u}}{\partial \tilde{x}^2} \\ \frac{\partial \tilde{v}}{\partial \tilde{t}} &= \kappa\alpha_1 f(\tilde{u})\tilde{v} - \mu\tilde{v} + D_2\frac{\partial^2 \tilde{v}}{\partial \tilde{x}^2} \end{aligned} \tag{3.1}$$

where $\tilde{u}$ and $\tilde{v}$ denote the population densities of the prey and predator, respectively. r is an intrinsic growth rate of prey, κ is a coefficient of food utilization, parameter μ is a natural mortality rate of the predator, b is a carrying capacity for the prey population, α_1 is a predation rate, while $f(\tilde{u})$ is function response which is a Holling type II, and H is half saturation abundance of prey. Their study explored the interactions between phytoplankton and zooplankton without the influence of toxic phytoplankton (TPP). The research uncovered complex and chaotic behaviour in the spatiotemporal dynamics of aquatic ecosystems, revealing the formation of intricate spatial patterns such as jagged and spiral structures. These patterns are shaped by factors like initial conditions and biological interactions, underscoring the role of non-linear dynamics in ecological modelling and enhancing the understanding of pattern formation in biological systems.

Recent research has extensively explored the fascinating phenomenon where toxic substances produced by phytoplankton significantly reduce the grazing pressure exerted by zooplankton. This interaction, known as toxic phytoplankton protection (TPP), has become a critical area of study due to its potential role as a natural biocontrol mechanism against harmful planktonic blooms ([12, 13, 16, 81, 15]).

In [17], a mathematical model based on the toxicity of phytoplankton was formulated using a system of ordinary differential equations, given by:

$$\begin{aligned} \frac{d\tilde{u}}{d\tilde{t}} &= r\tilde{u}\left(1-\frac{\tilde{u}}{b}\right)-\alpha_1 f(\tilde{u})\tilde{v}, \\ \frac{d\tilde{v}}{d\tilde{t}} &= \beta_1 f(\tilde{u})\tilde{v}-\mu\tilde{v}-\delta g(\tilde{u})\tilde{v}. \end{aligned} \tag{3.2}$$

Here, $\tilde{u}$ represents the density of the toxic phytoplankton (TPP) population, and $\tilde{v}$ represents the density of the zooplankton population. The parameter α_1 denotes the rate of zooplankton predation on the TPP population, while $f(\tilde{u})$ is the predation response function, and $g(\tilde{u})$ represents the distribution of toxic substances. These functions may correspond to different types of functional responses, such as Holling Type I, II, and III. Furthermore, β_1 denotes the ratio of biomass consumed by zooplankton for its growth, and δ is the rate of toxic liberation by TPP. In this study, they proposed that TPP can function as a biocontrol strategy, effectively mitigating the uncontrolled growth of plankton by altering the typical predator-prey dynamics between zooplankton and phytoplankton.

Building on this foundation, ([80]) developed a more sophisticated mathematical model that delves into the interactions between toxin-producing phytoplankton and zooplankton. Their study specifically investigates the occurrence of Hopf bifurcations within this system, which marks the transition from stable to oscillatory behaviour in population dynamics. Through detailed numerical simulations, they provided valuable insights into the complex and often counterintuitive dynamics driven by TPP.

Further extending the theoretical framework, ([61]) introduced a reaction-diffusion system that incorporates self-diffusion terms to model the spatial and temporal distributions of these interacting populations. Their work offers a comprehensive and rigorous analysis of the global dynamics of the system, revealing how TPP influences not only the population densities but also the spatial patterns and stability of the entire aquatic ecosystem. This body of research collectively enhances our understanding of the intricate biotic interactions that govern planktonic ecosystems and highlights the importance of TPP in maintaining ecological balance.

Mathematical modelling of toxic phytoplankton and zooplankton

In this study, we propose a system of partial differential equations (PDEs) to capture the spatiotemporal dynamics of toxic phytoplankton (denoted by u)and zooplankton (denoted by v). The model accounts for diffusion processes governing the spatial spread of these populations and reaction terms representing their growth, mortality, and interactions. By integrating diffusion and reaction mechanisms, our model aims to elucidate phytoplankton-zooplankton ecosystems' emergent patterns and stability properties.

The proposed PDE system is given by:

$$\begin{aligned}\frac{\partial \tilde{u}}{\partial \tilde{t}} &= r\tilde{u}\left(1-\frac{\tilde{u}}{b}\right)-\alpha_1 f(\tilde{u})\tilde{v}+D_1\frac{\partial^2\tilde{u}}{\partial\tilde{x}^2}+D_{12}\frac{\partial}{\partial\tilde{x}}\left(\tilde{u}\frac{\partial\tilde{v}}{\partial\tilde{x}}\right)\\ \frac{\partial \tilde{v}}{\partial \tilde{t}} &= \kappa\alpha_1 f(\tilde{u})\tilde{v}-\mu\tilde{v}-\delta g(\tilde{u})\tilde{v}+D_2\frac{\partial^2\tilde{v}}{\partial\tilde{x}^2}+D_{21}\frac{\partial}{\partial\tilde{x}}\left(\tilde{v}\frac{\partial\tilde{u}}{\partial\tilde{x}}\right)\end{aligned} \tag{3.3}$$

The above-proposed model was initially introduced by ([66]) in the absence of cross-diffusion and without incorporating the effects of toxicity on zooplankton. In this model, we introduce nonlinear cross-diffusion to represent the mutual avoidance between TPP and zooplankton, drawing on the concept from the experimental study by ([47]). Additionally, we include the toxicity effects proposed by [17], which suggest that TPP can be a biocontrol mechanism to prevent planktonic blooms. Here $\tilde{u}$ and $\tilde{v}$ are an abundance of toxic-producing phytoplankton and zooplankton, respectively, D_1, D_2 are self-diffusion coefficients, and D_{12}, D_{21} are cross-diffusion coefficients of TTP and zooplankton respectively. Cross diffusion is the phenomenon that tells how the gradient concentration of one species induces a flux of another species. Most of the studies where self and cross-diffusion terms are considered to focus on the mathematical properties of the system rather than pattern formation. In ([2], [100]), elaborating the importance of cross-diffusion on pattern formation from both experimental and theoretical points of view, the authors proposed minimal conditions of pattern formation in the presence of linear cross-diffusion terms with nonlinear kinetics. In recent studies, the researcher in ([32],[29],[34]) presented a complete analysis of the importance of cross-diffusion on the generation of Turing patterns from the mathematical point of view. The $f(u)$ represents the predation response function, and $g(u)$ is the distribution of toxic substances which ultimately lead to the death of the zooplankton population. The $f(u)$ and $g(u)$ both employ Holling type II functional response, which is the standard and intuitively obvious choice to describe grazing phenomena and is defined as $f(u) = g(u) = \frac{u}{u+H}$.

The above-coupled reaction-diffusion system can be re-written as,

$$\begin{aligned}\frac{\partial \tilde{u}}{\partial \tilde{t}} &= r\tilde{u}\left(1-\frac{\tilde{u}}{b}\right)-\alpha_1\left(\frac{\tilde{u}\tilde{v}}{\tilde{u}+H}\right)+D_1\frac{\partial^2\tilde{u}}{\partial\tilde{x}^2}+D_{12}\frac{\partial}{\partial\tilde{x}}\left(\tilde{u}\frac{\partial\tilde{v}}{\partial\tilde{x}}\right),\\ \frac{\partial \tilde{v}}{\partial \tilde{t}} &= \kappa\alpha_1\left(\frac{\tilde{u}\tilde{v}}{\tilde{u}+H}\right)-\mu\tilde{v}-\delta\left(\frac{\tilde{u}\tilde{v}}{\tilde{u}+H}\right)+D_2\frac{\partial^2\tilde{v}}{\partial\tilde{x}^2}+D_{21}\frac{\partial}{\partial\tilde{x}}\left(\tilde{v}\frac{\partial\tilde{u}}{\partial\tilde{x}}\right),\end{aligned} \tag{3.4}$$

κ is a coefficient of food utilization, parameter μ is an natural moratility rate of zooplankton, r is an intrinsic growth rate of TPP, b is an carrying capacity of TPP, α_1 predation rate of zooplankton, δ is the rate of toxin liberation by TPP, and H is half saturation abundance of TPP.

Parameters	Values	Source
β	0 - 2000	[70], [28]
η_1	0.6 - 30	[22] - [46]
η_2	0 - 2	[22] - [46]
m	0.06 - 3	[1]
γ	$0 < \gamma < 1$	Present study

TABLE 3.1: Numerical values of the parameters of the model (3.6), which have been used for the simulations for the present work.

The dimensionless form of the given model is represented as:

$$\begin{aligned}\frac{\partial u}{\partial t} &= u\left(1-u\right) - \left(\frac{uv}{u+\beta}\right) + \frac{\partial^2 u}{\partial x^2} + d_{12}\frac{\partial}{\partial x}\left(u\frac{\partial v}{\partial x}\right),\\ \frac{\partial v}{\partial t} &= \eta_1\left(\frac{uv}{u+\beta}\right) - mv - \eta_2\left(\frac{uv}{u+\beta}\right) + d\frac{\partial^2 v}{\partial x^2} + d_{21}\frac{\partial}{\partial x}\left(v\frac{\partial u}{\partial x}\right),\end{aligned} \tag{3.5}$$

where
$\tilde{u} = bu$, $\tilde{v} = \frac{rb}{\alpha_1}v$, $\tilde{x} = \sqrt{\frac{D_1}{r}}x$, $\tilde{t} = \frac{t}{r}$, $\eta_1 = \frac{\kappa\alpha_1}{r}$, $\eta_2 = \frac{\delta}{r}$, $\beta = \frac{H}{b}$, $m=\frac{\mu}{r}$, $d = \frac{D_2}{D_1}$, $d_{12} = \frac{D_{12}br}{\alpha_1 D_1}$, $d_{21} = \frac{D_{21}b}{D_1}$.

If we rewrite dimensionless system (3.5), as

$$\begin{aligned}\frac{\partial u}{\partial t} &= u\left(1-u\right) - \left(\frac{uv}{u+\beta}\right) + \frac{\partial^2 u}{\partial x^2} + d_{12}\frac{\partial}{\partial x}\left(u\frac{\partial v}{\partial x}\right),\\ \frac{\partial v}{\partial t} &= \eta\left(\frac{uv}{u+\beta}\right) - mv + d\frac{\partial^2 v}{\partial x^2} + d_{21}\frac{\partial}{\partial x}\left(v\frac{\partial u}{\partial x}\right),\end{aligned} \tag{3.6}$$

for simplicity, we defined $\eta = \eta_1 - \eta_2$, which will help us to understand the linear stability analysis in the next section. The value of the dimensionless parameters are summarised in table 3.1. Initial and boundary conditions must be added to the system. We are interested in self-organizing patterns in this article and shall impose the homogenous Neumann boundary conditions.The complete analysis of the proposed model (3.6) is discussed in the next chapters, (4 and 5).

Chapter 4

Stability Analysis and Turing Region

Chapter 4 focuses on the stability analysis of equilibrium solutions in a system described by partial differential equations, emphasising determining conditions for linear stability and Turing Instability. The chapter begins by introducing the concept of equilibrium solutions, particularly attracting equilibrium solutions, which are stable under small perturbations. The linear stability of these solutions is analyzed by linearizing the system around the equilibrium points and examining the eigenvalues of the resulting Jacobian matrix. Stability is ensured if all eigenvalues have negative real parts, a condition that is elaborated through the trace and determinant of the Jacobian. The chapter also discusses local stability in the context of ordinary differential equations (ODE) and introduces the concept of Hopf bifurcation, which occurs under specific parameter conditions. Numerical simulations illustrate the stability and instability regions, along with the occurrence of Hopf bifurcation under different scenarios (see sections 4.1 and 4.2). The latter part of the chapter delves into Turing instability, a phenomenon that occurs due to cross-diffusion in the system, leading to pattern formation. The conditions under which Turing instability arises are derived, highlighting the crucial role of cross-diffusion terms. The chapter concludes by establishing criteria for Turing instability and discussing its implications for the dynamics of the system (see sections 4.3 and 4.4).

4.1 Linear Stability Analysis

A prominent solution of great interest is the equilibrium solution of a partial differential equation. We are particularly interested in attracting equilibrium solutions, which are time-independent, stable solutions that can remain stable for small perturbations. Stability can take various forms, and our objective is to classify equilibrium as linearly stable.

Equilibrium solutions to (3.6) are solutions $(u^*, v^*)^T$ such that $u_t = v_t = 0$. Thus, (3.6) in absence of diffusion turns into

$$\begin{cases} f(u,v) = 0, \\ g(u,v) = 0. \end{cases}$$

So, for our model, equilibrium solutions in the absence of diffusion are those solutions $(u^*, v^*)^T$ which solve

$$f(u^*, v^*) = g(u^*, v^*) = 0.$$

Now, we address the stability of the equilibrium solutions by presenting the linearization of the system.

$$\begin{cases} u_t = f(u,v), \\ v_t = g(u,v). \end{cases} \tag{4.1}$$

Linearization

An equilibrium point $X^* \in \mathbb{R}^n$ of a nonlinear dynamical system is said to be stable if, for every neighbourhood O of X^*, there exists a smaller neighbourhood $O_1 \subset O$ such that any solution $X(t)$ of the system, with an initial condition $X(0) = X_0 \in O_1$, remains in O for all $t \geq 0$. In other words, small perturbations around X^* do not cause the system to diverge far from X^*. We define a perturbation of the equilibrium solution as

$$w = \begin{pmatrix} u - u^* \\ v - v^* \end{pmatrix}.$$

The functions f and g can be linearized using Taylor expansion about (u^*, v^*)

$$\begin{aligned} f(u,v) &\approx f(u^*,v^*) + f_u(u^*,v^*) \cdot (u-u^*) + f_v(u^*,v^*) \cdot (v-v^*), \\ &= f_u(u^*,v^*) \cdot (u-u^*) + f_v(u^*,v^*) \cdot (v-v^*), \end{aligned}$$

and

$$\begin{aligned} g(u,v) &\approx g(u^*,v^*) + g_u(u^*,v^*) \cdot (u-u^*) + g_v(u^*,v^*) \cdot (v-v^*) \\ &= g_u(u^*,v^*) \cdot (u-u^*) + g_v(u^*,v^*) \cdot (v-v^*). \end{aligned}$$

So, linearizing (4.1) about (u^*, v^*), we obtain

$$\begin{cases} u_t = [f_u(u^*,v^*) \cdot (u-u^*) + f_v(u^*,v^*) \cdot (v-v^*)], \\ v_t = [g_u(u^*,v^*) \cdot (u-u^*) + g_v(u^*,v^*) \cdot (v-v^*)]. \end{cases}$$

Which can be written in matrix form as

$$\mathbf{w}_t = J\mathbf{w}, \tag{4.2}$$

where

$$J = \begin{pmatrix} f_u(u^*,v^*) & f_v(u^*,v^*) \\ g_u(u^*,v^*) & g_v(u^*,v^*) \end{pmatrix} = \begin{pmatrix} f_u & f_v \\ g_u & g_v \end{pmatrix}_{(u^*,v^*)}.$$

Stability analysis

The solution $\mathbf{w}$ is said to be linearly stable if $|\mathbf{w}| \to 0$ as $t \to \infty$. We focus on determining the conditions on the eigenvalues of J, which make the solution w linearly stable. The solution $\mathbf{w}$ of equation (4.2) is linearly stable if and only if all eigenvalues of J have negative real parts.

Local stability

Let's review some of the fundamental stability theory of ordinary differential equations (ODE); for more details, refer to ([74]). The first important aspect to consider is the behaviour of solutions as t approaches $+\infty$. It is widely known that this behaviour heavily depends on the eigenvalues of J, which are denoted as λ_1 and λ_2. To calculate these eigenvalues, we need to solve the characteristic equation

$$
\begin{aligned}
&|J - \lambda I| = \left| \begin{pmatrix} f_u - \lambda & f_v \\ g_u & g_v - \lambda \end{pmatrix} \right| = 0, \\
&\Rightarrow (f_u - \lambda)(g_v - \lambda) - f_v g_u = 0, \\
&\Rightarrow \lambda_{1,2} = \frac{(f_u + g_v) \pm \sqrt{(f_u + g_v)^2 - 4(f_u g_v - f_v g_u)}}{2}.
\end{aligned}
$$

The linear stability is guaranteed if the trace of J is negative and its determinant is positive, i.e.

$$
\begin{cases} \operatorname{tr} J = f_u + g_v < 0, \\ \det J = f_u g_v - f_v g_u > 0. \end{cases}
$$

Our analysis determined that the linearized system (4.2) is stable only if the real parts of the eigenvalues of J are negative. If any eigenvalue is positive or has a positive real part, then (u^*, v^*) is unstable.
Now, we will determine the steady state of the equations (3.6) in the absence of diffusion. For that, using some simple calculation, we have to find three steady states of the system, which are (0, 0), (total extinction), (1, 0), (extinction of predator), and coexistence steady state (u^*, v^*). Where (0,0) is the saddle for all parameters values and (1,0) is the saddle if we choose parameters value from the ecological point of view; otherwise, it is a stable node if we choose $\beta > \frac{1-\gamma}{\gamma}$. The non-trivial steady state (u^*, v^*) (coexistence of prey and predator), which as defined

$$
u^* = \frac{\gamma\beta}{1-\gamma}, v^* = (1 - u^*)(\beta + u^*), \tag{4.3}
$$

where

$$
\gamma = \frac{m}{\eta}.
$$

From the ecological point of view, the steady state defined in Eq. (4.3) should be positive. We get the following condition on u^* and v^*

for

$$
u^* > 0, \text{ if } \gamma < 1,
$$

and for

$$
v^* > 0, \text{ if } \beta < \frac{1-\gamma}{\gamma}.
$$

The Jacobian matix around the neighbourhood of (u^*, v^*) is as follow:

$$
J = \begin{pmatrix} f_u & f_v \\ g_u & g_v \end{pmatrix}, \tag{4.4}
$$

where

$$f_u = u^*\left(-1+\frac{1-u^*}{(u^*+\beta)}\right) = \gamma\left(1-\beta\frac{1+\gamma}{1-\gamma}\right), \tag{4.5}$$

$$f_v = -\frac{u^*}{(u^*+\beta)} = -\gamma, \tag{4.6}$$

$$g_u = \frac{\eta v^*\beta}{(u^*+\beta)^2} = \eta(1-\gamma-\gamma\beta), \tag{4.7}$$

$$g_v = 0. \tag{4.8}$$

The positive coexistence steady state become stable if $\mathrm{tr}(J) < 0$ for that

$$f_u < 0, \Longrightarrow \beta > \frac{1-\gamma}{1+\gamma}, \tag{4.9}$$

so we get the following condition on β,

$$\beta \in \left(\frac{1-\gamma}{1+\gamma}, \frac{1-\gamma}{\gamma}\right), \tag{4.10}$$

and also, for stability $\mathrm{Det.}(J) > 0$, which we can see easily from Eqs. (4.5 - 4.8).

The eigenvalue of the system without diffusion can be defined as

$$\lambda = \frac{1}{2}[\gamma(1-\beta\frac{1+\gamma}{1-\gamma}) \mp \sqrt{\gamma^2(1-\beta\frac{1+\gamma}{1-\gamma})^2 - 4\gamma\eta(1-\gamma-\gamma\beta)}], \tag{4.11}$$

so Hopf bifurcation occurs at $\beta = \frac{1-\gamma}{1+\gamma}$.

4.2 Numerical Analysis of System Kinetics

This section delves into the numerical analysis of the stability and behaviour of a nonlinear dynamical system, focusing on the interactions between two species. In Figs. (4.1 and 4.2), we fix the parameter η and vary other parameters, particularly β, to observe the system's transition from stability to periodic oscillation and eventually instability. The bifurcation diagram illustrates two distinct regions: Region I, where the system exhibits stable equilibrium, and Region II, where the system becomes unstable. Between these two regions lies a boundary where the system exhibits periodic oscillations, marking a transition zone. As β changes its values, the system crosses this bifurcation point, transitioning from stable behaviour to periodic cycles and eventually leading to instability in Region II. Additionally, in Fig. 4.3, we fix the parameter m and explore how variations in β further affect system dynamics, demonstrating the system's progression through different dynamical states. These graphical representations provide a comprehensive view of the system's stability, periodic oscillations, and the transition to instability under varying parameters, highlighting the coexistence and bifurcation of steady states.

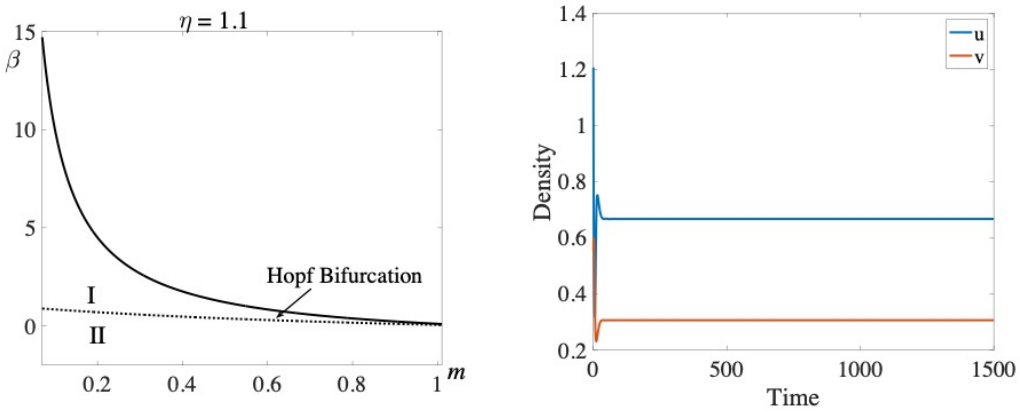

(a) (b)

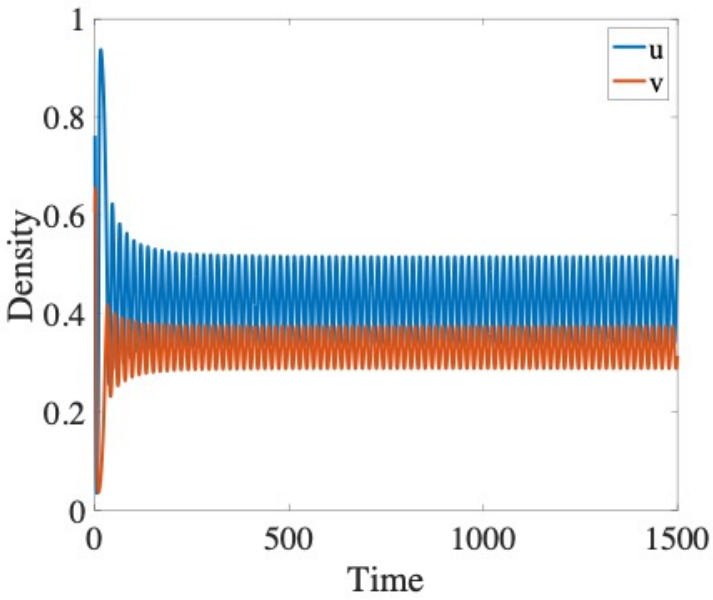

(c)

FIGURE 4.1: Stability analysis for a dynamical system at $\eta = 1.1$.

In Fig.4.1, a Graphical representation shows that the coexistence steady state will be stable in Region I; it is unstable in Region II and holds Hopf bifurcation on the dotted line. (a) We fix $\eta = 1.1$ and choose $m < \eta$ to obtain condition $0 < \gamma < 1$. (b) We are chosen parameters in the stable region by fixing $\beta = 0.25$, $\eta = 1.1$, $m = 0.8$, then $\gamma = 0.7273$, where $(u^*, v^*) = (0.6667, 0.3056)$. (c) We have chosen parameters where Hopf bifurcation occurs by selecting $\beta = 0.1579$; other parameters are the same as in (b) where (u^*, v^*)=$(0.4211, 0.3352)$.

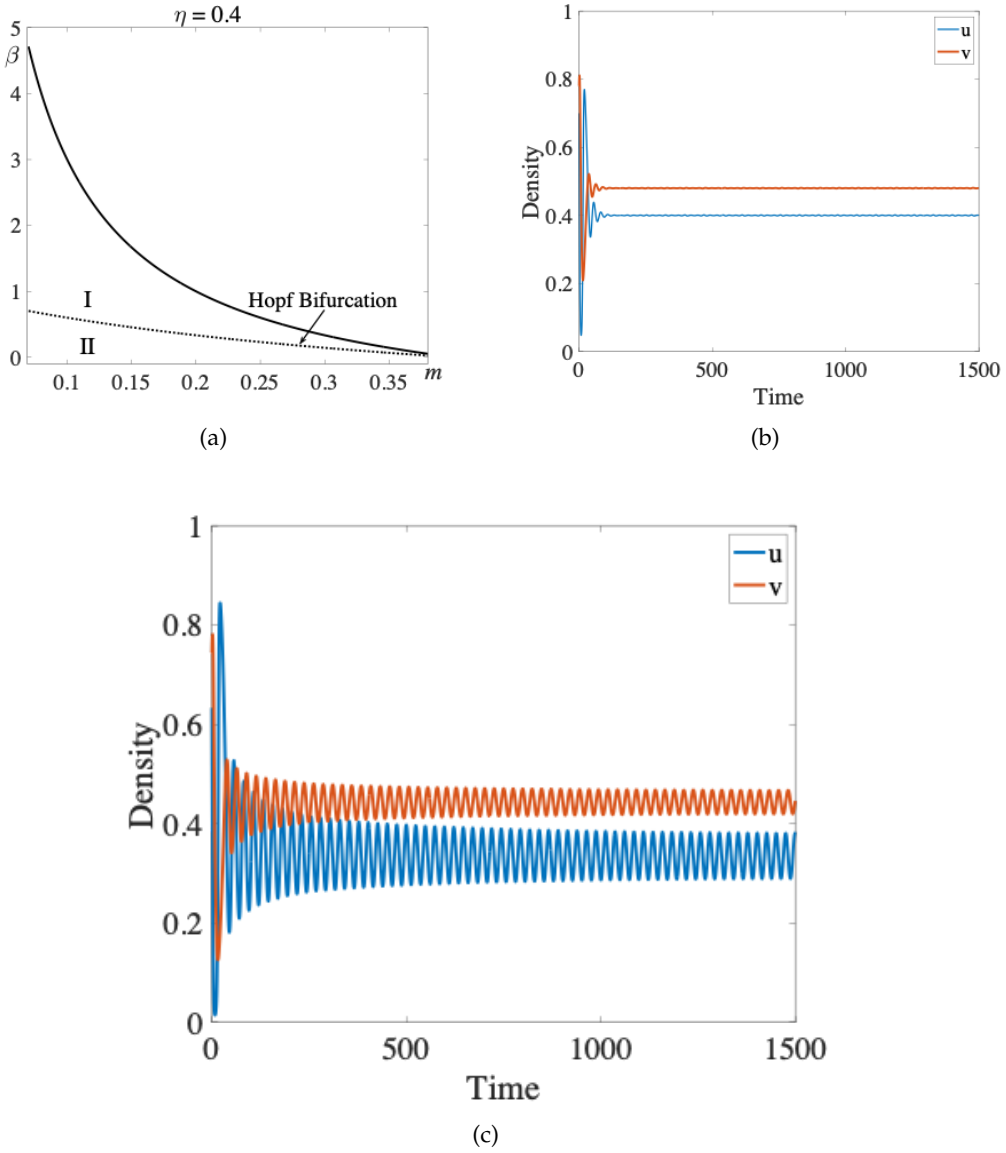

FIGURE 4.2: Stability analysis for a dynamical system at $\eta = 0.4$.

In Fig. 4.2, a Graphical representation shows that the coexistence steady state will be stable in Region I; it is unstable in Region II and holds Hopf bifurcation on the dotted line. (a) We fix $\eta = 0.4$ and choose $m < \eta$ to obtain condition $0 < \gamma < 1$. (b) We are chosen parameters in the stable region by fixing $\beta = 0.4$, $\eta = 0.4$, $m = 0.2$, then $\gamma = 0.5000$, where $(u^*, v^*) = (0.4000, 0.4800)$. (c) We have chosen parameters where Hopf bifurcation occurs by selecting $\beta = 0.3333$; other parameters are the same as in (b) where (u^*, v^*)=$(0.3333, 0.4444)$.

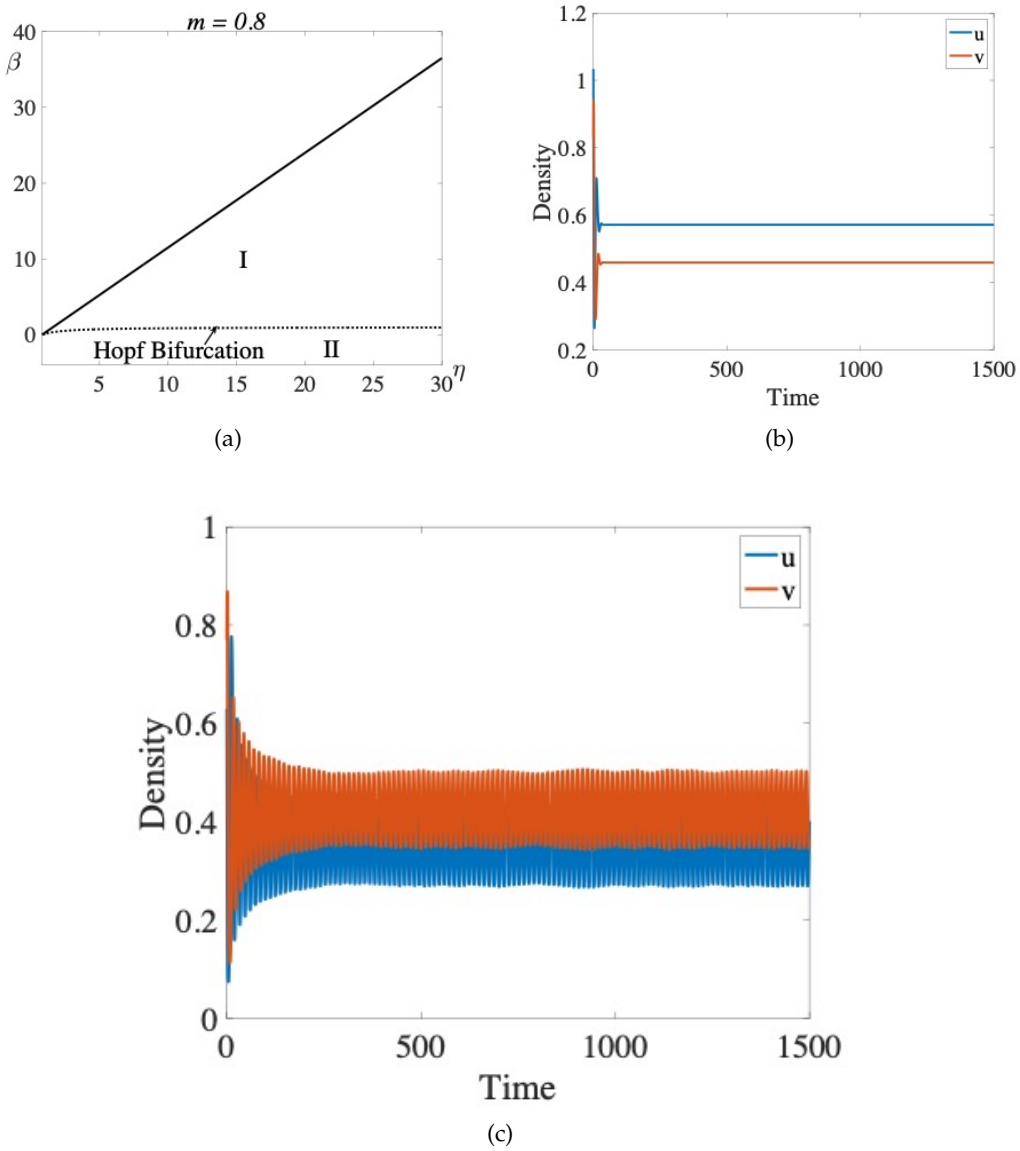

(a) (b)

(c)

FIGURE 4.3: Stability analysis for a dynamical system at $m = 0.8$.

In Fig. 4.3, a Graphical representation showing that the coexistence steady state will be stable in region I, it is unstable in region II and holds Hopf bifurcation on the dotted line.(a), We fix $m = 0.8$ and choose $m < \eta$ to obtain condition $0 < \gamma < 1$. (b) We are chosen parameters in the stable region by fixing $\beta = 0.5$, $m = 0.8$, $\eta = 1.5$, then $\gamma = 0.5333$, where $(u^*, v^*) = (0.5714, 0.459)$. (c) We have chosen parameters where Hopf bifurcation occurs by selecting $\beta = 0.3043$; other parameters are the same as in (b), where $(u^*, v^*) = (0.3478, 0.4253)$.

4.3 Linear Stability Analysis of Full System: Turing Instability

To obtain Turing instability, we linearized the original system (3.6) around the steady state. Then, we obtained the following linearized form of the system

$$\frac{\partial \mathbf{w}}{\partial t} = J\mathbf{w} + D\nabla^2\mathbf{w},\ \mathbf{w} = \begin{pmatrix} u-u^* \\ v-v^* \end{pmatrix}, \tag{4.12}$$

where

$$D = \begin{pmatrix} 1 & d_{12}u^* \\ d_{21}v^* & d \end{pmatrix}. \tag{4.13}$$

The dispersion relation, which gives the eigenvalue λ as a function of the wavenumber k:

$$\lambda^2 + (k^2\, tr(D) - tr(J))\lambda + h(k^2) = 0, \tag{4.14}$$

where

$$h(k^2) = Det(D)k^4 + qk^2 + Det(J), \tag{4.15}$$

with

$$Det(D) = 1 - d_{12}d_{21}u^*v^*,\ q = -df_u + d_{12}u^*g_u + d_{21}v^*f_v. \tag{4.16}$$

For Turing instability $Re(\lambda(k) > 0)$, for that either coefficient of λ in (4.14) is negative or $h(k^2) < 0$. As the coefficient of λ is positive, we are looking for those modes for which $h(k^2) < 0$. The only possibility for $h(k^2) < 0$ is $q < 0$. To check a sign of q, we have the following possibility

Remark 1: so if $d_{12} = d_{21} = 0 \Longrightarrow q > 0$ i.e. no Turing instability exists.

Remark 2: so if $d_{21} = 0 \Longrightarrow q > 0$ i.e. no Turing instability exists.

Remark 3: so if $d_{21} \neq 0 \Longrightarrow q < 0$ i.e. Turing instability exists.

Thus, the only potential destabilising mechanism is the presence of the cross-diffusion term, while linear diffusion plays a stabilising role; if this cross-diffusion is zero, there is no possible way to show that this reaction-diffusion system holds a Turing instability.

So, for the Turing instability, we want to show the following two conditions on $h(k^2)$,

$$q < 0, \tag{4.17}$$

and

$$q^2 - 4Det(D)Det(J) \geq 0. \tag{4.18}$$

The condition $q < 0$ shows that we get some positive value of k^2 on which $h(k^2)$ attains a minimum value. To get a minimum value of $h(k^2)$ negative for some finite width of the unstable wave number of k^2, we need to satisfy the condition as defined in equation (4.18). since $h(k^2)$ attains a minimum value at:

$$k_c^2 = -\frac{q}{2Det(D)}.$$

At the bifurcation, we require the following:

$$q^2 - 4Det(D)Det(J) = 0, \tag{4.19}$$

which, for fixed values for other parameters, defines the critical values d_{21}^c of the bifurcation parameter d_{21}.

To prove the condition on which $q < 0$, we write q in terms of system parameters, which is

$$q = -d\gamma\left(1 - \beta\frac{1+\gamma}{1-\gamma}\right) - \gamma d_{21}v^* + \eta(1-\gamma-\gamma\beta)u^* d_{12}, \tag{4.20}$$

if we define

$$\bar{d_{21}} = \frac{d}{v^*}(\beta\frac{1+\gamma}{1-\gamma} - 1) + \frac{\eta u^* d_{12}}{v^*\gamma}(1-\gamma-\gamma\beta), \tag{4.21}$$

as we see that q obtains a critical value when $d_{21} = \bar{d_{21}}$, so for $q < 0$,

$$d_{21} > \bar{d_{21}}. \tag{4.22}$$

For well-posedness condition, need to show that $d - d_{12}d_{21}u^*v^* > 0$, which gives the following condition

$$d_{21} < \frac{d}{d_{12}u^*v^*}, \tag{4.23}$$

so it means,

$$\bar{d_{21}} < \frac{d}{d_{12}u^*v^*}. \tag{4.24}$$

By solving (4.24), we get the following conditions on the parameters d and d_{12}, which are given by,

$$d = d_m > \frac{d_{12}\eta(1-\gamma-\gamma\beta)u^*}{\gamma\left(1 - \beta\frac{1+\gamma}{1-\gamma} + \frac{1}{d_{12}u^*}\right)}, \tag{4.25}$$

$$d_{12} < \frac{1}{\left(\beta\frac{1+\gamma}{1-\gamma} - 1\right)u^*}, \tag{4.26}$$

d_m is the point which gives the starting value in (d, d_{21})-plane, where both $q < 0$ and $d_{21} < \frac{d}{d_{12}u^*v^*}$ satisfied.

Then, we need to show the condition (4.18), which gives the threshold value of the parameter d_{21} on the equality. If we write (4.18) in terms of a system parameter, we get the following inequality,

$$v^{*2}\gamma^2 d_{21}^2 - 2d_{21}[v^{*2}\gamma^2\bar{d_{21}} - 2d_{12}u^*v^*Det(J)] + v^{*2}\bar{d_{21}}^2 - 4dDet(J) \geq 0. \tag{4.27}$$

The discriminant of (4.27) is

$$\Delta = 4Det(J)[d_{12}^2u^{*2}v^{*2}Det(J) + v^{*2}\gamma^2(d - \bar{d_{21}}d_{12}u^*v^*)], \tag{4.28}$$

as we see $\Delta > 0$ if $d > d_m$ from (4.25), then we will find the root d_{21}^c of (4.27) in which d_{21} lies above $\bar{d_{21}}$, by the following equality $d_{21} \geq d_{21}^c = \bar{d_{21}} + \epsilon^+$, where ϵ^+ is the root of following quadtratic polynimial

$$\epsilon^2 v^{*2}\gamma^2 + 4\epsilon d_{12}u^*v^*\mathrm{Det}(J) - 4\mathrm{Det}(J)(d - d_{12}\bar{d_{21}}u^*v^*) \geq 0. \tag{4.29}$$

The resulting quadratic polynomial in ϵ, given above by (4.29), admits only one real positive root ϵ^+. Thus, choosing $d > d_m$, a Turing instability sets in for $d_{21} \geq d_{21}^c = \bar{d}_{21} + \epsilon^+$.

From the above calculation, we get the following condition on diffusion coefficients to obtain a Turing instability:

$$d = d_m > \frac{d_{12}\eta(1-\gamma-\gamma\beta)u^*}{\gamma\left(1-\beta\frac{1+\gamma}{1-\gamma}+\frac{1}{\bar{d}_{12}u^*}\right)}, \tag{4.30}$$

$$d_{12} < \frac{1}{\left(\beta\frac{1+\gamma}{1-\gamma}-1\right)u^*}, \tag{4.31}$$

$$\frac{d}{d_{12}u^*v^*} > d_{21} > \bar{d}_{21} + \epsilon^+. \tag{4.32}$$

4.3.1 Conditions for diffusion instability

In this subsection, we will establish the conditions for the onset of diffusion instabilities of the system described by equations (3.6). These conditions will be determined based on the satisfaction of (4.17) - (4.18) and (4.23). We shall choose "d_{21}" as a bifurcation parameter.

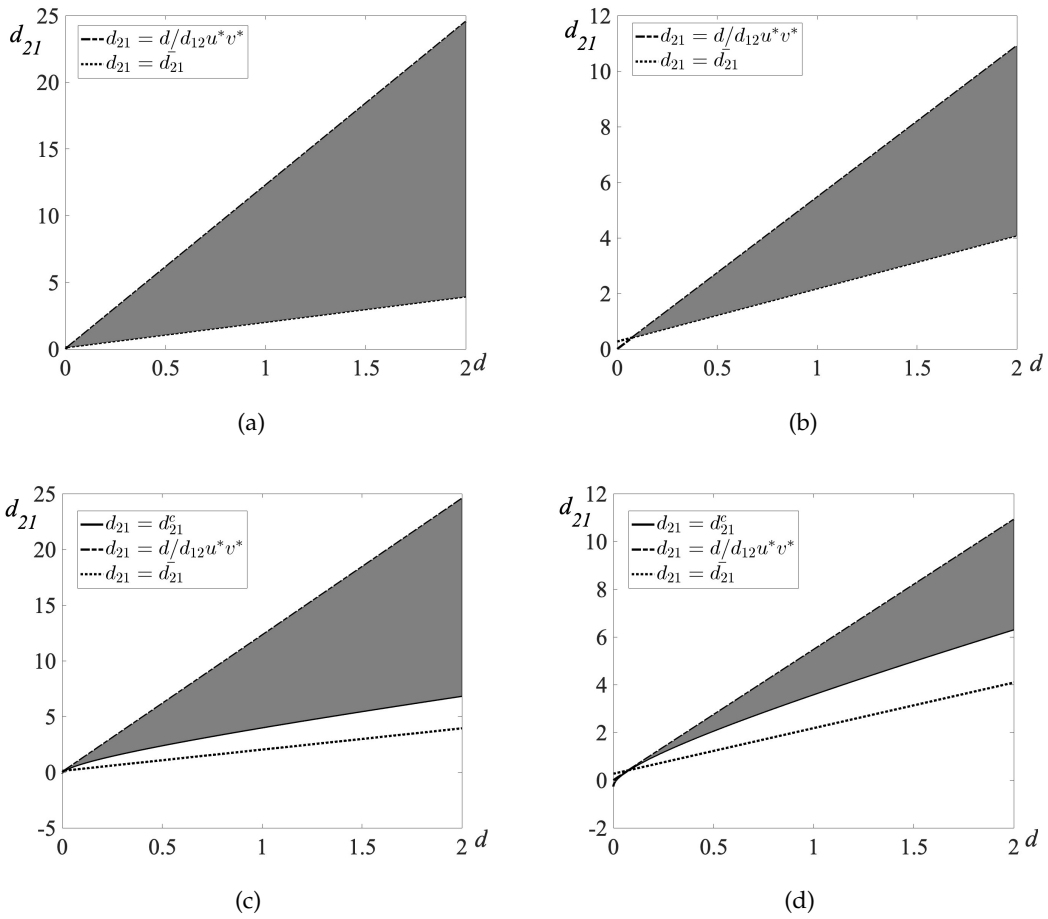

FIGURE 4.4: Parameter space of the system (3.6) showing the region where Turing instability occurs for case 1.

In Fig 4.4, there is a Graphical representation of the conditions for the diffusive-driven instability. (a-b) For two different choices of d_{12}, the region between $d_{21} = \bar{d_{21}}$ (dotted line) and $d_{21} = \frac{d}{d_{12}u^*v^*}$ (dash-dotted line) in (d, d_{21})-plane delineated by the two straight lines corresponds to fulfilment of the conditions (4.17) and (4.23). The other parameters are chosen as $\beta = 0.25$, $\eta = 1.1$, $m = 0.8$, then $\gamma = 0.7273$, so that $(u^*, v^*) = (0.6667, 0.3056)$. (a) $d_{12} = 0.4$, which gives $d_m = 0.0116$, (b) $d_{12} = 0.9$, which gives $d_m = 0.0762$. (c-d), For two different values d_{12}, the area between $d_{21} = d_{21}^c$ (solid line) and $d_{21} = \frac{d}{d_{12}u^*v^*}$ (dashed dotted line) in (d, d_{21})-plane fulfills the conditions (4.17), (4.23), and (4.27). (c) The parameters as chosen in (a). (d) The parameters as chosen in (b).

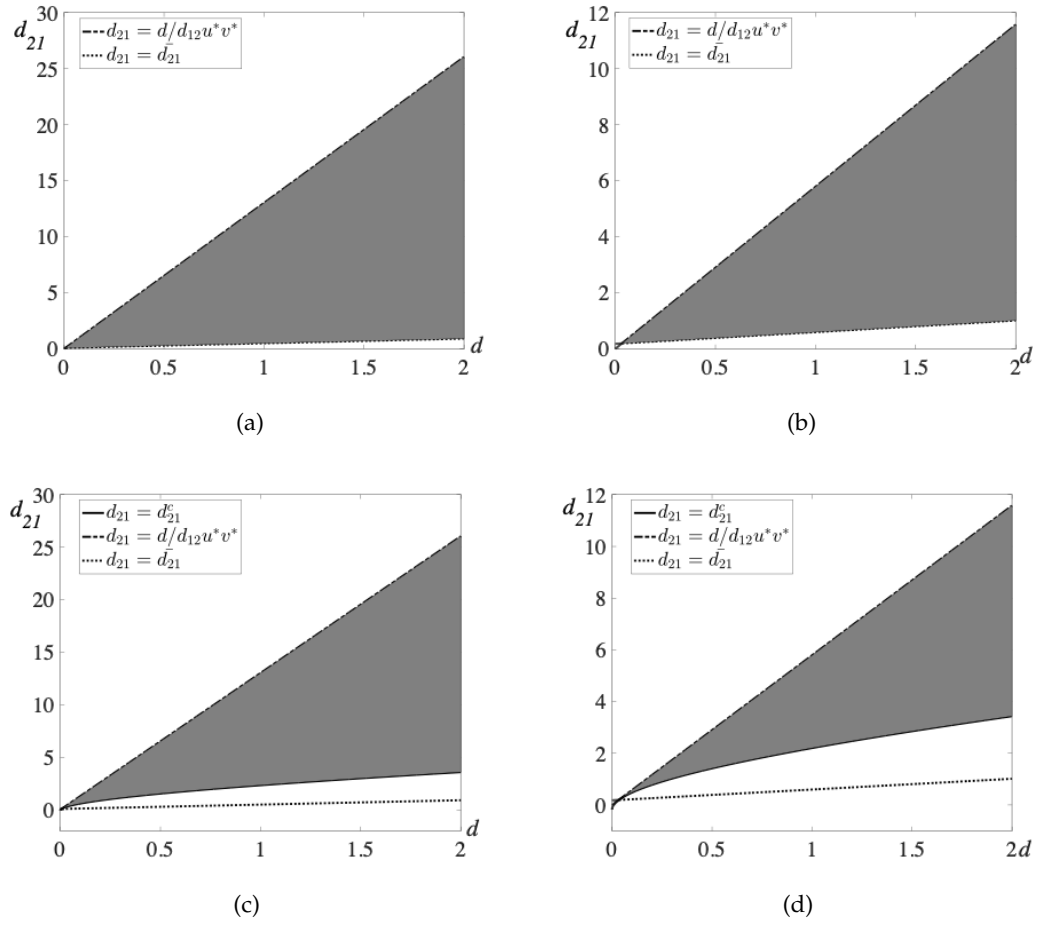

FIGURE 4.5: Parameter space of the system (3.6) showing the region where Turing instability occurs for case 2.

.

In Fig. 4.5, a graphical representation of the conditions for the diffusive-driven instability. (a-b) For two different choices of d_{12}, the region between $d_{21} = \bar{d_{21}}$ (dotted line) and $d_{21} = \frac{d}{d_{12}u^*v^*}$ (dash-dotted line) in (d, d_{21})-plane delineated by the two straight lines corresponds to fulfillment of the conditions (4.17) and (4.23). The other parameters are chosen as $\beta = 0.4$, $\eta = 0.4$, $m = 0.2$, then $\gamma = 0.5000$, so that $(u^*, v^*) = (0.4000, 0.4800)$. (a) $d_{12} = 0.4$, which gives $d_m = 0.0063$, (b) $d_{12} = 0.9$, which gives $d_m = 0.0335$. (c-d), For two different values d_{12}, the area between $d_{21} = d_{21}^c$ (solid line) and $d_{21} = \frac{d}{d_{12}u^*v^*}$ (dash-dotted line) in (d, d_{21})-plane fulfills

the conditions (4.17), (4.23), and (4.27). (c) The parameters as chosen in (a). (d) The parameters as chosen in (b),

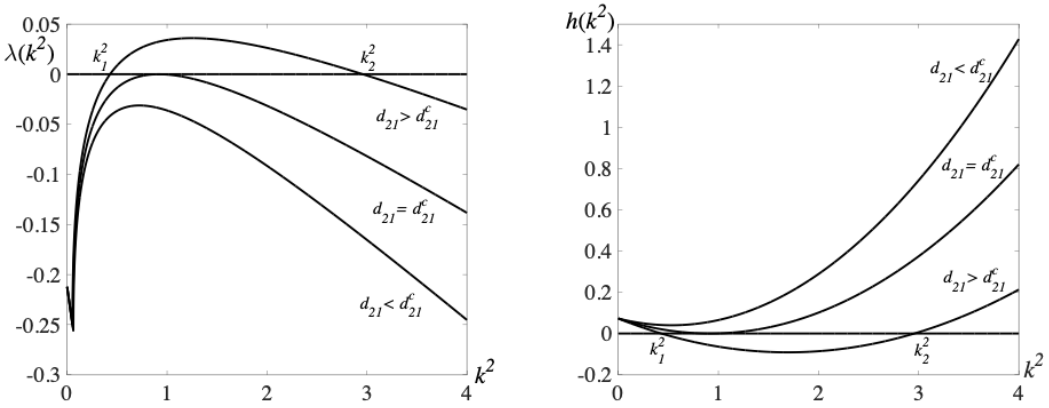

(a) (b)

FIGURE 4.6: Plots of the dispersion relations of the system (3.6) and $h(k^2)$ for various values of the bifurcation parameter in Case 1.

In Fig. 4.6, the curve in the above plot of (a) tells that real part of the eigenvalue is negative for the parametric values $\beta = 0.25$, $m = 0.8$, $\eta = 1.1$, then $\gamma = 0.7273$, $d = 0.41$, $d_{12} = 0.9$ and bifurcation parameter $d_{21} < d_{21}^c$, which shows that the homogenous steady state is stable for heterogenous pertubation. The corresponding curve tells that the real part of the eigenvalue is positive for a specific interval k^2 at which the model becomes unstable to heterogenous perturbation and produces Turing patterns when $d_{21} > d_{21}^c$. Similarly, in (b), the curve shows that $h(k^2) > 0$, which shows that a homogenous steady state is stable for heterogenous perturbation. The corresponding curve in (b) tells $h(k^2) < 0$ for a specific interval of k^2, at which the model becomes unstable to heterogenous perturbation and produces Turing patterns when $d_{21} > d_{21}^c$.

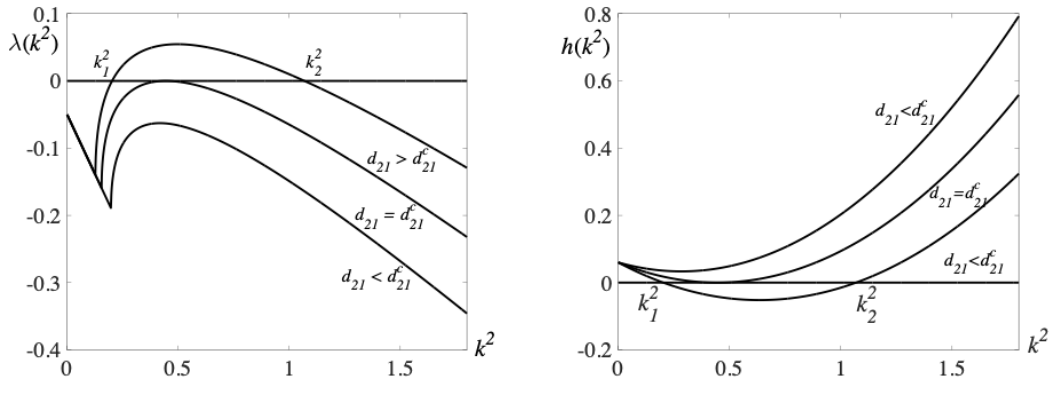

(a) (b)

FIGURE 4.7: Plots of the dispersion relations of the system (3.6) and $h(k^2)$ for various values of the bifurcation parameter in Case 2.

In Fig. 4.7, the curve in the above plot of (a) tells that real part of the eigenvalue is negative for the parametric values $\beta = 0.4$, $m = 0.2$, $\eta = 0.4$, then $\gamma = 0.5000$,

$d = 0.4095$, $d_{12} = 0.4$ and bifurcation parameter $d_{21} < d_{21}^c$, which shows that the homogenous steady state is stable for heterogenous pertubation. The corresponding curve tells that the real part of the eigenvalue is positive for a specific interval k^2 at which the model becomes unstable to heterogenous perturbation and produces Turing patterns when $d_{21} > d_{21}^c$. Similarly, in (b), the curve shows that $h(k^2) > 0$, which shows that a homogenous steady state is stable for heterogenous perturbation. The corresponding curve in (b) tells $h(k^2) < 0$ for a specific interval of k^2, at which the model becomes unstable to heterogenous perturbation and produces Turing patterns when $d_{21} > d_{21}^c$.

4.4 Numerical Simulations of Full System

In this section, we perform a numerical simulation of the reaction-diffusion system to verify stability analysis with or without cross-diffusion of the system (3.6), using the numerical scheme method of lines (MOL) in MATLAB.

Choose $m = 0.8$, $\eta = 1.1$, then $\gamma = m/\eta$, $\beta = 0.25$, $d = 0.41$, $d_{12} = 0$ and $d_{21} = 0$. The steady-state $(u^*, v^*) = (0.6667, 0.3056)$ is locally asymptotically stable, see Fig. 4.8. Choose $m = 0.8$, $\eta = 1.1$, then $\gamma = m/\eta$, $\beta = 0.25$, $d = 0.41$, $d_{12} = 9$ and $d_{21} = 1.7613 < d_{21}^c$. The steady-state $(u^*, v^*) = (0.6667, 0.3056)$ is locally asymptotically stable, see Fig. 4.9. Choose $m = 0.8$, $\eta = 1.1$, then $\gamma = m/\eta$, $\beta = 0.1579$, $d = 0.41$, $d_{12} = 0.9$ and $d_{21} = 1.6010$. The steady-state $(u^*, v^*) = (0.4211, 0.3352)$ holds Hopf bifurcation and get the periodic solution, see Fig. 4.10. Choose $m = 0.8$, $\eta = 1.1$, then $\gamma = m/\eta$, $d = 0.41$, $d_{12} = 0.9$, $d_{21} = 1.6519$ and $\beta = 0.14$, when β crosses the line of Hopf bifurcation see Fig. 4.1, then steady-state $(u^*, v^*) = (0.3733, 0.3217)$ becomes unstable and we get the asymptotic solution along time, see Fig. 4.11.

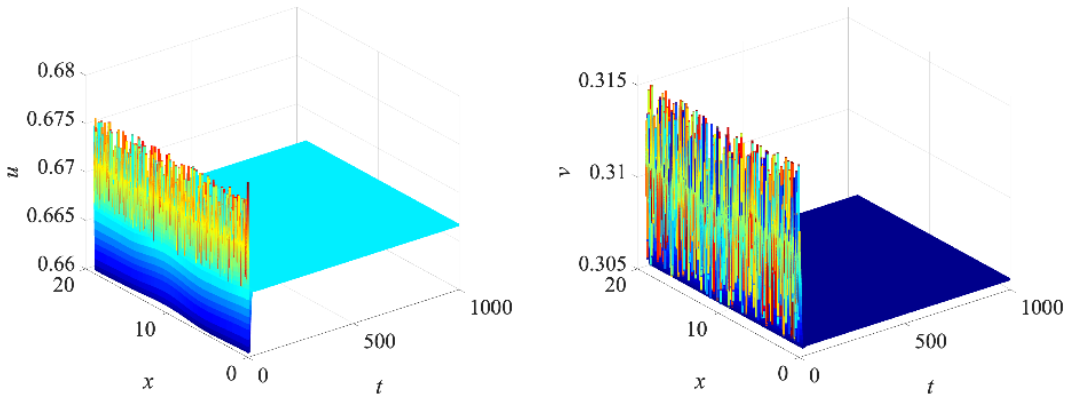

(a) (b)

FIGURE 4.8: The coexistence steady state of the system (3.6) is asymptotic stable for $m = 0.8$, $\eta = 1.1$, then $\gamma = 0.7273$, $\beta = 0.25$, $d_{12} = 0$, $d = 0.41$ and $d_{21} = 0$.

.

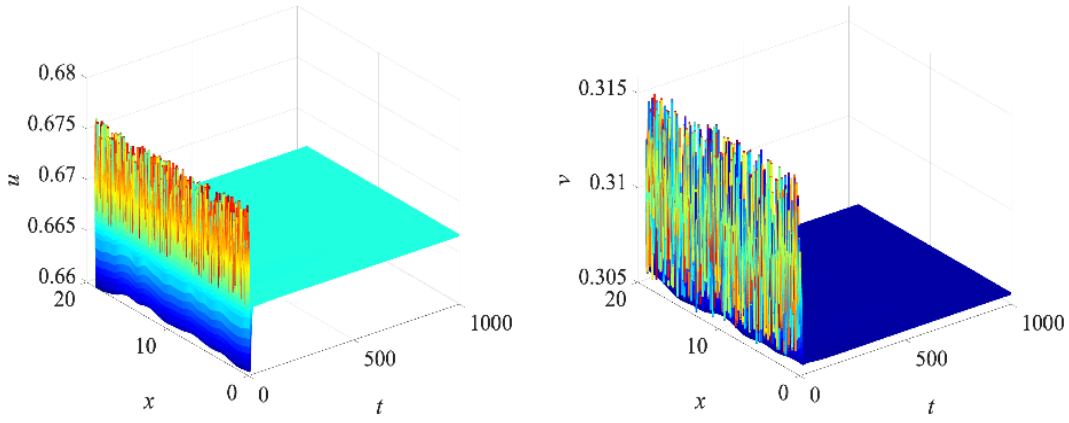

(a) (b)

FIGURE 4.9: The coexistence steady state of the system (3.6) is asymptotic stable for $m = 0.8$, $\eta = 1.1$, then $\gamma = 0.7273$, $\beta = 0.25$, $d_{12} = 0.9$, $d = 0.41$ and $d_{21} = 1.7613$.

.

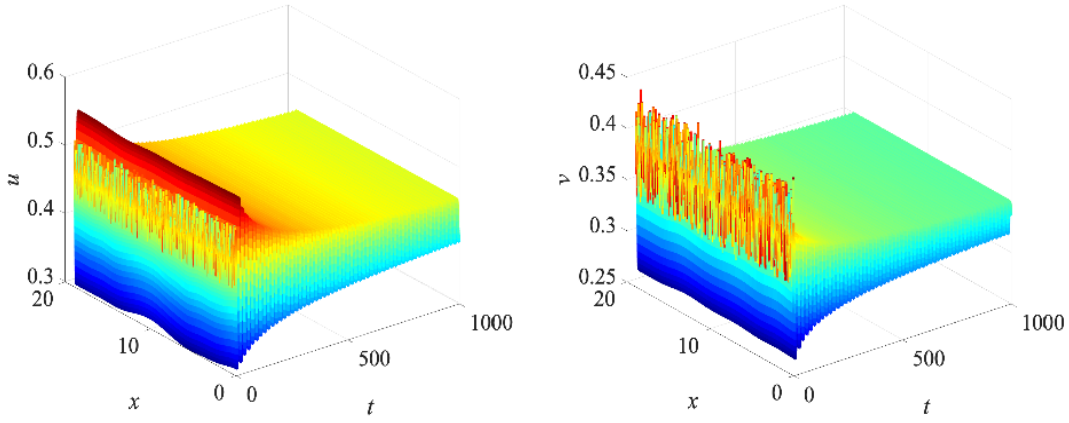

(a) (b)

FIGURE 4.10: The coexistence steady state of the system (3.6) holds Hopf bifurcation and get periodic solution for $m = 0.8$, $\eta = 1.1$, then $\gamma = 0.7273$, $\beta = 0.1579$, $d_{12} = 0.9$, $d = 0.41$ and $d_{21} = 1.6010$.

.

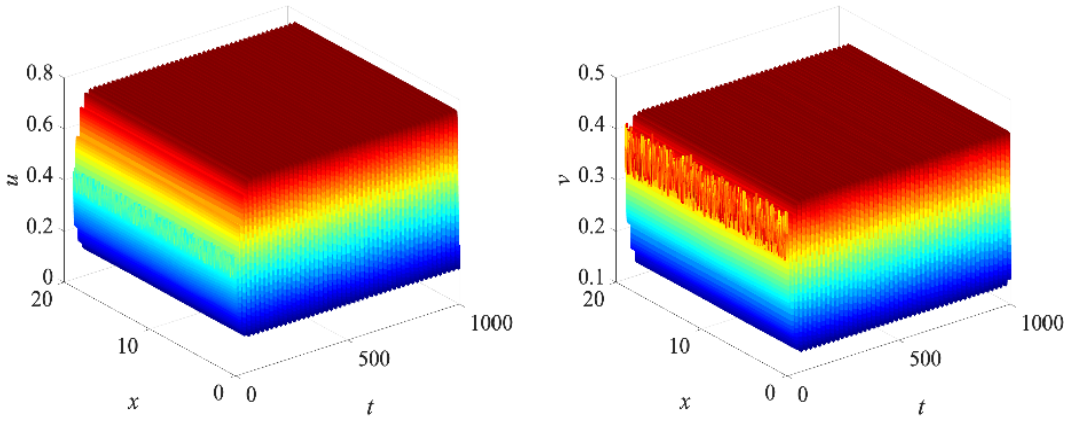

(a) (b)

FIGURE 4.11: The coexistence steady state of the system (3.6) becomes unstable and gets asymptotic solution along time for $m = 0.8, \eta = 1.1$, then $\gamma = 0.7273, \beta = 0.1400, d_{12} = 0.9, d = 0.41$ and $d_{21} = 1.6519$.

.

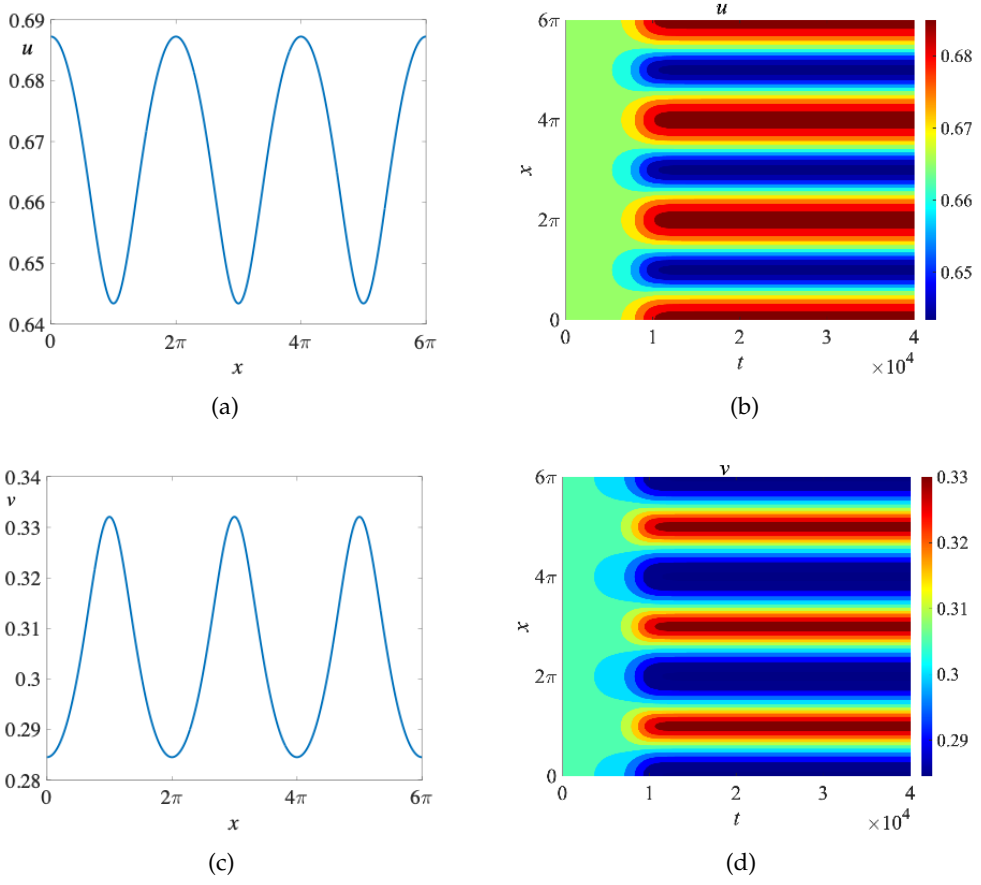

(a) (b)

(c) (d)

FIGURE 4.12: Turing pattern of the system (3.6) for $m = 0.8, \eta = 1.1$, then $\gamma = 0.7273, \beta = 0.25, d = 0.41, d_{12} = 0.9$, and $d_{21} = 1.7701 > d_{21}^c$.

Chapter 5

Amplitude and Turing Patterns Selection

This chapter delves into the weakly nonlinear analysis of Turing patterns in reaction-diffusion systems, particularly focusing on amplitude equations and pattern selection near the onset of diffusion-driven instability. By expanding the system's solution in terms of a small parameter (ϵ), which measures the distance from the critical threshold, the study explores the evolution of pattern amplitude on slow temporal scales. The analysis begins by deriving the Stuart-Landau equation, a key result that governs the amplitude of the pattern in the supercritical and subcritical regimes. The sign of the Landau coefficient (L) is crucial, as it determines whether the bifurcation is supercritical (where stable patterns emerge smoothly) or subcritical (where patterns can exhibit abrupt transitions). The chapter compares these analytical predictions with numerical simulations, demonstrating a strong agreement in the supercritical and subcritical cases (see section 5.1). Furthermore, the analysis is extended to two-dimensional systems, where the interaction of multiple modes leads to complex pattern formations (sec sections 5.2 and 5.3). The chapter concludes by emphasizing the critical role of nonlinear effects and the Fredholm solvability condition in selecting specific patterns and their stability, providing a comprehensive understanding of pattern formation mechanisms in reaction-diffusion systems.

5.1 Weakly Nonlinear Analysis

Once the conditions on the system parameters for the onset of diffusion-driven instability have been obtained, we perform a weakly nonlinear analysis to derive a reduced description of the near-critical bifurcation structure of the patterns in terms of their amplitude. Defining the control parameter as the dimensionless distance from the threshold $\epsilon = \frac{d_{21}-d_{21}^c}{d_{21}^c}$. The solution of the original system is written as a weakly nonlinear expansion in ϵ:

$$\mathbf{w} = \epsilon \mathbf{w}_1 + \epsilon^2 \mathbf{w}_2 + \epsilon^3 \mathbf{w}_3 + ..., \tag{5.1}$$

close to the bifurcation, the amplitude of the pattern evolves on a slow temporal scale; therefore, we separate the fast time t and slow time T:

$$\frac{\partial}{\partial t} = \epsilon \frac{\partial}{\partial T_1} + \epsilon^2 \frac{\partial}{\partial T_2} + \epsilon^3 \frac{\partial}{\partial T_3} + ..., \tag{5.2}$$

moreover, we expand the bifurcation parameter d_{21} as follows:

$$d_{21} = d_{21}^c + \epsilon d_{21}^1 + \epsilon^2 d_{21}^2 + ..., \tag{5.3}$$

separating the linear part from the nonlinear one, we can recast the given reaction-diffusion system for the perturbation $\mathbf{w}$= (w^u,w^v), in the following form:

$$\frac{\partial \mathbf{w}}{\partial t} = \mathcal{L}^d \mathbf{w} + \mathcal{N} + \begin{pmatrix} d_{12}(w^u \nabla^2 w^v + \nabla w^u \nabla w^v) \\ d_{21}(w^v \nabla^2 w^u + \nabla w^v \nabla w^u) \end{pmatrix}, \tag{5.4}$$

where $\mathcal{L}^d = J + D^d \nabla^2$ is a linear operator depending on the bifurcation parameter d_{21}^c and $\mathcal{N}$, which represents the nonlinear parts of the kinetics. Finally, the last term in Eq. (5.4) is the nonlinear diffusion terms.

Substituting all the above expansions into (5.4) and collecting the terms at each order in ϵ, one gets a sequence of equations for the $\mathbf{w}_i$.

$$\mathcal{O}(\epsilon) : \mathcal{L}^{d^c} \mathbf{w}_1 = 0, \tag{5.5}$$

$$\mathcal{O}(\epsilon^2) : \mathcal{L}^{d^c} \mathbf{w}_2 = \mathbf{F}, \tag{5.6}$$

$$\mathcal{O}(\epsilon^3) : \mathcal{L}^{d^c} \mathbf{w}_3 = \mathbf{G}. \tag{5.7}$$

The explicit expression of $\mathbf{F}$ and $\mathbf{G}$ is given in Appendix A. At order(ϵ), we have the linear problem $\mathcal{L}^{d^c} \mathbf{w}_1 = 0$, whose solution satisfying the Neumann boundary conditions is:

$$\mathbf{w}_1 = A(T)\mathbf{r} cos(k_c x), \tag{5.8}$$

with $\mathbf{r} \in ker(J - kc^2 D^{dc})$ where $A(T)$ is the amplitude of the pattern which is still arbitrary at this level, since $\mathcal{L}^{d^c}$ does not act on the slow scale T. The vector $\mathbf{r}$ = (r^u,r^v) is defined up to a constant and can be normalized in the following way:

$$\mathbf{r} = \begin{pmatrix} 1 \\ M \end{pmatrix}, with\ M = \frac{J_{21} - k_c^2 D_{21}^{d^c}}{D_{22}^{d^c} k_c^2 - J_{22}}, \tag{5.9}$$

where J and D^{d^c} $(i, j = 1, 2)$ are the i, j-entries of the matrices J and D^{d^c}.

The solvability condition for (A.8) gives the Stuart-Landau equation for the amplitude $A(T)$:

$$\frac{dA}{dT} = \sigma A - L A^3. \tag{5.10}$$

The coefficients σ and L are explicitly computed in terms of the system parameters and all the details can be found in Appendix A. Since the growth rate coefficient σ is always positive, the dynamics of the Stuart–Landau equation (5.10) can be divided into two qualitatively different cases depending on the sign of the Landau constant L: the supercritical case, when L is positive, and the subcritical case, when L is negative.

5.1.1 Supercritical case

The bifurcation is supercritical if the coefficients σ and L in (A.12) are positive. In this case, the stable equilibrium of the Stuart Landau equation is $A_\infty = \sqrt{\frac{\sigma}{L}}$ the asymptotic in-time behaviour of the solution is given by:

$$\mathbf{w} = \epsilon \mathbf{r} \sqrt{\frac{\sigma}{L}} \cos(k_c x) + \epsilon^2 \frac{\sigma}{L} (\mathbf{w_{20}} + \mathbf{w_{22}} cos(2k_c x)) + O(\epsilon^3) \tag{5.11}$$

where $\mathbf{r}$ is defined by (5.9) and $\mathbf{w_{2i}}, i = 0, 2$, are the solutions of the systems (A.6)-(A.7). To satisfy the Neumann boundary conditions ([24]), k_c should be an integer or semi-integer. We, therefore, define $\bar{k_c}$ as the first integer or semi-integer to become unstable as d_{21} crosses its critical value d_{21}^c and take as the weakly nonlinear approximation equation (5.11) in which k_c is replaced by $\bar{k_c}$.

In Figs. 5.1-5.2(c-d), we show the comparison between the stationary state predicted by weakly nonlinear analysis (solid line) and the stationary state reached from a random pertubation of the homogenous equilibrium $(u^*; v^*)$, computed by solving numerically system (3.6) (dotted line). Notice that in the weakly nonlinear solution, we have chosen $d_{21}^2 = d_{21}^c$ so that we measure the deviation from the critical value with d_{21}^c. Numerical results are in perfect agreement with what the weakly nonlinear analysis predicts. Thus, in this case, $(\sigma, L > 0)$ weakly nonlinear analysis can predict the instability's stationary nature, which leads to pattern and form and the pattern's amplitude.

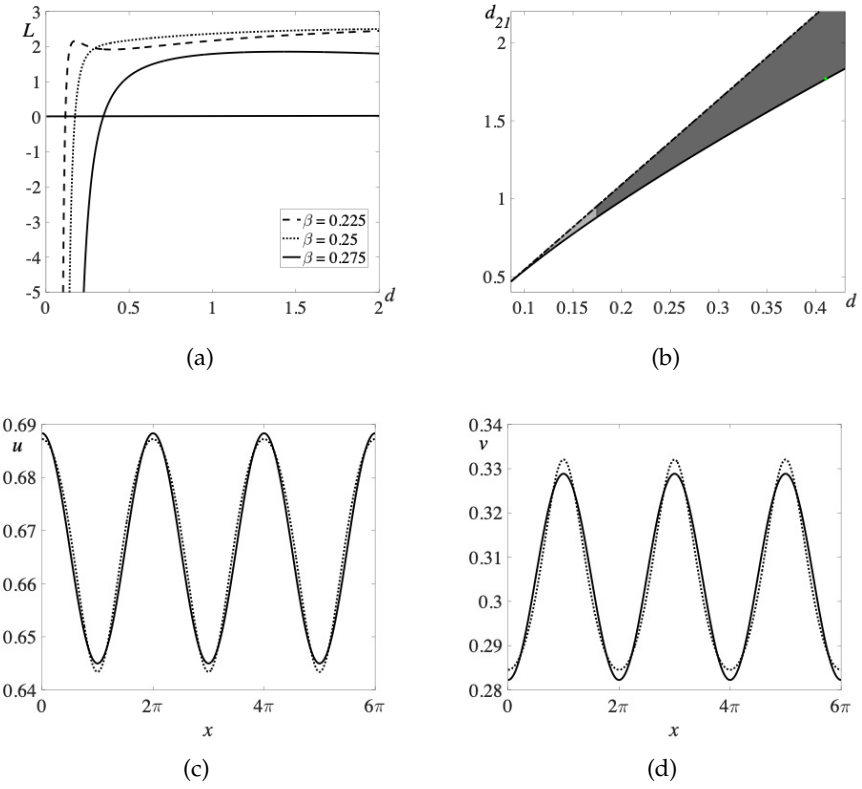

FIGURE 5.1: The Sign of Landau constant, bifurcation diagram, and Turing patterns in supercritical bifurcation for case 1.

In Fig. 5.1, (a) Shows the effect of β on the sign of Landau constant L as defined in (A.12). (b) Depicts the area between $d_{21} = d_{21}^c$ (solid line) and $d_{21} = \frac{d}{d_{12}u^*v^*}$ (dashed-dotted line) in the (d, d_{21}) plane, which is the region where Turing instability exists. In this region, subcritical bifurcation exists in the grey region and supercritical bifurcation in the dark grey region. (c-d) Compare the WNL approximated solution (solid line) and numerical solution of the original system (3.6) (dotted line). The chosen parameters are $\beta = 0.25$, $\eta = 1.1$, $m = 0.8$, $\gamma = 0.7273$, $d_{12} = 0.9$, and $d = 0.41$.

With these parameters, $d_{21} = d_{21}^c(1+\epsilon^2)$ and $\epsilon = 0.05$, resulting in $d_{21}^c = 1.7657$, while $\bar{k_c} \approx 1.0$. The corresponding point is marked by a plus sign in (b).

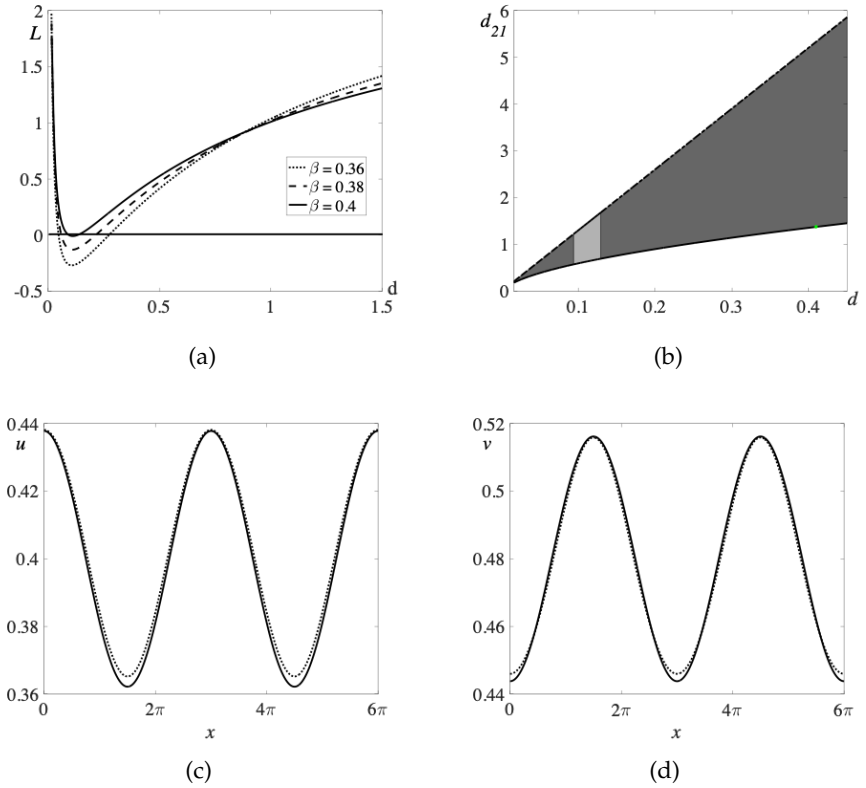

FIGURE 5.2: The Sign of Landau constant, bifurcation diagram, and Turing patterns in supercritical bifurcation for case 2.

In Fig. 5.2, (a) Shows the effect of β on the sign of Landau constant L as defined in (A.12). (b) Depicts the area between $d_{21} = d_{21}^c$ (solid line) and $d_{21} = \frac{d}{d_{12}u^*v^*}$ (dashed-dotted line) in the (d, d_{21}) plane, which is the region where Turing instability exists. In this region, subcritical bifurcation exists in the grey region and supercritical bifurcation in the dark grey region. (c-d) Compare the WNL approximated solution (solid line) and numerical solution of the original system (3.6) (dotted line). The chosen parameters are $\beta = 0.4$, $\eta = 0.4$, $m = 0.2$, $\gamma = 0.5000$, $d_{12} = 0.4$, and $d = 0.4095$. With these parameters, $d_{21} = d_{21}^c(1+\epsilon^2)$ and $\epsilon = 0.05$, resulting in $d_{21}^c = 1.3758$, while $\bar{k_c} \approx 0.67$. The corresponding point is marked by a plus sign in (b).

5.1.2 Subcritical case

When L is negative, the bifurcation is subcritical: in this case the weakly nonlinear expansion has to be pushed up to the fifth order. We therefore introduce the multiple time scales T and $T1$ as follows:

$$\frac{\partial}{\partial t} = \epsilon^2 \frac{\partial}{\partial T} + \epsilon^4 \frac{\partial}{\partial T_1} + ..., \tag{5.12}$$

and the following expansion of the bifurcation parameter:

$$d_{21} = d_{21}^c + \epsilon^2 d_{21}^1 + \epsilon^4 d_{21}^2 + \mathcal{O}(\epsilon^5). \tag{5.13}$$

Performing the weakly nonlinear analysis up to order (ϵ^5), one obtains the following quintic Stuart–Landau equation for the amplitude A:

$$\frac{\partial A}{\partial T} = \bar{\sigma}A - \bar{L}A^3 + \bar{Q}A^5, \tag{5.14}$$

where, $\bar{\sigma} = \sigma + \epsilon^2\tilde{\sigma}, \bar{L} = L + \epsilon^2\tilde{L}, \bar{Q} = \epsilon^2\tilde{Q}$.

The details of the analysis and the explicit expression of the coefficients appearing in (5.14) are given in Appendix B.

We compare the numerical solution of the system (3.6) with the weakly nonlinear approximation in Figs. 5.3-5.4(b-c). The dotted line represents the numerical solution, while the solid line depicts the weakly nonlinear approximation.

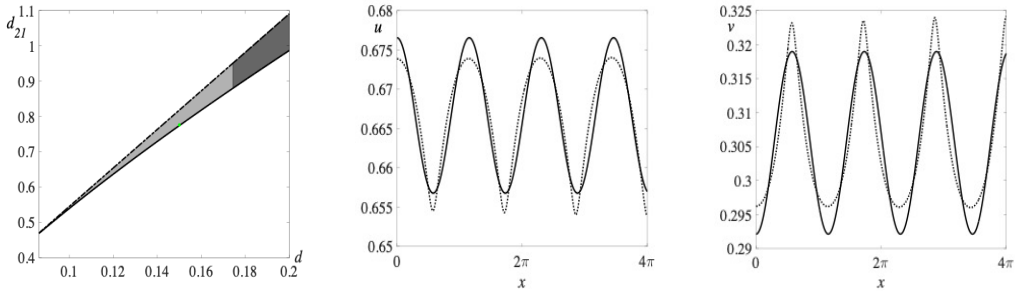

(a) (b) (c)

FIGURE 5.3: Bifurcation diagram, and Turing patterns in subcritical bifurcation for case 1.

In Fig. 5.3, (a) Depicts the area between $d_{21} = d_{21}^c$ (solid line) and $d_{21} = \frac{d}{d_{12}u^*v^*}$ (dashed-dotted line) in the (d, d_{21}) plane, which is the region where Turing instability exists. In this region, subcritical bifurcation exists in the grey region and supercritical bifurcation in the dark region. (b-c) Compare the WNL approximated solution (solid line) and numerical solution of the full system (3.6) (dotted line). The parameters chosen here are $\beta = 0.25$, $\eta = 1.1$, $m = 0.8$, $\gamma = 0.7273$, $d_{12} = 0.9$, $d = 0.15$, $\epsilon = 0.05$, $d_{21}^c = 0.7742$ and $\bar{k_c} \approx 1.73$. The corresponding point is marked by an asterisk sign in (a).

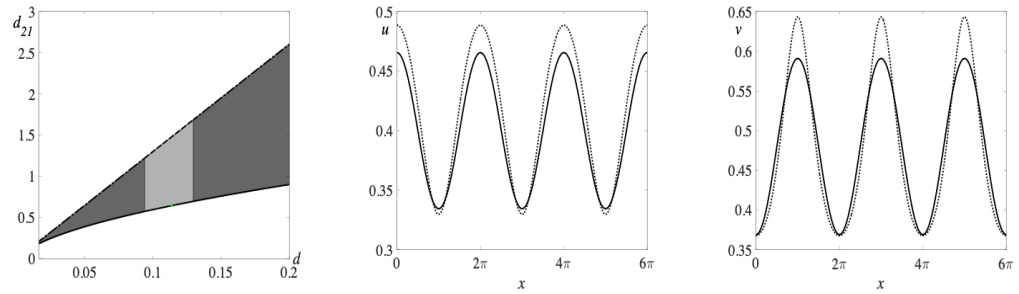

(a) (b) (c)

FIGURE 5.4: bifurcation diagram, and Turing patterns in subcritical bifurcation for case 2.

In Fig. 5.4, (a) depicts the area between $d_{21} = d_{21}^c$ (solid line) and $d_{21} = \frac{d}{d_{12}u^*v^*}$ (dashed-dotted line) in the (d, d_{21}) plane, which is the region where Turing instability exists. In this region, subcritical bifurcation exists in the grey region and supercritical bifurcation in the dark region. (b-c) Compare the WNL approximated solution (solid line) and numerical solution of the full system (3.6) (dotted line). The parameters chosen here are $\beta = 0.4$, $\eta = 0.4$, $m = 0.2$, $\gamma = 0.5000$, $d_{12} = 0.4$, $d = 0.1136$, $\epsilon = 0.1$, $d_{21}^c = 0.6442$ and $\bar{k_c} \approx 1.0$. The corresponding point is marked by an asterisk sign in (a).

5.2 Patterns Selection in 2D

In view of Fredholm solvability conditions, solving the Eq. (5.5) corresponding to the first order of ϵ yields

$$\begin{pmatrix} u_1 \\ v_1 \end{pmatrix} = \begin{pmatrix} \varphi \\ 1 \end{pmatrix} \left(\sum_{j=1}^{3} W_j \exp\left(\mathbf{i}\mathbf{k}_j \cdot \mathbf{q}\right) + \text{ c.c.} \right). \tag{5.15}$$

In the given expression, where $\varphi = \frac{J_{12} - k_c^2 D_{12}^{d^c}}{k_c^2 - J_{11}}$, and $|\mathbf{k}_j| = k_c$, with W_j representing the amplitude of the mode $e^{i\mathbf{k}_j \cdot \mathbf{q}}$ (where $j = 1, 2, 3$) under the first-order perturbation. Here, $\mathbf{q} = (x, y)$ is a spatial vector in two-dimensional space, and c.c. denotes the conjugate of the former terms. For the second order of ϵ as in Eq. (5.6), in order to ensure the existence of nontrivial solutions of the equation, the Fredholm solvability condition requires that the vector function of the right-hand side of this equation should be orthogonal to the zero eigenvectors of the operator $(\mathcal{L}^{d^c})^\dagger$, where $(\mathcal{L}^{d^c})^\dagger$ is the adjoint operator of the operator $\mathcal{L}^{d^c}$. In this context, the zero eigenvector of $(\mathcal{L}^{d^c})^\dagger$ is

$$\begin{pmatrix} 1 \\ \psi \end{pmatrix} \exp\left(-\mathrm{i}\mathrm{k}_j \cdot \mathbf{r}\right) + c.c., \quad j = 1, 2, 3 \tag{5.16}$$

where $\psi = \frac{J_{11} - k_c^2}{d_{21}^c v^* k_c^2 - J_{21}}$. Then, according to the orthogonality condition, this implies that

$$(1, \psi) \begin{pmatrix} F_u^j \\ F_v^j \end{pmatrix} = 0, \quad j = 1, 2, 3 \tag{5.17}$$

where F_u^j and F_v^j represent the coefficients corresponding to $\exp\left(\mathrm{i}\mathrm{k}_j \cdot \mathbf{q}\right)$ in F_u and F_v. Fredholm solvability condition for second and third order ϵ can be explained in Appendix C.

Finally,the amplitudes $A_j (j = 1, 2, 3)$ from 5.2,can be expanded as

$$\frac{\partial A_j}{\partial t} = \epsilon \frac{\partial A_j}{\partial T_1} + \epsilon^2 \frac{\partial A_j}{\partial T_2} + \cdots, \tag{5.18}$$

and on the other hand the amplitude A_j can be expressed as the coefficient of the term $e^{\mathbf{i}\mathbf{k}_j \cdot \mathbf{q}}$ in each order of ϵ :

$$\begin{pmatrix} A_j^u \\ A_j^v \end{pmatrix} = \epsilon \begin{pmatrix} \varphi \\ 1 \end{pmatrix} W_j + \epsilon^2 \begin{pmatrix} \varphi \\ 1 \end{pmatrix} V_j + \cdots,$$

setting

$$A_j = A_j^u = \epsilon\varphi W_j + \epsilon^2\varphi V_j + O\left(\epsilon^3\right). \tag{5.19}$$

Then together with (5.3), (C.1), (C.3), (5.18), and (5.19) we thus obtain the amplitude equations corresponding to A_1, A_2, A_3 as follows:

$$\begin{cases} \tau_0\frac{\partial A_1}{\partial t} = \mu A_1 + h_0\bar{A}_2\bar{A}_3 - \left[g_1\left|A_1\right|^2 + g_2\left(\left|A_2\right|^2 + \left|A_3\right|^2\right)\right]A_1, \\ \tau_0\frac{\partial A_2}{\partial t} = \mu A_2 + h_0\bar{A}_1\bar{A}_3 - \left[g_1\left|A_2\right|^2 + g_2\left(\left|A_1\right|^2 + \left|A_3\right|^2\right)\right]A_2, \\ \tau_0\frac{\partial A_3}{\partial t} = \mu A_3 + h_0\bar{A}_1\bar{A}_2 - \left[g_1\left|A_3\right|^2 + g_2\left(\left|A_1\right|^2 + \left|A_2\right|^2\right)\right]A_3, \end{cases} \tag{5.20}$$

where

$$\tau_0 = -\frac{\varphi+\psi}{d_{21}^c k_c^2 v^*\varphi\psi}, \quad \mu = \frac{d_{21}-d_{21}^c}{d_{21}^c}, \quad g_1 = -\frac{G_1}{d_{21}^c v^*\psi k_c^2\varphi^3}, \quad g_2 = -\frac{G_2}{d_{21}^c v^*\psi k_c^2\varphi^3},$$

$$h_0 = \frac{4(d_{21}-d_{21}^c)}{d_{21}^c v^*\varphi} + \frac{2\varphi^2 + 2(1-\eta\psi)\left(\frac{(1-\gamma)^2}{\beta}(\varphi - 2\varphi^2(1-\frac{\gamma\beta}{1-\gamma}))\right) + 4\varphi k_c^2(d_{12}+\psi d_{21}^c)}{d_{21}^c k_c^2 v^*\psi\varphi^2}.$$

5.2.1 Amplitude instability

In Eq. (5.20), each amplitude A_j can be decomposed as the following form

$$A_j = \rho_j \exp\left(\mathrm{i}\theta_j\right), j = 1,2,3, \tag{5.21}$$

where ρ_j represents mode and θ_j represents the corresponding phase angle. Substituting (5.21) into (5.20) and separating the real part and imaginary part yields

$$\begin{cases} \tau_0\frac{\partial\theta}{\partial t} = -h_0\frac{\rho_1^2\rho_2^2+\rho_1^2\rho_3^2+\rho_2^2\rho_3^2}{\rho_1\rho_2\rho_3}\sin\theta, \\ \tau_0\frac{\partial\rho_1}{\partial t} = \mu\rho_1 + h_0\rho_2\rho_3\cos\theta - g_1\rho_1^3 - g_2\left(\rho_2^2+\rho_3^2\right)\rho_1, \\ \tau_0\frac{\partial\rho_2}{\partial t} = \mu\rho_2 + h_0\rho_1\rho_3\cos\theta - g_1\rho_2^3 - g_2\left(\rho_1^2+\rho_3^2\right)\rho_2, \\ \tau_0\frac{\partial\rho_3}{\partial t} = \mu\rho_3 + h_0\rho_1\rho_2\cos\theta - g_1\rho_3^3 - g_2\left(\rho_1^2+\rho_2^2\right)\rho_3, \end{cases} \tag{5.22}$$

where $\theta = \theta_1+\theta_2+\theta_3$, consider the equation

$$(C_1): \tau_0\frac{\partial\theta}{\partial t} = -h_0\frac{\rho_1^2\rho_2^2+\rho_1^2\rho_3^2+\rho_2^2\rho_3^2}{\rho_1\rho_2\rho_3}\sin\theta.$$

In this context, when the system (5.22) reaches a steady-state solution, the phase of its amplitude depends solely on $\theta = 0$ and $\theta = \pi$. Assuming $\rho_j \geq 0$, if $h_0 < 0$ and $\theta = \pi$, then the solution of (C_1) is stable. Conversely, if $\theta = 0$, the solution is unstable. Here, only the stable solution of (C_1) is of interest, and its corresponding mode of equation is given by:

$$\begin{cases} \tau_0\frac{\partial\rho_1}{\partial t} = \mu\rho_1 + h_0\rho_2\rho_3\cos\theta - g_1\rho_1^3 - g_2\left(\rho_2^2+\rho_3^2\right)\rho_1, \\ \tau_0\frac{\partial\rho_2}{\partial t} = \mu\rho_2 + h_0\rho_1\rho_3\cos\theta - g_1\rho_2^3 - g_2\left(\rho_1^2+\rho_3^2\right)\rho_2, \\ \tau_0\frac{\partial\rho_3}{\partial t} = \mu\rho_3 + h_0\rho_1\rho_2\cos\theta - g_1\rho_3^3 - g_2\left(\rho_1^2+\rho_2^2\right)\rho_3, \end{cases} \tag{5.23}$$

System (5.23) has four solutions, and we will analyze their stability using linear stability analysis. To determine the stability of these four solutions, we introduce a

perturbation $(\epsilon\rho_1, \epsilon\rho_2, \epsilon\rho_3)$ to the variables (ρ_1, ρ_2, ρ_3) in system (3.19). By neglecting higher-order terms, we derive a linear perturbation system as follows:

$$\tau_0 \frac{\partial}{\partial t} \begin{pmatrix} \epsilon\rho_1 \\ \epsilon\rho_2 \\ \epsilon\rho_3 \end{pmatrix} = \begin{pmatrix} m_{11} & m_{12} & m_{13} \\ m_{21} & m_{22} & m_{23} \\ m_{31} & m_{32} & m_{33} \end{pmatrix} \begin{pmatrix} \epsilon\rho_1 \\ \epsilon\rho_2 \\ \epsilon\rho_3 \end{pmatrix} \tag{5.24}$$

where

$$m_{11} = \mu - 3g_1\rho_1^2 - g_2\left(\rho_2^2 + \rho_3^2\right), \quad m_{12} = |h_0|\rho_3 - 2g_2\rho_1\rho_2, \quad m_{13} = |h_0|\rho_2 - 2g_2\rho_3\rho_1,$$
$$m_{21} = |h_0|\rho_3 - 2g_2\rho_1\rho_2, \quad m_{22} = \mu - 3g_1\rho_2^2 - g_2\left(\rho_3^2 + \rho_1^2\right), \quad m_{23} = |h_0|\rho_1 - 2g_2\rho_2\rho_3,$$
$$m_{31} = |h_0|\rho_2 - 2g_2\rho_3\rho_1, \quad m_{32} = |h_0|\rho_1 - 2g_2\rho_2\rho_3, \quad m_{33} = \mu - 3g_1\rho_3^2 - g_2\left(\rho_1^2 + \rho_2^2\right).$$

Through the standard stability analysis of the system (5.23), we find that the system has four solutions.
One of them is a uniform steady-state solution $(\mathbf{O}) : \rho_1 = \rho_2 = \rho_3 = 0$.
By substituting $(0, 0, 0)$ into the perturbation equation (5.24), we obtain the characteristic equation $(\lambda - \eta)^3 = 0$, which gives the eigenvalue $\lambda = \eta$. This solution is stable when $\mu < \mu_2 = 0$ and unstable when $\mu > \mu_2 = 0$.
Another solution is a strip pattern solution $(\mathbf{S}) : \rho_1 = \sqrt{\frac{\mu}{g_1}} \neq 0, \rho_2 = \rho_3 = 0$, which exists under the condition $\mu > \mu_2 = 0$.
Substituting $(\rho_1, 0, 0)$ into the perturbation equation (5.24), we obtain:

$$\tau_0 \frac{\partial}{\partial t} \begin{pmatrix} \epsilon\rho_1 \\ \epsilon\rho_2 \\ \epsilon\rho_3 \end{pmatrix} = \begin{pmatrix} \mu - 3g_1\rho_1^2 & 0 & 0 \\ 0 & \mu - g_2\rho_1^2 & |h_0|\rho_1 \\ 0 & |h_0|\rho_1 & \mu - g_2\rho_1^2 \end{pmatrix} \begin{pmatrix} \epsilon\rho_1 \\ \epsilon\rho_2 \\ \epsilon\rho_3 \end{pmatrix} \tag{5.25}$$

The corresponding characteristic equation is given by:

$$(\lambda + 2\mu)\left[\left(\lambda - \mu + \frac{g_2}{g_1}\mu\right)^2 - \frac{h_0^2}{g_1}\mu\right] = 0.$$

The corresponding eigenvalues are $\lambda_1 = -2\mu$ and $\lambda_{2,3} = \mu\left(1 - \frac{g_2}{g_1}\right) \pm |h_0|\sqrt{\frac{\mu}{g_1}}$. Assume that $\mu > 0$ and $\frac{g_2}{g_1} > 1$. If $\mu > \mu_3 = \frac{h_0^2 g_1}{(g_2 - g_1)^2}$, then the eigenvalues are negative, indicating that the strip solution is stable, and system (5.23) exhibits the strip solution. Conversely, if $\mu < \mu_3 = \frac{h_0^2 g_1}{(g_2 - g_1)^2}$, the strip solution becomes unstable, meaning that system (5.23) does not exhibit the strip solution.

Two hexagonal configurations, $(\mathbf{H}_0, \mathbf{H}_\pi)$, are given by: $\rho_1 = \rho_2 = \rho_3 = \rho_\pm^* = \frac{|h_0| \pm \sqrt{h_0^2 + 4(g_1 + 2g_2)\mu}}{2(g_1 + 2g_2)}$. The condition for the existence of this solution is $\mu > \mu_1 = -\frac{h_0^2}{4(g_1 + 2g_2)}$.
By substituting (ρ_1, ρ_2, ρ_3) into the perturbation equation (5.24), we obtain:

$$\tau_0 \frac{\partial}{\partial t} \begin{pmatrix} \epsilon\rho_1 \\ \epsilon\rho_2 \\ \epsilon\rho_3 \end{pmatrix} = \begin{pmatrix} H_1 & H_2 & H_2 \\ H_2 & H_1 & H_2 \\ H_2 & H_2 & H_1 \end{pmatrix} \begin{pmatrix} \epsilon\rho_1 \\ \epsilon\rho_2 \\ \epsilon\rho_3 \end{pmatrix} \tag{5.26}$$

where $H_1 = \mu - (3g_1 + 2g_2)\rho^2$ and $H_2 = |h_0|\rho - 2g_2\rho^2$. The characteristic equation for this system is:

$$(H_1-\lambda)^3-3H_2^2(H_1-\lambda)+2H_2^3=0$$

which gives the corresponding eigenvalues as $\lambda_{1,2}=H_1-H_2$ and $\lambda_3=2H_2+H_1$. If

$$\rho_-^*=\frac{|h_0|-\sqrt{h_0^2+4(g_1+2g_2)\mu}}{2(g_1+2g_2)}$$

then $\lambda_3>0$, indicating that the hexagonal solution is unstable, and the system will not display a hexagonal solution. On the other hand, if

$$\rho_+^*=\frac{|h_0|+\sqrt{h_0^2+4(g_1+2g_2)\eta}}{2(g_1+2g_2)},\quad\text{and}\quad\mu<\mu_4=\frac{(2g_1+g_2)h_0^2}{(g_2-g_1)^2}$$

then all eigenvalues are negative, implying that the hexagonal solution is stable and the system will have a hexagonal configuration.

For a mixed structure solution (**MS**), where $\rho_1=\frac{|h_0|}{g_2-g_1},\rho_2=\rho_3=\sqrt{\frac{\mu-g_1\rho_1^2}{g_1+g_2}}$, the solution exists under the conditions $\mu>\mu_3$ and $g_2>g_1$.

By substituting (ρ_1,ρ_2,ρ_3) into the perturbation equation (5.24), we obtain:

$$\tau_0\frac{\partial}{\partial t}\begin{pmatrix}\epsilon\rho_1\\ \epsilon\rho_2\\ \epsilon\rho_3\end{pmatrix}=\begin{pmatrix}H_3 & H_5 & H_5\\ H_5 & H_4 & H_6\\ H_5 & H_6 & H_4\end{pmatrix}\begin{pmatrix}\epsilon\rho_1\\ \epsilon\rho_2\\ \epsilon\rho_3\end{pmatrix}\tag{3.23}$$

where

$$H_3=\mu-3g_1\rho_1^2-g_2(\rho_2^2+\rho_3^2),\quad H_4=\eta-3g_1\rho_2^2-g_2(\rho_1^2+\rho_2^2),$$
$$H_5=|h_0|\rho_2-2g_2\rho_1\rho_2,\quad H_6=|h_0|\rho_1-2g_2\rho_2^2.$$

The characteristic equation is:

$$\left[\lambda^2-(H_3+H_4+H_6)\lambda+H_3(H_4+H_6)-2H_5^2\right](\lambda-H_4+H_6)=0$$

The eigenvalues satisfy:

$$\lambda_1=H_4-H_6,\quad\lambda_2+\lambda_3=H_3+H_4+H_6,\quad\lambda_2\lambda_3=H_3(H_4+H_6)-2H_5^2.$$

For all eigenvalues to be negative, the following conditions must be met:

$$\text{(a) }\lambda_1<0,\quad\text{(b) }\lambda_2+\lambda_3<0,\quad\text{(c) }\lambda_2\lambda_3>0.$$

For $\lambda_1<0$, we have:

$$\mu<\frac{(2g_1+g_2)h_0^2}{(g_1-g_2)^2}$$

and for $\lambda_2\lambda_3>0$, we require:

$$\mu>\frac{(2g_1+g_2)h_0^2}{(g_1-g_2)^2}.$$

These two conditions are contradictory, indicating that the mixed structure solution is unstable, and thus, the system (5.23) will not be stable.

From the above analysis, we conclude that $\mu_1 < \mu_2 = 0 < \mu_3 < \mu_4$, leading to the following conclusions.

Theorem 2 *: Stability Analysis of Amplitude Equations*
Assume that $g_1 > 0$ and $g_2 > 0$. The original reaction-diffusion system exhibits different types of patterns if the steady-state solution of the system (5.22) satisfies the following conditions:

1. *The homogeneous stationary state $(\mathbf{O})$ is defined by:*

$$\rho_1 = \rho_2 = \rho_3 = 0.$$

This state $(\mathbf{O})$ is stable when $\mu < \mu_2 = 0$, and becomes unstable when $\mu > \mu_2 = 0$.

2. *The strip pattern formation $(\mathbf{S})$ occurs if:*

$$\rho_1 = \sqrt{\frac{\mu}{g_1}} \neq 0, \quad \rho_2 = \rho_3 = 0, \quad with \quad \mu > \mu_2 = 0.$$

This strip pattern $(\mathbf{S})$ is stable when $\mu > \mu_3 = \frac{h_0^2 g_1}{(g_2 - g_1)^2}$, and unstable when $\mu < \mu_3$.

3. *The two hexagonal patterns $(\mathbf{H}_0, \mathbf{H}_\pi)$ are given by:*

$$\rho_1 = \rho_2 = \rho_3 = \rho_\pm^* = \frac{|h_0| \pm \sqrt{h_0^2 + 4(g_1 + 2g_2)\mu}}{2(g_1 + 2g_2)},$$

with $\theta = 0$ or $\theta = \pi$. These patterns exist when $\mu > \mu_1 = -\frac{h_0^2}{4(g_1+2g_2)}$. The solution $\rho_+^* = \frac{|h_0|+\sqrt{h_0^2+4(g_1+2g_2)\mu}}{2(g_1+2g_2)}$ is stable when $\mu < \mu_4 = \frac{(2g_1+g_2)h_0^2}{(g_2-g_1)^2}$. However, the solution $\rho_-^* = \frac{|h_0|-\sqrt{h_0^2+4(g_1+2g_2)\mu}}{2(g_1+2g_2)}$ is always unstable.

4. *The mixed structure state (MS) is defined by:*

$$\rho_1 = \frac{|h_0|}{g_2 - g_1}, \quad \rho_2 = \rho_3 = \sqrt{\frac{\mu - g_1\rho_1^2}{g_1 + g_2}},$$

which exists under the conditions $\mu > \mu_3$ and $g_2 > g_1$. However, this solution is always unstable.

Theorem 3 *In the range where Turing patterns are generated, the parameters $\eta, \beta, m, \gamma, d, d_{12}$, and d_{21} are considered variables. The behaviour of the system (3.6) can be described as follows:*

1. *When $\mu_2 < \mu < \mu_3$, the system exhibits a spot pattern.*
2. *When $\mu_3 < \mu < \mu_4$, the system can display either a spot pattern or a stripe pattern, depending on the initial conditions.*
3. *When $\mu > \mu_4$, the spot pattern in the system transitions to a stripe pattern.*

In Fig. 5.5, we change the value of bifurcation parameter d_{21} and fix the other parameters in system (3.6), then we can calculate the values of h_0, μ, μ_1, μ_3, μ_4 and know that $\mu_1 < \mu_2 < \mu_3 < \mu_4$, according to theorem (2). The bifurcation diagram

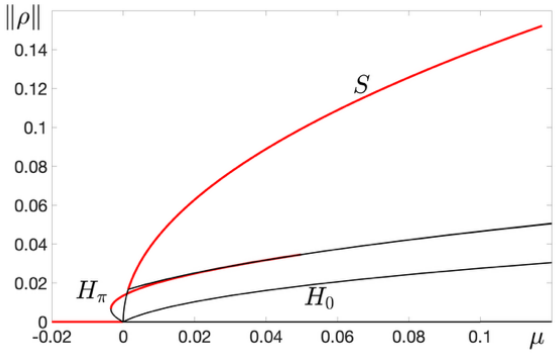

FIGURE 5.5: In the bifurcation diagram of amplitude equations' solutions, the red lines represent stable solutions, while the black lines signify unstable ones. In this context, the symbol H_0 denotes the hexagonal state with $\theta = 0$, H_π represents the hexagonal state with $\theta = \pi$, and S is indicative of stripe patterns.

illustrates how the mode of ρ changes with μ. Here we fix parameters $m = 0.8$, $\eta = 1.5$, $\beta = 0.35$, $\gamma = m/\eta$, $d = 1.6$, $d_{12} = 0.9$. Then we get the critical value of Turing bifurcation is $d_{21}^c = 4.7556$. Choosing the control parameter value $d_{21} = 4.8032 > d_{21}^c$,we get $h_0 = -1.8960$, $g_1 = 5.0648$, $g_2 = 114.7297$, $\mu = 0.0100$, $\mu_1 = -0.0038$, $\mu_2 = 0$, $\mu_3 = 0.0015$ and $\mu_4 = 0.0373$.

5.3 Numerical Simulations in 2D

In this section, we conducted numerical simulations of the original system (3.6). We used the same set of parameters to generate a bifurcation diagram see Fig. 5.5. For that set of parameters, the coexisting steady state is $(0.4000, 0.4500)$. We determined the following values: $h_0 = -1.8960$, $g_1 = 5.0648$, $g_2 = 114.7297$, $\mu = 0.0100$, $\mu_1 = -0.0038$, $\mu_2 = 0$, $\mu_3 = 0.0015$, and $\mu_4 = 0.0373$. It's important to note that for this set of parameters, $h_0 < 0$ and $g_1 < g_2$. Therefore, since $h_0 < 0$, H_0 is always unstable for this set of parameters. Additionally, as $\mu \in (\mu_3, \mu_4)$, both hexagonal and strip patterns are stable.

In the numerical experiment shown in Fig. 5.6, we pick the parameters in such a way that in the rectangular domain with $L_x = 8\pi$ and $L_y = 8\sqrt{3}\pi$, the only admitted unstable mode is $\bar{k}_c \approx 0.75$. For the chosen set of parameters, the bifurcation diagram in Fig. 5.5 shows a bi-stability regime of hexagonal and roll patterns, which will appear strictly depending on the initial data. Performing three thousand simulations, starting from different randomly chosen initial conditions, we have found that the shape of the pattern is a hexagon shown in Fig. 5.6; furthermore, performing five thousand simulations and obtained rolls as shown in Fig. 5.7. In Fig. 5.8, we selected parameters such that $\mu \in (\mu_4, \infty)$, where only strip patterns are stable. For the numerical simulation, we used the same rectangular domain that we used for the numerical experiments in the bi-stability region shown in Figs. 5.6-5.7. Performing ten thousand simulations, we obtained roll patterns as shown in Fig. 5.8.

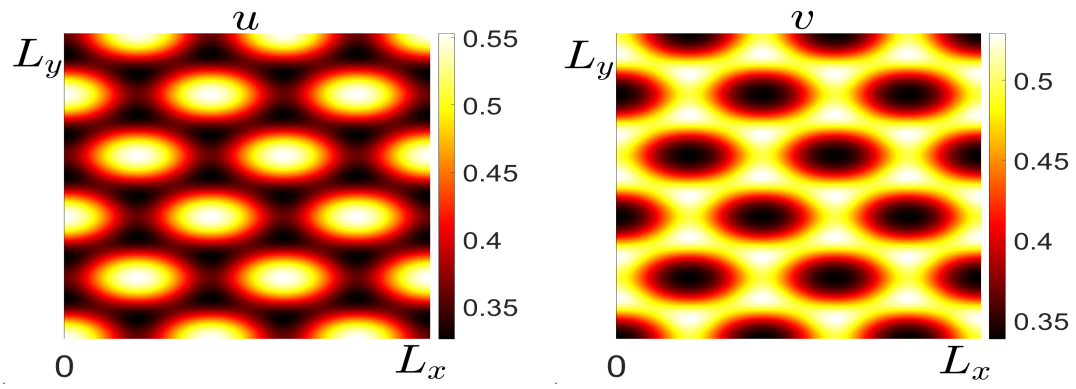

(a) (b)

FIGURE 5.6: Hexagonal patterns, the numerical solution u and v of the original system (3.6).

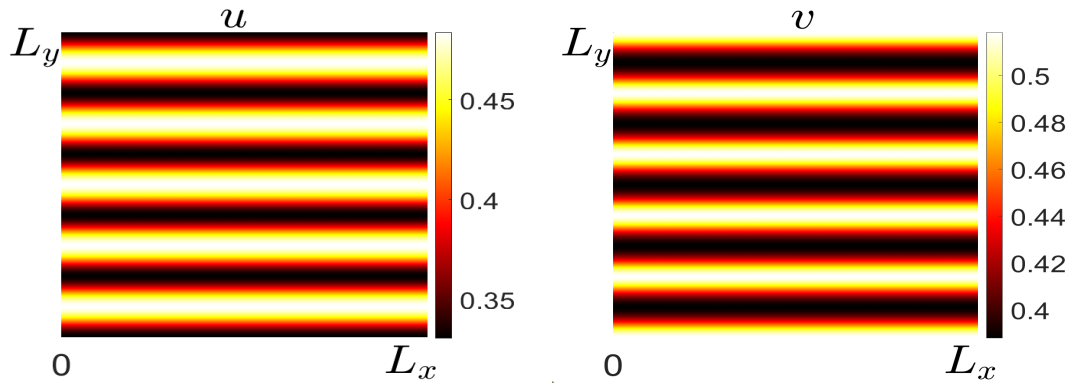

(a) (b)

FIGURE 5.7: Roll patterns, the numerical solution u and v of the original system (3.6).

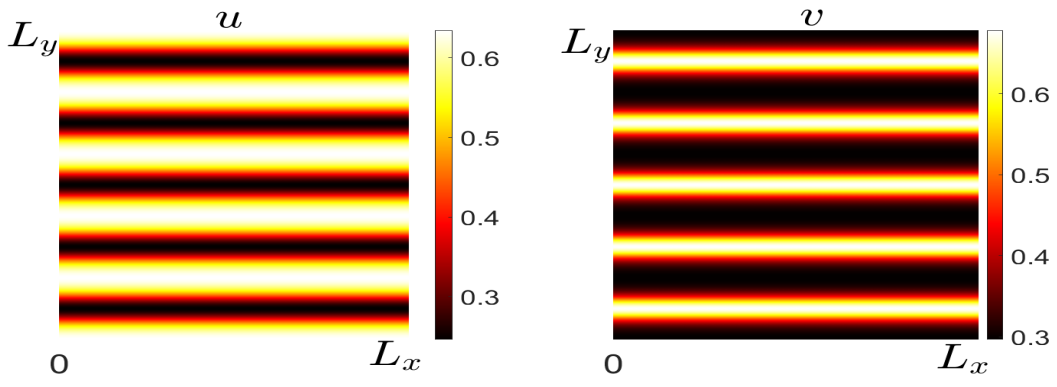

(a) (b)

FIGURE 5.8: Roll patterns, the numerical solution u and v of the original system (3.6).

Chapter 6

Mathematical Modelling and Numerical Results of Tumor Growth Model

The chapter presents a mathematical model for tumor growth that accounts for the interplay between normal cells, tumor cells, and the concentration of H^+ ions in the tumor microenvironment. The model considers logistic growth for each population, as well as competition effects between normal and tumor cells. The spatial and temporal dynamics of the system are described by a system of partial differential equations (PDE) (see sections 6.1, 6.2, and 6.3). We can discretise the mathematical model using the method of lines to obtain a system of ordinary differential equations (ODE) that can be numerically integrated. The numerical results illustrate how the competition parameters affect the evolution of normal cells, tumor cells, H^+ ion concentration, and the resulting pH changes over time (see sections 6.4, and 6.5). The chapter highlights the importance of considering the acid-mediated tumor invasion process in a radially symmetric geometry to better capture the spherical nature of tumor growth at the microscopic level, as discussed in our work ([56]).

6.1 Introduction of Tumor Growth

The idea of tumor cell invasion was given by ([102]). He said that metabolism is the process by which cancer cells and normal cells will grow; metabolism has two types: anaerobic and aerobic. Aerobic is the process in which the breakdown of glucose is done in the presence of oxygen; during this process, carbon dioxide and energy are produced; the normal cell uses this energy to run the function of the human body, and the carbon dioxide is released during the respiration process. While anaerobic processes are done in the absence of oxygen, during this process, tumour cells will be growing, and a concentration of H^+ ions is produced, which is a dangerous environment for normal cells.

Researchers are particularly intrigued by the low pH of the tumor microenvironment in cancer invasion studies ([20]). Cancer cells' anaerobic glycolysis generates H^+ ions, lowering the pH of the primary tumor's surroundings. This acidic environment facilitates the formation of secondary tumors, a process known as metastasis. The heightened metabolic activity produces substantial lactic acid, resulting in an excess of H^+ ions. This acidity affects normal cells in the tumor vicinity, creating conditions favorable for tumor growth while causing normal cell death ([14], [74],

[88]). While normal cells thrive in blood with a pH of 7.1-7.4, tumor cells can survive in a more acidic environment with a pH of 6.5-7([48], [83], [79]).

([35]) pioneered a mathematical model for acid-mediated tumor invasion. Subsequent experimental work supported this model, demonstrating that tumor cells' anaerobic glycolysis produces H^+ ions ([36], [37]). This leads to local acidification and destruction of normal cells, facilitating tumor cell invasion ([35], [37], [75]). Normal cells struggle to survive in acidic conditions, creating a favourable environment for tumor growth. The reaction-diffusion model ([35]) describes how the population of normal cells, tumor cells, and the concentration of H^+ ions evolve over time due to their interactions. In 2013, ([64]) extended the model of ([35]) by adding the competition of tumor cells on normal call in logistic growth of normal cells, but the effect of the normal cells on tumour cells was not be added in tumour cell equation. Subsequently, ([65]) further developed the model by introducing mutual competition between normal and tumor cells and accounted for acid-mediated tumor cell death, noting that tumors cannot survive in environments more acidic than pH 6.3 ([14], [74]).

In 2017, ([43]) extended the model by including the time-varying carrying capacities in the normal and tumour cell equations and solved the system using the dual reciprocity boundary element method. Tumour cells grow in acidic environments, but an acidic environment does not suit the tumour cells. That's why the carrying capacity must depend on the excess concentration of lactic acid.

In this work, we propose a modified form of the mathematical model, which was first reported in ([35]). More concretely, we will assume that the growth rate for normal cells, cancer cells, and concentration of H^+ ions obey logistic-type regimes. This is an important difference from previously published works in which, for example, the concentration of H^+ ions is considered to be an exponential growth rate. The reason behind this correction is that the growth of the concentration of H^+ ions depends on the growth of the tumor, which is logistic according to the empirical data mentioned in the previous paragraphs. We also add nonzero competition terms of normal and tumour cell growth following the approach based on the Lotka–Volterra competition model ([101]). Those parameters will be represented by α_1 and α_2, respectively. Moreover, we will consider a radially symmetric form of the mathematical model in order to account for the approximately spherical geometry of tumors at the microscopic level.

6.2 Mathematical Modelling of Tumor Growth

Let r and t denote the radial position in one spatial dimension (cm) and time (s), respectively. Define the following parameters related to a tumor growth model:

Temporal and spatial distribution of normal cells

Let N_n denote be the normal cells density (in cells $/\mathrm{cm}^3$), r_1 be a growth rate of normal cells (in s^{-1}) and r_2 be rate in which concentration of H^+ ions effect the normal cells (in $\mathrm{M}^{-1}\mathrm{sec}^{-1}$) since ($\mathrm{M} = \frac{\mathrm{g\,mol}}{1000\,\mathrm{cm}^3}$) . We take the logistic growth of Normal cells in which we use Lotka–Volterra competition, i.e. how tumor cells will affect the

normal cells; the competition parameter is denoted by α_1.

The above phenomenon gives the governing equation of normal cells that can be described as

$$\frac{\partial N_n}{\partial t} = r_1 N_n \left(1 - \frac{N_n}{K_n} - \alpha_1 \frac{N_t}{K_t}\right) - r_2 H N_n, \tag{6.1}$$

here K_n denotes the carrying capacity of normal cells.

Temporal and spatial distribution of tumor cells

Let $N_t(r,t)$ denote tumor cells density (in cells /cm^3), r_3 be static growth rate of tumor cells (in s^{-1}), and K_t be carrying capacity of tumor cells(in cells/ cm^2). In this section, we will also discuss the diffusion term of tumor cells and how they affect the normal cells, which is denoted by $D(N_n)$. The diffusion term of tumor cells depends on normal cells. We also take the logistic growth of tumour cells as we took the growth of normal cells in Eq. (6.1) and the competition effect of normal cells on tumour cells. The competition parameter is denoted by α_2.

The governing Equation of tumor cells will be described as

$$\frac{\partial N_t}{\partial t} = r_3 N_t \left(1 - \frac{N_t}{K_t} - \alpha_2 \frac{N_n}{K_n}\right) + \frac{1}{r^2}\frac{\partial}{\partial r}\left(r^2 D(N_n)\frac{\partial N_t}{\partial r}\right), \tag{6.2}$$

where

$$D(N_n) = D_t \left(1 - \frac{N_n}{K_n}\right),$$

here D_t be a Diffusion rate of tumor cells (in cm^2/sec).

Temporal and spatial distribution of H^+ ions

In this subsection, we discuss the mathematical modelling of concentration of H^+ ions and how they affect the surrounding environment in which tumour cells promote, and normal cells will decay in this environment. We also discuss in numerical results how pH will change as time increases, which depends on the concentration of H+ ions, which will be calculated by the following formula $-\log(H^+)$.

Let $C_h(r,t)$ is the concentration of H^+, r_4 in(M cm^3/s) rate of growth for excess of H^+ions and r_5 is rate constant for excess H^+ (in s^{-1}) and D_h is a constant diffusion rate of H^+ ions.

The above phenomena give the governing concentration equation of C_h ions

$$\frac{\partial C_h}{\partial t} = r_4 N_t \left(1 - \frac{N_t}{K_t} - \alpha_2 \frac{N_n}{K_n}\right) - r_5 H + \frac{1}{r^2}\frac{\partial}{\partial r}\left(r^2 D_h \frac{\partial C_h}{\partial r}\right). \tag{6.3}$$

It is worth pointing out that there is a remarkable difference between the present model and that investigated in ([35]). Indeed, the authors of that paper assumed that the concentration of H^+ions for tumor cells followed an exponential law, while we assume a logistic distribution. The rationale behind this assumption obeys the hypothesis that H^+ions affect the normal cells, and lactic acid helps promote tumor invasion. Moreover, we suppose also that the normal cells affect the tumor cells but

in milder form ([65]). Also, it is essential to point out that the partial derivative with respect to r in the second and third equations of the model represents a divergence operator of the diffusion term in spherical coordinates. This diffusion term considers a non-constant diffusion coefficient, which makes the model more realistic and general.

In order to solve the diffusive-reactive system (6.1) -(6.3), we will require suitable initial conditions of the form

$$\begin{cases} N_n(r,0) = f_n(r) \\ N_t(r,0) = f_t(r) \\ C_h(r,0) = f_h(r) \end{cases} \tag{6.4}$$

where $f_n(r), f_t(r)$ and $f_h(r)$ represent the initial distribution of normal cells and tumor cells and the initial concentration of H^+ ions, respectively. In addition, we will impose homogeneous Neumann boundary conditions on both ends of the interval $[0,\infty)$, that is,

$$\frac{\partial N_t}{\partial \mathbf{n}}(0,t) = \frac{\partial C_h}{\partial \mathbf{n}}(0,t) = 0, \quad \forall t \geq 0 \tag{6.5}$$

$$\lim_{r\to\infty} \frac{\partial N_t}{\partial \mathbf{n}}(r,t) = \lim_{r\to\infty} \frac{\partial C_h}{\partial \mathbf{n}}(r,t) = 0, \quad \forall t \geq 0 \tag{6.6}$$

Biologically, homogeneous Neumann boundary conditions are usually employed to simulate a free boundary.

The nonlinear diffusion term of tumor cells, the third term on the right-hand side of Eq. (6.2), required additional analysis at $r = 0$, i.e. at $r = 0$, the diffusion term is undetermined. Hence, this term is an application of L'Hôpital's rule ([69]). Expanding the derivative of the proposed term is given below:

$$\begin{aligned} \frac{1}{r^2}\frac{\partial}{\partial r}\left(r^2 D(N_n)\frac{\partial N_t}{\partial r}\right) &= \frac{1}{r^2}\left[r^2\frac{\partial}{\partial r}\left(r^2 D(N_n)\frac{\partial N_t}{\partial r}\right)\right] + \frac{1}{r^2}\left[2r\left(D(N_n)\frac{\partial N_t}{\partial r}\right)\right], \\ &= \frac{\partial}{\partial r}\left(D(N_n)\frac{\partial N_t}{\partial r}\right) + \frac{2}{r}D(N_n)\frac{\partial N_t}{\partial r}, \\ &= \mathrm{D(N_n)}\frac{\partial^2 N_t}{\partial r^2} + \frac{dD(N_n)}{dN_n}\frac{\partial N_n}{\partial r}\frac{\partial N_t}{\partial r} + \frac{2}{r}D(N_n)\frac{\partial N_t}{\partial r}, \\ &= \mathrm{D(N_n)}\frac{\partial^2 N_t}{\partial r^2} + \left(-\frac{D_t}{K_n}\right)\frac{\partial N_n}{\partial r}\frac{\partial N_t}{\partial r} + \frac{2}{r}D(N_n)\frac{\partial N_t}{\partial r} \end{aligned} \tag{6.7}$$

The third term of Eq. (6.7) is not determined at $r = 0$, which is an application of L'Hôpital's rule, so we apply this rule to solve this term as given below.

$$\begin{aligned} \lim_{r\to 0}\left[\frac{2}{r}D(N_n)\frac{\partial N_t}{\partial r}\right] &= 2\mathrm{D(N_n)}\frac{\partial^2 N_t}{\partial r^2} + 2\frac{dD(N_n)}{dN_n}\frac{\partial N_n}{\partial r}\frac{\partial N_t}{\partial r} \\ &= 2\mathrm{D(N_n)}\frac{\partial^2 N_t}{\partial r^2} + 2\left(-\frac{D_t}{K_n}\right)\frac{\partial N_n}{\partial r}\frac{\partial N_t}{\partial r} \end{aligned} \tag{6.8}$$

Using BCs ((6.5) and (6.6)) and combining Eqs. ((6.7) and (6.8)), we get

$$\frac{1}{r^2}\frac{\partial}{\partial r}\left(r^2 D(N_n)\frac{\partial N_t}{\partial r}\right) = 3\mathrm{D}(\mathrm{N_n})\frac{\partial^2 N_t}{\partial r^2} \tag{6.9}$$

Similarly, the diffusion term of concentration of H^+ions is also undermined at $r = 0$, so we solve this term the same manner as we solve the diffusion term of tumor cells: we get the following term after solving.

$$\frac{1}{r^2}\frac{\partial}{\partial r}\left(r^2 D_h\frac{\partial H}{\partial r}\right) = 3D_h\frac{\partial^2 H}{\partial r^2} \tag{6.10}$$

It is worth pointing out that the dynamical behaviour of this system was already investigated in ([65]) using Cartesian coordinates. In our case, we investigate the radially symmetric scenario. However, the determination of the equilibrium points of this system and the stability analysis is the same as for Cartesian coordinates.

6.3 Cell Balacing

In this section, we will balance our system of PDE, which will show that our system that we define is balanced, i.e. the equations (6.1-6.3), left and right-hand sides is balance in normal cells/s, tumor cells/s and H^+/s, respectively. This will be presented in the subsections ((6.3.1), (6.3.2) and (6.3.3)).

6.3.1 Normal cells balance

Equation (6.1) is a conservation balance for normal cells in the Spherical coordinates system starting with the terms:

LHS-1: $(4\pi r^2)\frac{\partial N_n}{\partial t}$ – Accumulation of normal cells in a differential volume $(4\pi r^2)$. Note that the units of this term are $(\mathrm{cm}^3)(\frac{\text{normal cells}}{\mathrm{cm}^3})(\frac{1}{\mathrm{s}}) = (\frac{\text{normal cells}}{\mathrm{s}})$, that is, the accumulation of normal cells/s (or the depletion of normal cells if the derivative in t is negative).

RHS-1: $(4\pi r^2)r_1 N_n\left(1 - \frac{N_n}{K_n} - \alpha_1\frac{N_t}{K_t}\right)$ – A logistic rate for the increase in the number of normal cells, N_n, in a differential volume $(4\pi r^2)$. Note that as $\frac{N_n}{K_n} \to 1$, this rate approaches zero again, and the net units are normal cells/s, as in LHS-1.

RHS-2: $(4\pi r^2 dr)r_2 N_n C_h$ - Finally, the last term on the right-hand side of (6.1) represents the rate of reduction in the number of normal cells within a differential volume given by $4\pi r^2 dr$. Note that this rate is proportional to the product of the variables C_h and N_n, so it is nonlinear. The net units are normal cells/s, as in the case of the terms above.

6.3.2 Tumor cells balance

Equation (6.2) is a conservation balance for tumor cells in a spherical coordinates system starting with the terms:

LHS-1: $(4\pi r^2 dr)\frac{\partial N_t}{\partial t}$ – Accumulation of tumor cells in a differential volume $(4\pi r^2 dr)$. Note that the units of this term are $(\mathrm{cm}^3)(\frac{\text{tumor cells}}{\mathrm{cm}^3})(\frac{1}{\mathrm{s}}) = (\frac{\text{tumor cells}}{\mathrm{s}})$, that is, the accumulation of tumor cells/s (or the depletion of tumor cells if the derivative in t is

negative).

RHS-1: $(4\pi r^2 dr) r_3 N_t \left(1 - \frac{N_t}{K_t} - \alpha_2 \frac{N_n}{K_n}\right)$ - A logistic rate for the increase in the number of tumor cells, N_t, in a differential volume $(4\pi r^2 dr)$. Note that as $\frac{N_t}{K_t} \to 1$, this rate approaches zero. Again, the net units are tumor cells/s, as in LHS-1.

RHS-2: $(4\pi r^2) D_t \left(1 - \frac{N_n}{K_n}\right) \frac{\partial N_t}{\partial t}$ at r. Rate of diffusion of tumor cells into the differential volume $(4\pi r^2 dr)$ at r. This is an application of Fick's Law for diffusion. The net units are tumor cells/s, as in LHS-1 and RHS-1. Note the diffusivity of N_t is a function of N_n to reflect the decrease in the rate of diffusion of tumor cells as the number of normal cell increases; this is a nonlinear effect that can be accommodated within the normal approach to the solution of equation (6.2), to be discussed subsequently.

RHS-3: $(4\pi (r+dr)^2) D_t \left(1 - \frac{N_n}{K_n}\right) \frac{\partial N_t}{\partial t}$ at $r + dr$. Rate of diffusion of tumor cells out of differential volume $(4\pi r^2 dr)$ at $r + dr$. The net units are tumor cells/s, as in LHS-1, RHS-1,and RHS-2.

If these four terms are placed in a balence for N_t (with $D(N_n) = D_t\left(1 - \frac{N_n}{K_n}\right)$) in equation (6.2), we set

$$\begin{aligned}(4\pi r^2 dr)\frac{\partial N_t}{\partial t} =& (4\pi r^2 dr) r_3 N_t \left(1 - \frac{N_t}{K_t} - \alpha_2 \frac{N_n}{K_n}\right) - (4\pi r^2 dr) - \\ & (4\pi r^2) D_t \left(1 - \frac{N_n}{K_n}\right) \frac{\partial N_t}{\partial t}|_r + (4\pi r^2) D_t \left(1 - \frac{N_n}{K_n}\right) \frac{\partial N_t}{\partial t}|_{r+dr}\end{aligned} \tag{6.11}$$

After some arrangements, the above equation can be written as

$$\frac{\partial N_t}{\partial t} = r_3 N_t \left(1 - \frac{N_t}{K_t} - \alpha_2 \frac{N_n}{K_n}\right) + \frac{1}{r^2} \frac{\partial}{\partial r}\left(r^2 D(N_n) \frac{\partial N_t}{\partial r}\right) \tag{6.12}$$

6.3.3 H^+ balance

Equation (6.3) is a conservation balance for H^+ ion in spherical coordinates system starting with the terms:

LHS-1: $(4\pi r^2 dr) \frac{\partial C_h}{\partial t}$ – Accumulation of H^+ ion in a differential volume $(4\pi r^2 dr)$. Note that the units of this term are $(\text{cm}^3)(\frac{\text{H}^+ \text{ ion}}{\text{cm}^3})(\frac{1}{\text{s}}) = (\frac{\text{H}^+ \text{ ion}}{\text{s}})$, that is, the accumulation of H^+ ion per second (or the depletion of H^+ ion if the derivative in t is negative).

RHS-1: $(4\pi r^2 dr) r_4 N_t \left(1 - \frac{N_t}{K_t} - \alpha_2 \frac{N_n}{K_n}\right)$ - A logistic rate for the increase in the number of H^+ ion, in a differential volume $(4\pi r^2 dr)$. Note that as $\frac{N_t}{K_t} \to 1$, this rate approaches zero. Again, the net units are H^+ ion/s, as in LHS-1.

RHS-2: $(4\pi r^2)D_h\left(\frac{\partial C_h}{\partial t}\right)$ at r. Rate of diffusion of H^+ ion into the differential volume $(4\pi r^2 dr)$ at r. This is an application of Fick's Law for diffusion. The net units are H^+ ion/sec, as in LHS-1 and RHS-1.

RHS-3:$(4\pi(r+dr)^2)D_h\left(\frac{\partial C_h}{\partial t}\right)$ at $r+dr$. Rate of diffusion of H^+ ion out of differential volume $(4\pi r^2 dr)$ at $r+dr$. The net units are H^+ ion/sec, as in LHS-1, RHS-1 and RHS-2.

If these terms are placed in a balance for H^+ ion, into the equation (6.3), we get

$$\begin{aligned}(4\pi r^2 dr)\frac{\partial C_h}{\partial t} =&(4\pi r^2 dr)r_4 N_t\left(1-\frac{N_t}{K_t}-\alpha_2\frac{N_n}{K_n}\right)-(4\pi r^2 dr)r_5 C_h\\ &-(4\pi r^2)D_h\left(\frac{\partial C_h}{\partial t}\right)|_r+(4\pi(r+dr)^2)D_h\left(\frac{\partial C_h}{\partial t}\right)|_{r+dr}\end{aligned} \tag{6.13}$$

After some simplification, the above equation can be written as

$$\frac{\partial C_h}{\partial t} = r_4 N_t\left(1-\frac{N_t}{K_t}-\alpha_2\frac{N_n}{K_n}\right)-r_5 C_h + D_h\frac{1}{r^2}\frac{\partial}{\partial r}\left(r^2\frac{\partial C_h}{\partial r}\right) \tag{6.14}$$

6.4 Discretization of the Mathematical Model using MOL

The MOL's core concept is to use algebraic approximations to substitute the PDE's spatial (boundary value) derivatives. Once this has been accomplished, the spatial derivatives are no longer expressed explicitly in terms of the spatial independent variables. As a result, in a physical problem, just the initial variable remains, which is usually time. In other words, we have a system of ODEs that approximates the original PDEs having only one independent variable. Once this is done, we can use any integration algorithm to solve the ODEs.

To illustrate this procedure, we consider the MOL solution for the mathematical model described in Equations (6.1) to (6.3). First, we need to replace the spatial derivatives with an algebraic approximation. f_r and f_{rr} represents the first and second order derivative respectively. We used a finite difference (FD) five-point (fourth-order accurate) formula to discretize the model. For Neuman boundary conditions as defined in eq. (6.5), we used five-point forward and backward formulas for the endpoints and five-point central difference formulas for the interior points. We used index i, which is an index designating a position along a grid in r, and Δr is the spacing in r along the grid, assumed constant for the time being. Thus, for the left end value of r, $i=1$, and for the right end value of r, $i=n$, i.e., the grid in r has n points

The discretization form of the first-order derivative at the left endpoints is given as

$$f_r = \frac{-25f_i+48f_{i+1}-36f_{i+2}+16f_{i+3}-3f_{i+4}}{12\Delta r}, \qquad i=1 \tag{6.15}$$

$$f_r = \frac{-3f_{i-1} - 10f_i + 18f_{i+2} - 6f_{i+3} + f_{i+4}}{12\Delta r}, \qquad i = 2 \tag{6.16}$$

at right end points,

$$f_r = \frac{25f_i - 48f_{i-1} + 36f_{i-2} - 16f_{i-3} + 3f_{i-4}}{12\Delta r}, \qquad i = n \tag{6.17}$$

$$f_r = \frac{-f_{i-4} + 6f_{i-3} - 18f_{i-2} + 10f_{i-1} + 3f_i}{12\Delta r}, \qquad i = n-1 \tag{6.18}$$

for interior points,

$$f_r = \frac{f_{i-2} - 8f_{i-1} - 0 * f_i + 8f_{i+1} + f_{i+2}}{12\Delta r} \tag{6.19}$$

The discretization form of the order derivative at the left endpoints is given as

$$f_{rr} = \frac{45f_i - 154f_{i+1} + 214f_{i+2} - 156f_{i+3} + 61f_{i+4} - 10f_{i+5}}{12\Delta r^2} \qquad i = 1 \tag{6.20}$$

$$f_{rr} = \frac{10f_{i-1} - 15f_i - 4f_{i+1} + 14f_{i+2} - 6f_{i+3} + f_{i+4}}{12\Delta r^2}, \qquad i = 2 \tag{6.21}$$

at right endpoints

$$f_{rr} = \frac{45f_i - 154f_{i-1} + 214f_{i-2} - 156f_{i-3} + 61f_{i-4} - 10f_{i-5}}{12\Delta r^2}, \qquad i = n \tag{6.22}$$

$$f_{rr} = \frac{10f_{i+1} - 15f_i - 4f_{i-1} + 14f_{i-2} - 6f_{i-3} + f_{i-4}}{12\Delta r^2}, \qquad i = n-1 \tag{6.23}$$

for interior points,

$$f_{rr} = \frac{-f_{i-2} + 16f_{i-1} - 30f_i + 16f_{i+1} - f_{i+2}}{12\Delta r^2} \tag{6.24}$$

Now we can see that if we put these algebraic expressions as defined in equations (6.15 - 6.24) to the given system (6.1 - 6.3), we get a system of ODEs that approximates the original PDEs. Then, to compute the solution of the PDEs, we compute a solution to the approximating system of ODEs. As we know $1 \leq i \leq n$ so we get n system ODES. To solve this system of ODEs, we used an ODEs integration algorithm, ode45 and ode15s ([38]), to get the numerical results, as discussed in the next section.

6.5 Numerical Results and Discussion

For numerical results, we used MATLAB R2016a user-defined functions developed for the analysis and ran it on a laptop with 8 GB RAM and 1.61 GHz processes. The operating system is 64-bit and Windows 10. The computational cost on each case is given in Table 6.1, and the parametric numerical value is given in Table 6.2.

We will use no flux Neumann BCs as we define in equations (6.5) and (6.6). We also assume the initial normal cells are half of their carrying capacity, while tumor cells can be close to theirs and thus prone to invade the surrounding tissue as given in ([65]). Since pH level is lowered due to the concentration of H^+ ions which is produced due to tumour cells. By using this assumption, we define the initial condition

of normal cells, tumor cells and concentration H^+ ions as given below

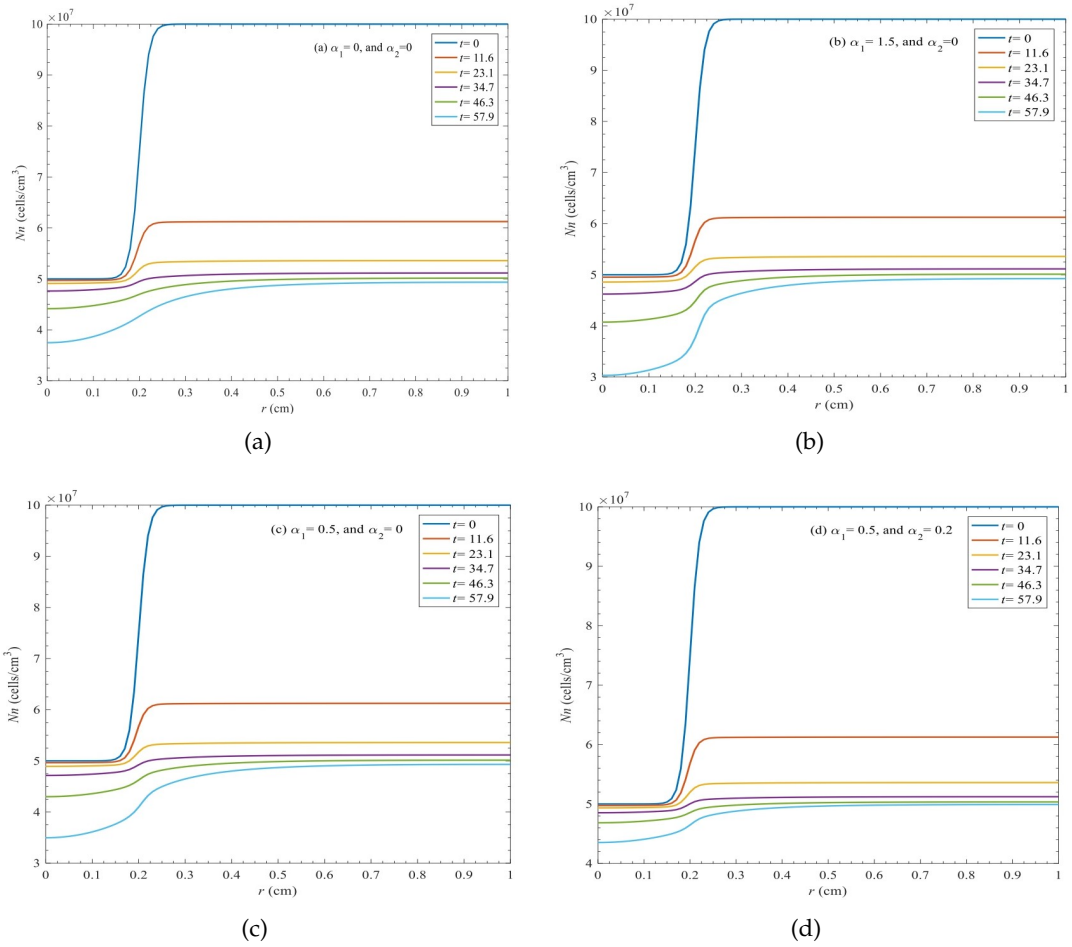

(a) (b)

(c) (d)

FIGURE 6.1: Numerical results for normal cells for $0 \leq r \leq 1$, t=0, 11.6, 23.1, 34.7. 46.3, 57.9 days (top to bottom)

.

$$r_s = 50 \tag{6.25}$$

$$num = e^{(rs(r-r(21)))} - e^{(-rs(r-r(21)))}$$

$$den = e^{(rs(r-r(21)))} + e^{(-rs(r-r(21)))}$$

$$tanh(r) = \frac{num}{den} \tag{6.26}$$

$$Nn_o(r,0) = 5.0 \times 10^7 \times \frac{1 - tanh(r)}{2} + 1.0 \times 10^8 \times \frac{1 + tanh(r)}{2} \tag{6.27}$$

The above equation (6.27) is the initial condition for normal cells.

Now we define the initial condition for tumor cells, which can be written as

$$Nt_o(r,0) = 1.0 \times 10^5 \times \frac{1 - tanh(r)}{2} + 1.0 \times 10^3 \times \frac{1 + tanh(r)}{2} \tag{6.28}$$

Above equation (6.28) is the initial condition for tumor cells here *tanhr* is same as defined in equation (4.14). Now we define initial condition of concentration of H^+

ions,

$$num = e^{(rs(r-r(11)))} - e^{(-rs(r-r(11)))}$$
$$den = e^{(rs(r-r(11)))} + e^{(-rs(r-r(11)))}$$
$$tanh(r) = \frac{num}{den} \tag{6.29}$$
$$Ch_o(r,0) = 1.0 \times 10^{-9} \times \frac{1 - tanh(r)}{2} \tag{6.30}$$

which is the initial condition for the concentration of H^+ ions.The equations (6.27), (6.28) and (6.30) are the initial conditions for normal cells, tumour cells and concentration of H^+ ions, respectively.
The previous work on acid-mediated tumour growth has been done in the Cartesian coordinates system, and their results were not so much precise about the behaviour of tumour expansion and how much it affects the normal cells ([50],[65]). But here, we are dealing with the tumour growth in spherical coordinates, which gives a better approximation to the geometry of the tumour. Also, we analyze how the pH varies due to the effect of the concentration of H^+ ion.

The variation of normal cells is presented in Fig. 6.1 (a - d) for different cases. In these plots, α_1 represents the effect of tumor cells on normal cells. On the other hand, α_2 represents the effect of normal cells on tumour cells see Fig.6.1(a - d)).

First, we considered a case in which both $\alpha_1 = \alpha_2 = 0$ as ([35]) taken in his article and later on ([7]) and discussed the numerical results. The normal cells decay with time variation, which clearly indicates the effect of tumor cells sec Fig. 5.1(a). In a second case, see Fig.6.1(b), when we take a competition term of tumor on normal cells is nonzero and using interspecific competition as taken in, we see that as time varies normal cells decay more rapidly see Fig. 6.1(b) as compared to the case when competition term is zero.
In Fig. 6.1(c), when we used intraspecific competition as taken ([65]) then, we see that the decay rate of normal cells is less as compared to the first two cases see Fig. 5.1(a-b). Also, in the last case, when we take an intraspecific competition, both α_1 and α_2 are nonzero as see Fig. 6.1(d) decay of normal cells very less as compared to the other three cases as discussed above.
The variation of tumor cells is presented in Fig. 6.2(a-d) for different cases. For the first case, we take both the competition terms as zero, i.e. $\alpha_1 = \alpha_2 = 0$. For this case, we clearly see that tumor cells expand with time variations and affect the normal cells in that area see Fig. 6.2(a). If we choose one of the competition terms as nonzero, i.e. interspecific competition, then we clearly see that expand rate of tumor cells is fast as compared to the first case see Fig. 6.2(b).

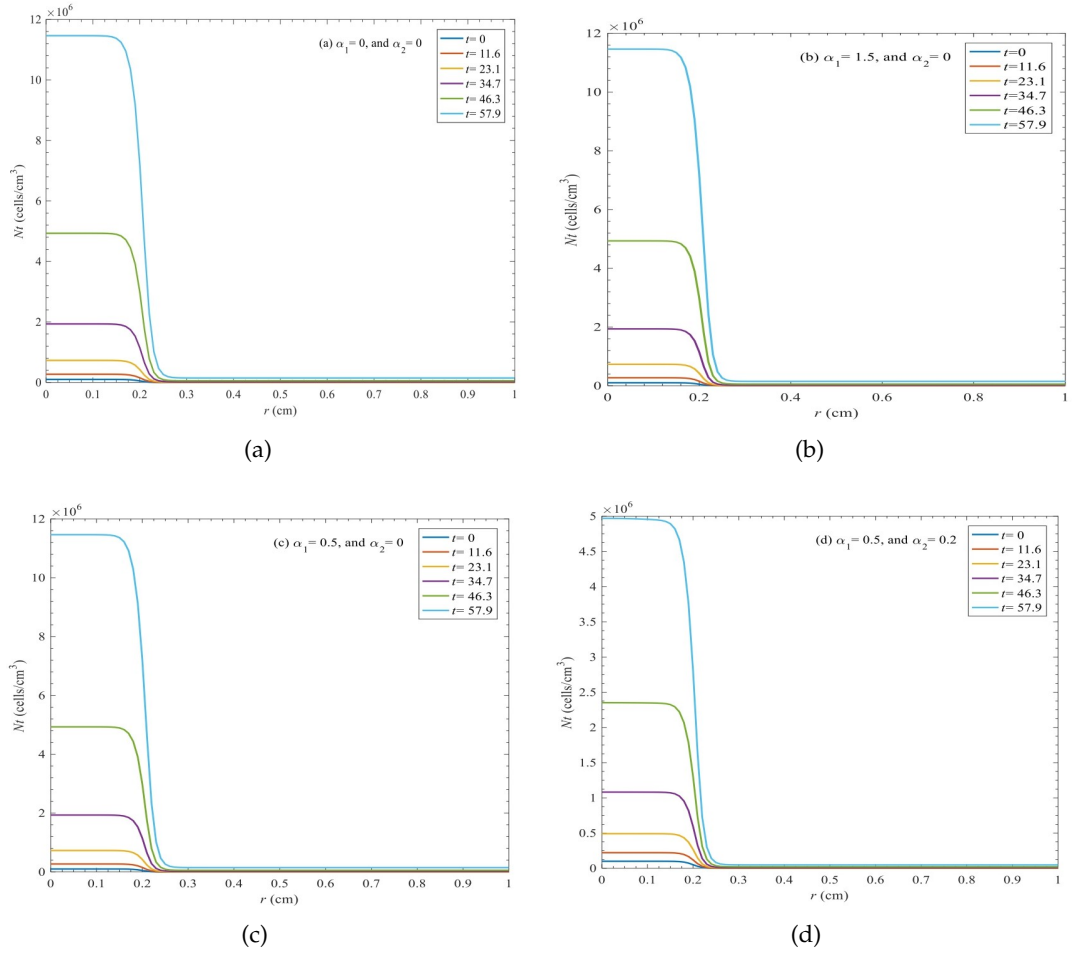

(a) (b)

(c) (d)

FIGURE 6.2: Numerical results for tumor cells for $0 \leq r \leq 1$, t=0, 11.6, 23.1, 34.7. 46.3, 57.9 days (bottom to top)

.

Also, we considered a case in which we take an intraspecific competition of tumor cells, and we see that in that case, the tumor expansion rate is a little bit slow but not affect too much to slow down the expansion rate of the tumor see Fig. 6.2(c). In the last case, when we considered both competition terms as nonzero, then we see that the spread rate of tumor is much slower as compared to other cases see Fig. 6.2(d). The variation of concentration of H^+ is presented in Fig. 6.3(a-d) for different cases. For the case $\alpha_1 = \alpha_2 = 0$ see Fig. 6.3(a), we see how the concentration of H^+ ions increases in that area where tumor cells spread with time variation.

On the other hand, as we see in Fig. 6.3(b-c), the variation of concentration H^+ ions looks the same as compared to the first case see Fig.6.3(a). The reason behind this is that in case 2 when we choose $\alpha_1 > 1$ as an interspecific competition of tumor on normal due to this reason tumor effect normal in that area, but the variation concentration of H^+ looks same as we see in the first case see Fig. 6.3 (a) and when we choose intraspecific competition then we see that variation of H^+ ions remain looks same because tumor cells do not effect on each other see Fig. 6.3(c). In the last case, when chosen, both competition terms are nonzero as we see a variation of H^+ ions is much slower as compared to the other three cases see Fig.6.3(d).

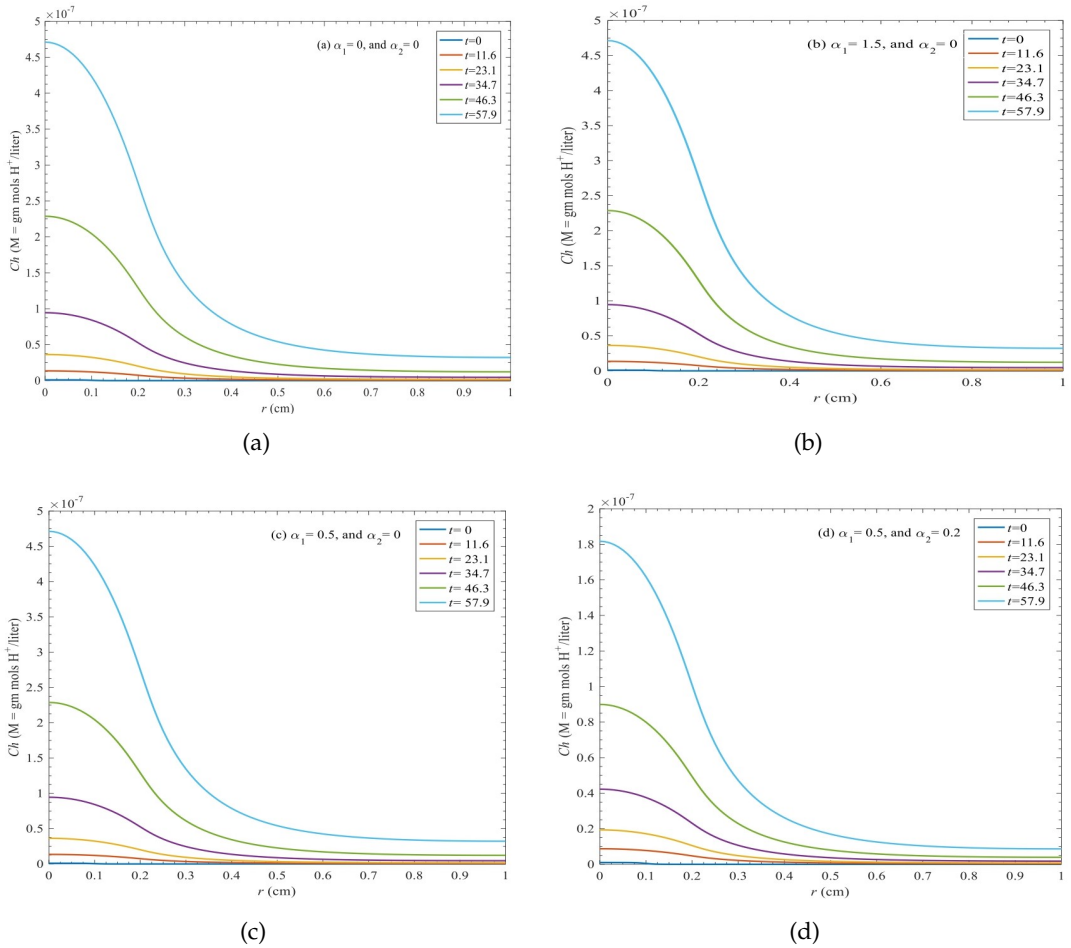

(a) (b)

(c) (d)

FIGURE 6.3: Numerical results for concentration of H^+ ions for $0 \leq r \leq 1$, t=0, 11.6, 23.1, 34.7. 46.3, 57.9 days (bottom to top)

.

The Variation of pH is presented in Fig 6.4 (a - d) for different cases. For the first case, see Fig. 6.4(a) in which both competition terms are zero, we see how pH decreases with time variation in that area where the concentration of H^+ increases with time (see Fig. 6.3 (a)).

On the other hand, if we choose $\alpha_1 > 1$, then we see that the variation of pH with time looks the same (see Fig. 6.4 (b)), the reason behind this is that we use competition of tumor on normal cells is nonzero that's why the growth rate of tumor same but in that case, normal cells decay fast as compare to the first case see Fig. 6.4(a-b). In case three, when we choose intraspecific competition of tumour cells, then we see that tumour cells do not affect themselves see Fig. 6.4 (c). In the last case, when we choose that both the competition terms are nonzero, then a variation of pH is too slow as compared to other cases see Fig. 6.4 (d).

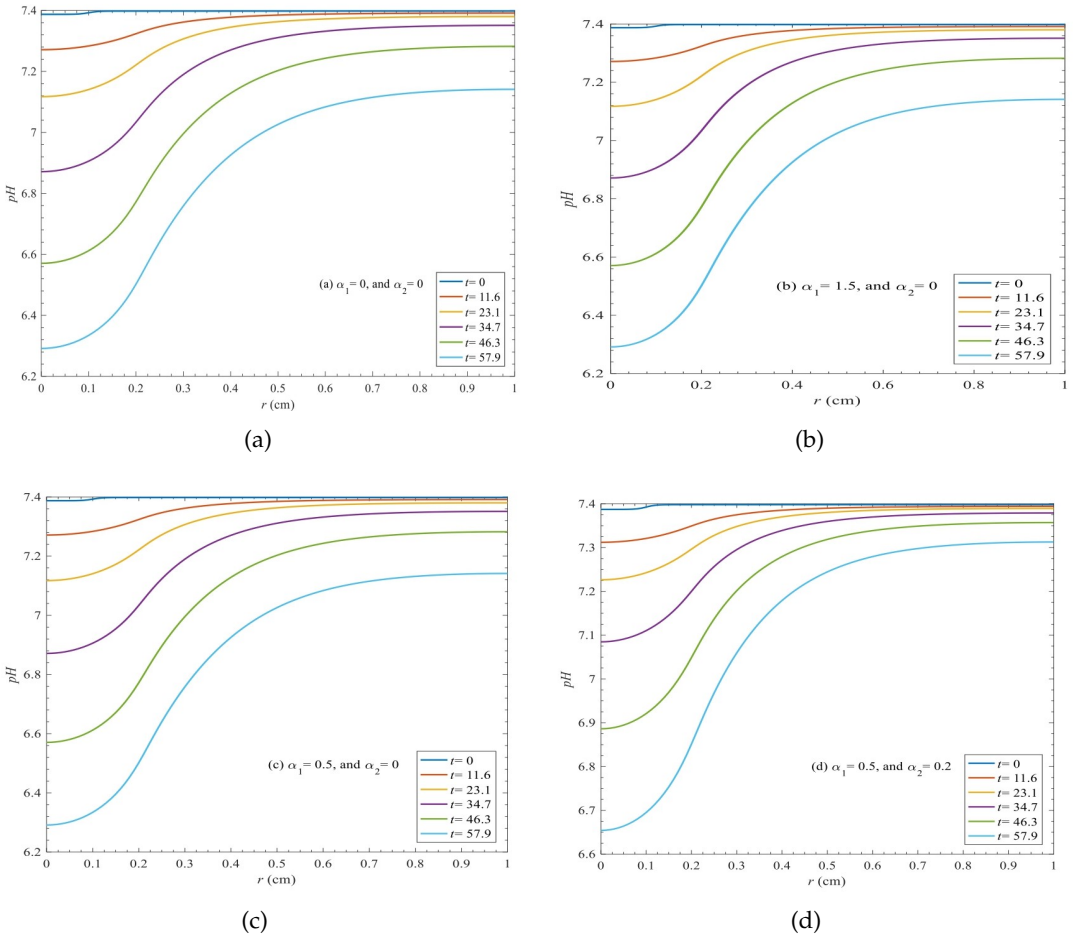

(a) (b)

(c) (d)

FIGURE 6.4: Numerical results for pH for $0 \leq r \leq 1$, t=0, 11.6, 23.1, 34.7. 46.3, 57.9 days (top to bottom)

.

TABLE 6.1: Computational Cost

Cases	Elapsed Time in seconds
Case 1	3.3023373
Case 2	3.485992
Case 3	3.749872
Case 4	3.749877

TABLE 6.2: Numerical Values of Parameters

Parameter	Value	Unit
r_1	1×10^{-6}	s^{-1}
r_2	$0 - 10$	$M^{-1}s^{-1}$
r_3	1×10^{-6}	s^{-1}
r_5	2.2×10^{-17}	$M\,cm^3\,s^{-1}$
r_6	1.1×10^{-4}	s^{-1}
K_n	5.0×10^{7}	cm^3
K_t	5.0×10^{7}	cm^3
D_t	2.0×10^{-10}	cm^2s^{-1}
D_h	2.0×10^{-6}	cm^2s^{-1}

Chapter 7

Conclusion

In this thesis, we studied how patterns form when toxic phytoplankton and zooplankton interact in a reaction-diffusion system with nonlinear cross-diffusion. We identified the parameter ranges where diffusion-driven instability occurs and patterns emerge. Using a weakly nonlinear expansion, we predicted the pattern's shape and amplitude and derived the amplitude equations, including up to quintic order terms, for supercritical and subcritical bifurcation cases. We used two cases of kinetic parameters to draw patterns in supercritical and subcritical bifurcation regions; in supercritical bifurcation, both cases' numerical solutions perfectly match the weakly nonlinear approximation see Figs. (5.1-5.2), but in subcritical bifurcation, for the first case, our numerical result does not perfectly match with WNL approximation because the numerical scheme MOL can not run the solution for a long time, so we do not get perfect stationary patterns as we expected, but for the second case of parameters, numerical solution perfectly matches with WNL approximation see Figs. (5.3 – 5.4), the difference between the last two simulations is about 10^{-13}. Also, we performed numerical simulations of the system that show that without cross-diffusion, the system does not hold diffusion-driven instability see Figs. (4.8-4.9). For the non-spatial model, we predict the region where the coexistence steady state will be stable, where it holds Hopf bifurcation and where it becomes unstable see Figs. (4.1-4.3).

Additionally, we examine the pattern transition in the 2D domain by deriving an amplitude equation for the activated modes near the onset ($d_{21} = d_{21}^c$) on the central manifold, using cross-diffusion rate as a bifurcation parameter. The linear stability analysis of amplitude equations effectively explains the structural transitions and stability of various forms of Turing patterns. It is found that the system described in equation (3.6) can give rise to different types of Turing patterns, such as spot patterns, stripe patterns, and a combination of spot and stripe patterns, depending on the varying cross-diffusivity see Figs. (5.6-5.8).

In this thesis, we also proposed a mathematical model of acid-mediated tumour invasion as a system of reaction-diffusion equations. The partial differential equations in this model describe the dynamics for the rate of change of normal and tumor cell densities and the concentration of H^+ ions. The cancer cells consistently rely on anaerobic glycolysis to convert glucose to ATP molecules, even in the presence of oxygen. Due to anaerobic glycolysis, the H^+ ions are produced, causing local acidification. The excess amount of H^+ ions causes the destruction of normal cells, which helps the tumor to propagate. The mathematical model considers the effect of tumor cells on normal cells and vice-versa. We checked our results for different values of the dimensionless competition parameters and observed the dynamics of normal and tumour cells vary in a bounded interval and at different times. The spatial interval considered in this work was the interval $[0, 1]$ in R. Under the initial conditions employed in this work, the normal cells tend to concentrate the radial

model in $[0.1, 1]$ as time increases. For tumor cells, the concentration area is within the interval $[0, 0.1]$, and the concentration increases with time. On the other hand, the concentration of H^+ ions is more saturated around $[0, 0.1]$. The reason for this effect is that cancer cells produce H^+ ions, and this production increases with time. Consequently, the concentration of H+ ions and the population of cancer cells are directly related. On the other hand, H^+ ions are inversely related to the pH level. So, when H^+ ions increase, the pH decreases, and the normal cells begin to die if the pH remains below 7.1. This situation facilitates tumor invasion. From our simulations, it is clear that the normal cells decrease more rapidly when both competition parameters are equal to zero. In that case, the effect of H^+ ions on the normal cells is more evident than its effect on the tumor. In this case, tumor invasion is relatively fast. Meanwhile, the tumor invasion rate is slower when either of the competition parameters is nonzero. Various other interesting physical implications were drawn from our simulations, and the potential applications of our approach are promising see Figs. (6.1-6.4).

It is important to point out that the idea behind using the reaction-diffusion system in this work is that it consists of two components. The first is the kinetics part, which models the interaction between normal and tumor cells. On the other hand, due to the interaction of normal cells, if a tumor develops in some part of the body, it may be transferred to another part through a process called metastatic cancer. Using Fick's law to account for this phenomenon, we added the diffusion term to the model. Our results confirmed that when tumor cells have more concentration at the primary part, they move to a lower concentration. This is the process through which tumor develops in other parts of the human body.

Appendix A

Derivation of Stuart–Landau Equation

Considering the solution at the lowest order given by (5.8). Equating the coefficients at $\mathcal{O}(\epsilon^2)$, and $\mathcal{O}(\epsilon^3)$, gives the following equations:

$$\mathcal{O}(\epsilon^2) : \mathcal{L}^{d^c}\mathbf{w}_2 = \mathbf{F}, \tag{A.1}$$

$$\mathcal{O}(\epsilon^3) : \mathcal{L}^{d^c}\mathbf{w}_3 = \mathbf{G}, \tag{A.2}$$

with

$$\begin{aligned}\mathbf{F} =& \frac{\partial \mathbf{w}_1}{\partial T_1} - \begin{pmatrix} 0 & 0 \\ d_{21}^1 v^* & 0 \end{pmatrix} \nabla^2 \mathbf{w}_1 + \begin{pmatrix} u_1^2 \\ 0 \end{pmatrix} - \left[\frac{(1-\gamma)^2}{\beta}(u_1 v_1 - 2u_1^2 \times \right. \\ & \left. (1 - \frac{\gamma\beta}{1-\gamma})) \right] \begin{pmatrix} -1 \\ \eta \end{pmatrix} - \begin{pmatrix} d_{12}(u_1 \nabla^2 v_1 + \nabla u_1 \nabla v_1) \\ d_{21}^c (v_1 \nabla^2 u_1 + \nabla v_1 \nabla u_1) \end{pmatrix},\end{aligned} \tag{A.3}$$

$$\begin{aligned}\mathbf{G} =& \frac{\partial \mathbf{w}_1}{\partial T_2} + \frac{\partial \mathbf{w}_2}{\partial T_1} - \begin{pmatrix} 0 & 0 \\ v^* & 0 \end{pmatrix} (d_{21}^2 \nabla^2 \mathbf{w}_1 + d_{21}^1 \nabla^2 \mathbf{w}_2) + \begin{pmatrix} 2u_1 u_2 \\ 0 \end{pmatrix} \\ & - \left[\frac{(1-\gamma)^2}{\beta}(u_1 v_2 + u_2 v_1 - 4u_1 u_2 (1 - \frac{\gamma\beta}{1-\gamma})) + 2\frac{(1-\gamma)^3}{\beta^2} \times \right. \\ & \left. (3u_1^3 (1 - \frac{\gamma\beta}{1-\gamma}) - u_1^2 v_1) \right] \begin{pmatrix} -1 \\ \eta \end{pmatrix} - \begin{pmatrix} 0 \\ d_{21}^1 (v_1 \nabla^2 u_1 + \nabla v_1 \nabla u_1) \end{pmatrix} \\ & - \begin{pmatrix} d_{12}(u_1 \nabla^2 v_2 + u_2 \nabla^2 v_1 + \nabla u_1 \nabla v_2 + \nabla u_2 \nabla v_1) \\ d_{21}^c (v_1 \nabla^2 u_2 + v_2 \nabla^2 u_1 + \nabla v_1 \nabla u_2 + \nabla v_2 \nabla u_1) \end{pmatrix}.\end{aligned} \tag{A.4}$$

At $\mathcal{O}(\epsilon^2)$, we obtain the following system,

$$\begin{aligned}\mathcal{L}^{d^c}\mathbf{w}_2 =& \left(\frac{\partial A}{\partial T_1} r + \begin{pmatrix} 0 \\ d_{21}^1 v^* k_c^2 \end{pmatrix} \right) cos(k_c x) + \begin{pmatrix} \frac{A^2}{2} \\ 0 \end{pmatrix} - \left[\frac{A^2(1-\gamma)^2}{2\beta}(M - 2(1 - \frac{\gamma\beta}{1-\gamma})) \right] \times \\ & \begin{pmatrix} -1 \\ \eta \end{pmatrix} + \left(\begin{pmatrix} \frac{A^2}{2} \\ 0 \end{pmatrix} - \left[\frac{A^2(1-\gamma)^2}{2\beta}(M - 2(1 - \frac{\gamma\beta}{1-\gamma})) \right] \begin{pmatrix} -1 \\ \eta \end{pmatrix} \right. \\ & \left. + \begin{pmatrix} d_{12} \\ d_{21}^c \end{pmatrix} M k_c^2 \right) cos(2k_c x).\end{aligned} \tag{A.5}$$

By the Fredholm alternative, Eq. (A.5) admits solution if and only if $\langle \mathbf{F}, \boldsymbol{\psi} \rangle = 0$ and $\boldsymbol{\psi} \in ker(J - kc^2 D^{d^c})^\dagger$. since

$$\boldsymbol{\psi} = \mathbf{r}^* cos(k_c x), \text{ with } \mathbf{r}^* = \begin{pmatrix} 1 \\ M^* \end{pmatrix}, \text{ with } M^* = \frac{J_{12} - k_c^2 D_{12}^{d^c}}{D_{22}^{d^c} k_c^2 - J_{22}}.$$

By this condition, we find the amplitude equation of the following form:

$$\frac{\partial A}{\partial T1} = \alpha A,$$

where $\alpha = -\frac{k_c^2 M^* d_{21}^1 v^*}{1+MM^*}$. The above amplitude equation does not indicate anything about the asymptotic behavior of the amplitude of patterns.Hence, the secular terms presented in $\mathbf{F}$ can be conquered by imposing $T_1 = 0$ and $d_{21}^1 = 0$ and automatically the condition holds. Now, we can calculate the solution of (A.5) as follows:

$$\mathbf{w}_2 = A^2 \mathbf{w}_{20} + A^2 \mathbf{w}_{22} cos(2k_c x),$$

where $\mathbf{w}_{2i}, i = 0, 2$, are solutions of the following linear systems:

$$(J)(\mathbf{w}_{20}) = \begin{pmatrix} \frac{1}{2} \\ 0 \end{pmatrix} - \left[\frac{(1-\gamma)^2}{2\beta} (M - 2(1 - \frac{\gamma\beta}{1-\gamma})) \right] \begin{pmatrix} -1 \\ \eta \end{pmatrix}, \tag{A.6}$$

$$\begin{aligned}(J - 4k_c^2 D^{d^c})(\mathbf{w}_{22}) = &(J - 4k_c^2 D^{d^c})(\mathbf{w}_{22}) = \begin{pmatrix} \frac{1}{2} \\ 0 \end{pmatrix} - \left[\frac{(1-\gamma)^2}{2\beta} (M - 2(1 - \frac{\gamma\beta}{1-\gamma})) \right] \times \\ &\begin{pmatrix} -1 \\ \eta \end{pmatrix} + \begin{pmatrix} d_{12} \\ d_{21}^c \end{pmatrix} M k_c^2.\end{aligned} \tag{A.7}$$

At $\mathcal{O}(\epsilon^3)$,

$$\mathcal{L}^{d^c} \mathbf{w}_3 = \left(\frac{dA}{dT_2} + A\mathbf{G}_1^1 + A^3 \mathbf{G}_1^3 \right) \cos(k_c x) + A^3 \mathbf{G}_3 \cos(3k_c x), \tag{A.8}$$

with

$$\mathbf{G}_1^1 = k_c^2 d_{21}^2 \begin{pmatrix} 0 \\ v^* \end{pmatrix}, \tag{A.9}$$

$$\begin{aligned}\mathbf{G}_1^3 = &\begin{pmatrix} 2w_{20}^u + w_{22}^u \\ 0 \end{pmatrix} - \frac{(1-\gamma)^2}{\beta} \left(M w_{20}^u + \frac{1}{2} M w_{22}^u + w_{20}^v + \frac{1}{2} w_{22}^v - (1 - \frac{\gamma\beta}{1-\gamma}) \times \right. \\ &\left. (4w_{20}^u + 2w_{22}^u) \right) \begin{pmatrix} -1 \\ \eta \end{pmatrix} - 2\frac{(1-\gamma)^3}{\beta^2} \left(\frac{9}{4}(1 - \frac{\gamma\beta}{(1-\gamma)}) - \frac{3}{4} M \right) \begin{pmatrix} -1 \\ \eta \end{pmatrix} \\ &+ \begin{pmatrix} d12 k_c^2 (w_{22}^v - \frac{1}{2} M w_{22}^u + M w_{20}^u) \\ d_{21}^c k_c^2 (M w_{22}^u - \frac{1}{2} M w_{22}^v + w_{20}^v) \end{pmatrix},\end{aligned} \tag{A.10}$$

$$\begin{aligned}\mathbf{G}_3 = &\begin{pmatrix} w_{22}^u \\ 0 \end{pmatrix} - \frac{(1-\gamma)^2}{\beta} \left(\frac{1}{2} w_{22}^v + \frac{M}{2} w_{22}^u - 2(1 - \frac{\gamma\beta}{1-\gamma}) w_{22}^u \right) \begin{pmatrix} -1 \\ \eta \end{pmatrix} \\ &- 2\frac{(1-\gamma)^3}{\beta^2} \left((1 - \frac{\gamma\beta}{(1-\gamma)}) \frac{3}{4} - \frac{1}{4} M) \right) \begin{pmatrix} -1 \\ \eta \end{pmatrix} \\ &+ \begin{pmatrix} d12 k_c^2 (3w_{22}^v + \frac{3}{2} M w_{22}^u) \\ d_{21}^c k_c^2 (3M w_{22}^u + \frac{3}{2} M w_{22}^v) \end{pmatrix}.\end{aligned} \tag{A.11}$$

The solvability condition $\langle \mathbf{G}, \boldsymbol{\psi} \rangle = 0$ for Eq. (A.2) leads to Eq. (5.10), which represents the Stuart–Landau equation for the amplitude $A(T)$. The expressions for σ and L are provided as follows:

$$\sigma = -\frac{(\mathbf{G}_1^1, \boldsymbol{\psi})}{(\mathbf{r}, \boldsymbol{\psi})}, \text{ and } L = \frac{(\mathbf{G}_1^3, \boldsymbol{\psi})}{(\mathbf{r}, \boldsymbol{\psi})}. \tag{A.12}$$

In the region of the parameter space where the pattern can develop, as long as $d_{21} > d_{21}^c$, it can be easily proven that the coefficient σ is always positive. Meanwhile, the Landau constant L can be either positive or negative, depending on the system parameters. Therefore, the dynamics of the Stuart-Landau equation can be categorized into two qualitatively different cases: the supercritical case, when $L > 0$, and the subcritical case, when $L < 0$.

Appendix B

Derivation of the Quintic Stuart–Landau Equation

B.1 Quintic Stuart–Landau equation

This appendix provides a detailed derivation of the quintic Stuart–Landau equation (5.14). By substituting expansions (5.12), (5.13), and (5.1) into (5.4), up to $\mathcal{O}(\epsilon^3)$, we obtain the same equations as in section 5.1. At $\mathcal{O}(\epsilon^3)$, the solvability condition $\langle \mathbf{G}, \boldsymbol{\psi} \rangle = 0$ for (A.2) leads once again to (5.10) for the amplitude, where the derivative with respect to T is now a partial derivative, denoted as $A = A(T; T1)$. If this condition is satisfied, the solution is:

$$\mathbf{w}_3 = (A\mathbf{w_{31}} + A^3\mathbf{w}_{32})cos(k_c x) + A^3\mathbf{w}_{33}cos(3k_c x),$$

where $\mathbf{w}_{3i}, i = 1, 2, 3$ are solutions of the following linear systems:

$$(J - k_c^2 D^{d^c})(\mathbf{w}_{31}) = \sigma\mathbf{r} + \mathbf{G}_1^1, \tag{B.1}$$

$$(J - k_c^2 D^{d^c})(\mathbf{w}_{32}) = -L\mathbf{r} + \mathbf{G}_1^3, \tag{B.2}$$

$$(J - 9k_c^2 D^{d^c})(\mathbf{w}_{33}) = \mathbf{G}_3. \tag{B.3}$$

At $\mathcal{O}(\epsilon^4)$:

$$\begin{aligned}\mathcal{L}^{d^c}\mathbf{w}_4 =& 2A\frac{\partial A}{\partial T}\mathbf{w}_{20} + A^2\mathbf{H}_0^2 + A^4\mathbf{H}_0^4 + \left(2A\frac{\partial A}{\partial T}\mathbf{w}_{22} + A^2\mathbf{H}_2^2 + A^4\mathbf{H}_2^4\right)\cos(2k_c x) \\ &+ A^4\mathbf{H}_4\cos(4k_c x),\end{aligned} \tag{B.4}$$

where $\mathbf{H}_0^2$, $\mathbf{H}_0^4$, $\mathbf{H}_2^2$, $\mathbf{H}_2^4$, $\mathbf{H}_4$ are explicitly computed in terms of the system parameters.

$$\mathbf{H}_0^2 = \begin{pmatrix} w_{31}^u \\ 0 \end{pmatrix} - \frac{(1-\gamma)^2}{\beta}\left(\frac{1}{2}w_{31}^v + \frac{1}{2}Mw_{31}^u - 2w_{31}^u\left(1 - \frac{\gamma\beta}{1-\gamma}\right)\right)\begin{pmatrix} -1 \\ \eta \end{pmatrix}$$

$$\mathbf{H}_0^4 = \begin{pmatrix} \frac{1}{2}w_{22}^{u^2} + w_{20}^{u^2} + w_{32}^{u} \\ 0 \end{pmatrix} - \frac{(1-\gamma)^2}{\beta}\Big(\frac{1}{2}w_{32}^{v} + \frac{1}{2}Mw_{22}^{u} + w_{20}^{u}w_{20}^{v} + \frac{1}{2}(w_{22}^{u}w_{22}^{v}) - 2w_{32}^{u}(1-\frac{\gamma\beta}{1-\gamma}) - (1-\frac{\gamma\beta}{1-\gamma})(2w_{20}^{u^2} + w_{22}^{u^2})\Big)\begin{pmatrix} -1 \\ \eta \end{pmatrix} + \frac{2(1-\gamma)^3}{\beta^2}\Big(\frac{1}{2}w_{20}^{v} + \frac{1}{4}w_{22}^{v} + Mw_{20}^{u} + \frac{1}{2}Mw_{22}^{u} - (\frac{9}{2}w_{20}^{u} + \frac{9}{4}w_{22}^{u})(1-\frac{\gamma\beta}{1-\gamma})\Big)\begin{pmatrix} -1 \\ \eta \end{pmatrix} - \frac{9}{4}\frac{(1-\gamma)^4}{\beta^3}\times \Big(M - 4(1-\frac{\gamma\beta}{1-\gamma})\Big)\begin{pmatrix} -1 \\ \eta \end{pmatrix},$$

$$\mathbf{H}_2^2 = \begin{pmatrix} w_{31}^{u} \\ 0 \end{pmatrix} - \frac{(1-\gamma)^2}{\beta}\Big(\frac{1}{2}w_{31}^{v} + \frac{1}{2}Mw_{31}^{u} - 2w_{31}^{u}(1-\frac{\gamma\beta}{1-\gamma})\Big)\begin{pmatrix} -1 \\ \eta \end{pmatrix} + k_c^2 d_{21}^{c}\begin{pmatrix} 0 \\ 4v^{*}w_{22}^{u} + M \end{pmatrix} + \begin{pmatrix} d_{12}k_c^2(w_{31}^{v} + Mw_{31}^{u}) \\ d_{21}k_c^2(w_{31}^{v} + Mw_{31}^{u}) \end{pmatrix},$$

$$\mathbf{H}_2^4 = \begin{pmatrix} 2w_{22}^{u}w_{20}^{u} + w_{32}^{u} + w_{33}^{u} \\ 0 \end{pmatrix} - \frac{(1-\gamma)^2}{\beta}\Big(\frac{1}{2}w_{32}^{v} + \frac{1}{2}w_{33}^{v} + \frac{1}{2}Mw_{22}^{u} + \frac{1}{2}Mw_{33}^{u} + w_{20}^{u}w_{22}^{v} + w_{22}^{u}w_{20}^{v} - 2(w_{32}^{u} + w_{33}^{u} + 2w_{20}^{u}w_{22}^{u})(1-\frac{\gamma\beta}{1-\gamma})\Big)\begin{pmatrix} -1 \\ \eta \end{pmatrix} + 2\frac{(1-\gamma)^3}{\beta^2}\times \Big(\frac{1}{2}w_{20}^{v} + \frac{1}{2}w_{22}^{v} + Mw_{22}^{u} + Mw_{20}^{u} - (\frac{9}{2}w_{22}^{u} + \frac{9}{2}w_{20}^{u})(1-\frac{\gamma\beta}{1-\gamma})\Big)\begin{pmatrix} -1 \\ \eta \end{pmatrix} - 3\frac{(1-\gamma)^4}{\beta^3}\Big(M - 4(1-\frac{\gamma\beta}{1-\gamma})\Big)\begin{pmatrix} -1 \\ \eta \end{pmatrix} + \begin{pmatrix} d_{12}k_c^2\,(4w_{20}^{u}w_{22}^{v} + w_{32}^{v} + 3w_{33}^{v} + M(w_{32}^{u} - w_{33}^{u}) \\ d_{21}^{c}k_c^2\,(4w_{20}^{v}w_{22}^{u} + M(w_{32}^{u} + 3w_{33}^{u}) + w_{32}^{v} - w_{33}^{v}) \end{pmatrix},$$

$$\mathbf{H}_4 = \begin{pmatrix} \frac{1}{2}w_{22}^{u^2} + w_{33}^{u} \\ 0 \end{pmatrix} - \frac{(1-\gamma)^2}{\beta}\Big(\frac{1}{2}w_{33}^{v} + \frac{1}{2}Mw_{33}^{u} + \frac{1}{2}w_{22}^{u}w_{22}^{v} - (2w_{33}^{u} + w_{22}^{u^2})\times (1-\frac{\gamma\beta}{1-\gamma})\Big)\begin{pmatrix} -1 \\ \eta \end{pmatrix} + 2\frac{(1-\gamma)^3}{\beta^2}\Big(\frac{1}{4}w_{22}^{v} + \frac{1}{2}Mw_{22}^{u} - \frac{9}{4}w_{22}^{u}(1-\frac{\gamma\beta}{1-\gamma})\Big)\times \begin{pmatrix} -1 \\ \eta \end{pmatrix} - \frac{3}{4}\frac{(1-\gamma)^4}{\beta^3}\Big(M - 4(1-\frac{\gamma\beta}{1-\gamma})\Big)\begin{pmatrix} -1 \\ \eta \end{pmatrix} + \begin{pmatrix} d_{12}k_c^2\,(4w_{22}^{v}w_{22}^{u} + 2Mw_{33}^{u} + 6w_{33}^{v}) \\ d_{21}^{c}k_c^2\,(4w_{22}^{v}w_{22}^{u} + 6Mw_{33}^{u} + 2w_{33}^{v}) \end{pmatrix}.$$

The solvability condition for (B.4) is automatically satisfied and the solution is:

$$\mathbf{w}_4 = A^2\mathbf{w}_{40} + A^4\mathbf{w}_{41} + (A^2\mathbf{w}_{42} + A^4\mathbf{w}_{43})cos(2k_c x) + A^4\mathbf{w}_{44}cos(4k_c x),$$

where $\mathbf{w}_{4i}, i = 0, 1, 2, 3, 4$ are solutions of the following linear systems:

$$(J)(\mathbf{w}_{40}) = 2\sigma\mathbf{w}_{20} + \mathbf{H}_0^2, \tag{B.5}$$

$$(J)(\mathbf{w}_{41}) = -2L\mathbf{w}_{20} + \mathbf{H}_0^4, \tag{B.6}$$

$$(J - 4k_c^2 D^{d^c})(\mathbf{w}_{42}) = 2\sigma\mathbf{w}_{22} + \mathbf{H}_2^2, \tag{B.7}$$

$$(J - 4k_c^2 D^{d^c})(\mathbf{w}_{43}) = -2L\mathbf{w}_{22} + \mathbf{H}_2^4, \tag{B.8}$$

$$(J - 16k_c^2 D^{d^c})(\mathbf{w}_{44}) = \mathbf{H}_4. \tag{B.9}$$

At $\mathcal{O}(\epsilon^5)$:

$$\mathcal{L}^{d^c}\mathbf{w}_5 = \mathbf{P}, \tag{B.10}$$

where

$$\begin{aligned}\mathbf{P} =& \left(2A\frac{\partial A}{\partial T_1}\mathbf{r} + \frac{\partial A}{\partial T}\mathbf{w}_{31} + 3A^2\frac{\partial A}{\partial T}\mathbf{w}_{32} + A\mathbf{P}_1^1 + A^3\mathbf{P}_1^3 + A^5\mathbf{P}_1^5\right)\cos(k_c x) + \\ & \left(3A^2\frac{\partial A}{\partial T}\mathbf{w}_{33} + A^3\mathbf{P}_3^3 + A^5\mathbf{P}_3^5\right)\cos(3k_c x) + A^5\mathbf{P}_5\cos(5k_c x),\end{aligned} \tag{B.11}$$

where $\mathbf{P_1^1}$, $\mathbf{P_1^3}$, $\mathbf{P_1^5}$, $\mathbf{P_3^3}$, $\mathbf{P_3^5}$, $\mathbf{P_5}$ are explicitly computed in terms of the system parameters.

$$\mathbf{P_1^1} = k_c^2 v^* \begin{pmatrix} 0 \\ d_{21}^c w_{31}(u) + d_{21}^c \end{pmatrix}$$

$$\begin{aligned}\mathbf{P_1^3} =& \begin{pmatrix} 2w_{40}^u + w_{42}^u + 2w_{31}^u w_{20}^u + w_{22}^u w_{31}^u \\ \\ 0 \end{pmatrix} \\ & - \frac{(1-\gamma)^2}{\beta}\big(w_{40}^v + \frac{1}{2}w_{42}^v + w_{20}^u w_{31}^v + \frac{1}{2}w_{22}^u w_{31}^v + w_{20}^v w_{31}^u + \frac{1}{2}w_{22}^v w_{31}^u + Mw_{40}^u + \\ & \frac{1}{2}Mw_{42}^u - (4w_{40}^u + 2w_{42}^u + 4w_{31}^u w_{20}^u + 2w_{22}^u w_{31}^u(1 - \frac{\gamma\beta}{1-\gamma}))\begin{pmatrix} -1 \\ \eta \end{pmatrix} + \\ & 2\frac{(1-\gamma)^3}{\beta^2}(\frac{1}{4}w_{31}^v + \frac{1}{2}Mw_{31}^u - \frac{9}{4}w_{31}^u(1 - \frac{\gamma\beta}{1-\gamma}))\begin{pmatrix} -1 \\ \eta \end{pmatrix} + \begin{pmatrix} 0 \\ \\ (d_{21}^c k_c^2)(w_{32}^u v^* + Mw_{22}^u \end{pmatrix} \\ & + \begin{pmatrix} (d_{12}k_c^2)\begin{pmatrix} w_{42}^v + w_{31}^v w_{20}^u - \frac{1}{2}w_{31}^v w_{22}^u + w_{22}^v w_{31}^u \\ +Mw_{40}^u - \frac{1}{2}Mw_{42}^u \end{pmatrix} \\ (d_{21}^c k_c^2)\begin{pmatrix} Mw_{42}^u + w_{31}^u w_{20}^v - \frac{1}{2}w_{31}^u w_{22}^v + w_{22}^u w_{31}^v \\ +w_{40}^v - \frac{1}{2}w_{42}^v \end{pmatrix} \end{pmatrix}\end{aligned}$$

$$\mathbf{P_1^5} = \begin{pmatrix} 2w_{41}^u + w_{43}^u + 2w_{32}^u w_{20}^u + w_{22}^u w_{32}^u + w_{22}^u w_{33}^u \\ \\ 0 \end{pmatrix}$$
$$- \frac{(1-\gamma)^2}{\beta}\Big(w_{41}^v + \frac{1}{2}w_{43}^v + w_{20}^u w_{32}^v + \frac{1}{2}w_{22}^u w_{32}^v + \frac{1}{2}w_{22}^u w_{33}^v + w_{20}^v w_{32}^u + \frac{1}{2}w_{22}^v w_{32}^u +$$
$$\frac{1}{2}w_{22}^v w_{33}^u + Mw_{41}^u + \frac{1}{2}Mw_{43}^u - \big(4w_{41}^u + 2w_{43}^u + 4w_{32}^u w_{20}^u + 2w_{22}^u w_{32}^u + 2w_{22}^u w_{33}^u\big)\times$$
$$(1 - \frac{\gamma\beta}{1-\gamma})\Big)\begin{pmatrix} -1 \\ \eta \end{pmatrix} + 2\frac{(1-\gamma)^3}{\beta^2}\Big(\frac{1}{4}w_{32}^v + \frac{1}{4}w_{33}^v + 2w_{20}^u w_{20}^v + w_{20}^u w_{22}^v + w_{22}^u w_{20}^v +$$
$$w_{22}^u w_{22}^v + \frac{1}{2}Mw_{32}^u + \frac{1}{2}Mw_{33}^u + Mw_{20}^{u^2} + \frac{1}{2}M^{u^2}w_{22} + Mw_{20}^u w_{22}^u - 9\big(\frac{1}{4}w_{32}^u + \frac{1}{4}w_{33}^u +$$
$$w_{20}^{u^2} + \frac{1}{2}w_{22}^{u^2} + w_{20}^u w_{22}^u\big)(1 - \frac{\gamma\beta}{1-\gamma})\Big)\begin{pmatrix} -1 \\ \eta \end{pmatrix} - 6\frac{(1-\gamma)^4}{\beta^3}\big(\frac{1}{4}w_{22}^v + \frac{1}{4}w_{20}^v + \frac{3}{4}Mw_{20}^u +$$
$$\frac{3}{4}Mw_{22}^u - 4(w_{22}^u + w_{20}^u(1 - \frac{\gamma\beta}{1-\gamma}))\begin{pmatrix} -1 \\ \eta \end{pmatrix} + 15\frac{(1-\gamma)^5}{\beta^4}\big(M - 5(1 - \frac{\gamma\beta}{1-\gamma})\big)\begin{pmatrix} -1 \\ \eta \end{pmatrix}$$
$$+ \begin{pmatrix} (d_{12}k_c^2)\begin{pmatrix} w_{43}^v + w_{32}^v w_{20}^u - \frac{1}{2}w_{32}^v w_{22}^u + \frac{3}{2}w_{22}^u w_{33}^v \\ +w_{22}^v w_{32}^u - w_{33}^u w_{22}^v + Mw_{41}^u - \frac{1}{2}Mw_{43}^u \end{pmatrix} \\ (d_{21}^c k_c^2)\begin{pmatrix} Mw_{43}^v + w_{32}^u w_{20}^v - \frac{1}{2}w_{32}^u w_{22}^v + \frac{3}{2}w_{22}^v w_{33}^u \\ +w_{22}^u w_{32}^v - w_{33}^v w_{22}^u + w_{41}^v - \frac{1}{2}w_{43}^v \end{pmatrix} \end{pmatrix}.$$

The solvability condition for (B.11) is

$$\frac{\partial A}{\partial T1} = \tilde{\sigma}A - \tilde{L}A^3 + \tilde{Q}A^5 \tag{B.12}$$

where,

$$\tilde{\sigma} = -\frac{(\sigma w_{31} + P_1^1, \psi)}{(r,\psi)},\ \tilde{L} = -\frac{(-Lw_{31} + 3\sigma w_{32} + P_1^3, \psi)}{(r,\psi)},\ \text{and}\ \tilde{Q} = -\frac{(3Lw_{32} - P_1^5, \psi)}{(r,\psi)}.$$

adding up (5.14) to (B.12), one gets the quintic Stuart-Landau equation

$$\frac{\partial A}{\partial T} = \bar{\sigma}A - \bar{L}A^3 + \bar{Q}A^5 \tag{B.13}$$

where, $\bar{\sigma} = \sigma + \epsilon^2\tilde{\sigma}, \bar{L} = L + \epsilon^2\tilde{L}, \bar{Q} = \epsilon^2\tilde{Q}$.

Appendix C

Description of Amplitude Equations for 2D Patterns Selection

This appendix provides a detailed description of the amplitude equation for 2D pattern selection. By applying the Fredholm solvability condition to the second order of (ϵ), we derive

$$\begin{cases} (\varphi+\psi)\dfrac{\partial W_1}{\partial T_1} = -d_{21}^c k_c^2 \varphi\psi v^* W_1 - \Big[2\varphi^2 + 2(1-\eta\psi)\left(\dfrac{(1-\gamma)^2}{\beta}(\varphi - 2\varphi^2(1-\dfrac{\gamma\beta}{1-\gamma}))\right) \\ \qquad\qquad +4\varphi k_c^2(d_{12}+\psi d_{21}^c)\Big]\bar{W}_2\bar{W}_3, \\ (\varphi+\psi)\dfrac{\partial W_2}{\partial T_1} = -d_{21}^c k_c^2 \varphi\psi v^* W_2 - \Big[2\varphi^2 + 2(1-\eta\psi)\left(\dfrac{(1-\gamma)^2}{\beta}(\varphi - 2\varphi^2(1-\dfrac{\gamma\beta}{1-\gamma}))\right) \\ \qquad\qquad +4\varphi k_c^2(d_{12}+\psi d_{21}^c)\Big]\bar{W}_1\bar{W}_3, \\ (\varphi+\psi)\dfrac{\partial W_3}{\partial T_1} = -d_{21}^c k_c^2 \varphi\psi v^* W_3 - \Big[2\varphi^2 + 2(1-\eta\psi)\left(\dfrac{(1-\gamma)^2}{\beta}(\varphi - 2\varphi^2(1-\dfrac{\gamma\beta}{1-\gamma}))\right) \\ \qquad\qquad +4\varphi k_c^2(d_{12}+\psi d_{21}^c)\Big]\bar{W}_1\bar{W}_2. \end{cases} \tag{C.1}$$

Then substituting (5.15) into (5.6) and solving it, we obtain

$$\begin{aligned} \begin{pmatrix} u_2 \\ v_2 \end{pmatrix} = \begin{pmatrix} U_0 \\ V_0 \end{pmatrix} + \sum_{j=1}^{3}\begin{pmatrix} U_j \\ V_j \end{pmatrix} e^{\mathrm{i}\mathbf{k}_j\cdot\mathbf{q}} + \sum_{j=1}^{3}\begin{pmatrix} U_{jj} \\ V_{jj} \end{pmatrix} e^{2\mathrm{i}\mathbf{k}_j\cdot\mathbf{q}} + \begin{pmatrix} U_{12} \\ V_{12} \end{pmatrix} e^{\mathrm{i}(\mathbf{k}_1-\mathbf{k}_2)\cdot\mathbf{q}} \\ + \begin{pmatrix} U_{23} \\ V_{23} \end{pmatrix} e^{\mathrm{i}(\mathbf{k}_2-\mathbf{k}_3)\cdot\mathbf{q}} + \begin{pmatrix} U_{31} \\ V_{31} \end{pmatrix} e^{\mathrm{i}(\mathbf{k}_3-\mathbf{k}_1)\cdot\mathbf{q}} + \mathbf{c.c.}, \end{aligned} \tag{C.2}$$

where

$$\begin{pmatrix} U_0 \\ V_0 \end{pmatrix} = \begin{pmatrix} u_{00} \\ v_{00} \end{pmatrix}\left(|W_1|^2+|W_2|^2+|W_3|^2\right), \quad U_j = \varphi V_j$$
$$\begin{pmatrix} U_{jj} \\ V_{jj} \end{pmatrix} = \begin{pmatrix} u_{11} \\ v_{11} \end{pmatrix} W_j^2, \qquad \begin{pmatrix} U_{jl} \\ V_{jl} \end{pmatrix} = \begin{pmatrix} u_\star \\ v_\star \end{pmatrix} W_j\bar{W}_l,$$

$$\begin{cases} (J)\begin{pmatrix} u_{00} \\ v_{00} \end{pmatrix} = \begin{pmatrix} 2\varphi^2 \\ 0 \end{pmatrix} + \left[\frac{2(1-\gamma)^2}{\beta}(\varphi - 2\varphi^2(1-\frac{\gamma\beta}{1-\gamma}))\right]\begin{pmatrix} 1 \\ -\eta \end{pmatrix}, \\ (J-4k_c^2D^{d_c})\begin{pmatrix} u_{11} \\ v_{11} \end{pmatrix} = \begin{pmatrix} \varphi^2 \\ 0 \end{pmatrix} + \left[\frac{(1-\gamma)^2}{\beta}(\varphi - 2\varphi^2(1-\frac{\gamma\beta}{1-\gamma}))\right]\begin{pmatrix} 1 \\ -\eta \end{pmatrix} + \\ \qquad\qquad \begin{pmatrix} 2\varphi k_c^2 d_{12} \\ 2\varphi k_c^2 d_{21}^c \end{pmatrix}, \\ (J-3k_c^2D^{d_c})\begin{pmatrix} u_* \\ v_* \end{pmatrix} = \begin{pmatrix} 2\varphi^2 \\ 0 \end{pmatrix} + \left[\frac{2(1-\gamma)^2}{\beta}(\varphi - 2\varphi^2(1-\frac{\gamma\beta}{1-\gamma}))\right]\begin{pmatrix} 1 \\ -\eta \end{pmatrix}. \end{cases}$$

For the third-order of ϵ in Eq. (5.7), let $\left(H_u^1, H_v^1\right)^T$ represent the coefficient of $e^{\mathbf{i}\mathbf{k}_1\cdot\mathbf{q}}$ in the right-hand side term of Eq. (5.7). Then, one can obtain

$$\begin{aligned} H_u^1 =& \varphi\frac{\partial V_1}{\partial T_1} + \varphi\frac{\partial W_1}{\partial T_2} + \left(I_1\left|W_1\right|^2 + I_2\left(\left|W_2\right|^2 + \left|W_3\right|^2\right)\right)W_1 + \\ & \left(2\varphi^2 + 2\left(\frac{(1-\gamma)^2}{\beta}(\varphi - 4\varphi^2(1-\frac{\gamma\beta}{1-\gamma})\right) + 4\varphi k_c^2 d_{12}\right)(\bar{W}_2\bar{V}_3 + \bar{W}_3\bar{V}_2), \\ H_v^1 =& \frac{\partial V_1}{\partial T_1} + \frac{\partial W_1}{\partial T_2} + \varphi k_c^2 v^*(d_{21}^1 V_1 + d_{21}^2 W_1)W_1 + \left(J_1\left|W_1\right|^2 + J_2\left(\left|W_2\right|^2 + \left|W_3\right|^2\right)\right)W_1 + \\ & \left(-2\eta\left(\frac{(1-\gamma)^2}{\beta}(\varphi - 2\varphi^2(1-\frac{\gamma\beta}{1-\gamma})\right) + 4\varphi k_c^2 d_{21}^c\right)(\bar{W}_2\bar{V}_3 + \bar{W}_3\bar{V}_2), \end{aligned}$$

where

$$\begin{aligned} I_1 =& 2\varphi(u_{11}+u_{00}) + \frac{(1-\gamma)^2}{\beta}\left(\varphi v_{00} + \varphi v_{11} + u_{00} + u_{11} - 4\varphi(u_{00}+u_{11})(1-\frac{\gamma\beta}{1-\gamma})\right) \\ & + 2\frac{(1-\gamma)^3}{\beta^2}\left(9\varphi^3(1-\frac{\gamma\beta}{1-\gamma}) - 3\varphi^2\right) + d_{12}k_c^2(2\varphi v_{11} + u_{00} - u_{11}), \\ I_2 =& 2\varphi(u_{00}+u_*) + \frac{(1-\gamma)^2}{\beta}\left(\varphi v_{00} + \varphi v_* + u_{00} + u_* - 4\varphi(u_{00}+u_*)(1-\frac{\gamma\beta}{1-\gamma})\right) \\ & + 2\frac{(1-\gamma)^3}{\beta^2}\left(18\varphi^3(1-\frac{\gamma\beta}{1-\gamma}) - 6\varphi^2\right) + d_{12}k_c^2 6\varphi v_* + u_{00} + 4u_*), \\ J_1 =& -\eta\frac{(1-\gamma)^2}{\beta}\left(\varphi v_{00} + \varphi v_{11} + u_{00} + u_{11} - 4\varphi(u_{00}+u_{11})(1-\frac{\gamma\beta}{1-\gamma})\right) \\ & - 2\eta\frac{(1-\gamma)^3}{\beta^2}\left(9\varphi^3(1-\frac{\gamma\beta}{1-\gamma}) - 3\varphi^2\right) + d_{21}^c k_c^2(2u_{11} + \varphi v_{00} - \varphi v_{11}), \\ J_2 =& -\eta\frac{(1-\gamma)^2}{\beta}\left(\varphi v_{00} + \varphi v_* + u_{00} + u_* - 4\varphi(u_{00}+u_*)(1-\frac{\gamma\beta}{1-\gamma})\right) \\ & - 2\eta\frac{(1-\gamma)^3}{\beta^2}\left(18\varphi^3(1-\frac{\gamma\beta}{1-\gamma}) - 6\varphi^2\right) + d_{21}^c k_c^2(6u_* + \varphi v_{00} + 4\varphi v_*). \end{aligned}$$

Utilizing Fredholm solvability condition in $O\left(\epsilon^3\right)$ again, we get

$$\begin{cases} (\varphi+\psi)\left(\dfrac{\partial V_1}{\partial T_1}+\dfrac{\partial W_1}{\partial T_2}\right) = -k_c^2 v^* \varphi\psi\left(d_{21}^1 V_1 + d_{21}^2 W_1\right) - 4k_c^2 d_{21}^1 \varphi\psi \bar{W}_2 \bar{W}_3 - \\ \qquad\qquad G_3\left(\bar{W}_2\bar{V}_3 + \bar{W}_3\bar{V}_2\right) - \left[G_1\left|W_1\right|^2 + G_2\left(\left|W_2\right|^2 + \left|W_3\right|^2\right)\right] W_1, \\ (\varphi+\psi)\left(\dfrac{\partial V_2}{\partial T_1}+\dfrac{\partial W_2}{\partial T_2}\right) = -k_c^2 v^* \varphi\psi\left(d_{21}^1 V_2 + d_{21}^2 W_2\right) - 4k_c^2 d_{21}^1 \varphi\psi \bar{W}_1 \bar{W}_3 - \\ \qquad\qquad G_3\left(\bar{W}_3\bar{V}_1 + \bar{W}_1\bar{V}_3\right) - \left[G_1\left|W_2\right|^2 + G_2\left(\left|W_3\right|^2 + \left|W_1\right|^2\right)\right] W_2, \\ (\varphi+\psi)\left(\dfrac{\partial V_3}{\partial T_1}+\dfrac{\partial W_3}{\partial T_2}\right) = -k_c^2 v^* \varphi\psi\left(d_{21}^1 V_3 + d_{21}^2 W_3\right) - 4k_c^2 d_{21}^1 \varphi\psi \bar{W}_1 \bar{W}_2 - \\ \qquad\qquad G_3\left(\bar{W}_1\bar{V}_2 + \bar{W}_2\bar{V}_1\right) - \left[G_1\left|W_3\right|^2 + G_2\left(\left|W_1\right|^2 + \left|W_2\right|^2\right)\right] W_3, \end{cases} \tag{C.3}$$

where $G_1 = I_1 + \psi J_1$, $\quad G_2 = I_2 + \psi J_2$, $\quad G_3 = 2\varphi^2 + 2(1-\eta\psi)\left(\frac{(1-\gamma)^2}{\beta}\left(\varphi - 2\varphi^2\left(1 - \frac{\gamma\beta}{1-\gamma}\right)\right)\right) + 4\varphi k_c^2(d_{12} + \psi d_{21}^c)$

Bibliography

[1] T. A. Al-Karkhi, R. Kusdiantara, H. Susanto, and E. A. Codling. "Bloom Formation and Turing Patterns in an Infochemical Mediated Multitrophic Plankton Model". In: *International Journal of Bifurcation and Chaos* 30.10 (2020), p. 2030028.

[2] Y. Almirantis and S. Papageorgiou. "Cross-diffusion effects on chemical and biological pattern formation". In: *Journal of theoretical biology* 151.3 (1991), pp. 289–311.

[3] Vivi Andasari, Alf Gerisch, Georgios Lolas, Andrew P South, and Mark AJ Chaplain. "Mathematical modeling of cancer cell invasion of tissue: biological insight from mathematical analysis and computational simulation". In: *Journal of Mathematical Biology* 63.1 (2011), pp. 141–171.

[4] Donald M Anderson. "Approaches to monitoring, control and management of harmful algal blooms (HABs)". In: *Ocean & coastal management* 52.7 (2009), pp. 342–347.

[5] Donald M Anderson, Joann M Burkholder, William P Cochlan, Patricia M Glibert, Christopher J Gobler, Cynthia A Heil, Raphael M Kudela, Michael L Parsons, JE Jack Rensel, David W Townsend, et al. "Harmful algal blooms and eutrophication: examining linkages from selected coastal regions of the United States". In: *Harmful algae* 8.1 (2008), pp. 39–53.

[6] Donald M. Anderson, Allan D. Cembella, and Gustaaf M. Hallegraeff. "Progress in understanding harmful algal blooms: paradigm shifts and new technologies for research, monitoring, and management". In: *Annual Review of Marine Science* 4 (2012), pp. 143–176.

[7] Brian H Andrew, R R Marianito, and Alfred H Miguel. "A model for acid-mediated tumor growth with nonlinear acid production term". In: *Applied Mathematics and Computation* 227.1 (2014), pp. 176–198.

[8] Rhodora V. Azanza, Michael L. Brosnahan, Donald M. Anderson, Inga Hense, and Marina Montresor. "The role of life cycle characteristics in harmful algal bloom dynamics". In: *Global Ecology and Oceanography of Harmful Algal Blooms*. Springer, Cham, 2019, pp. 133–161.

[9] Deborah Banas, Benoite Lapeyre, Sylvie Chifflet, Jason Woodhouse, Thierry Homere, and Ian Jenkinson. "Sublethal effects on crustacean larvae by toxic microalgae can be moderated by nutrient degree and ratios in coastal waters". In: *Limnology and Oceanography* 52.2 (2007), pp. 824–835.

[10] Elisa Berdalet, Lora E Fleming, Richard Gowen, Keith Davidson, Philipp Hess, Lorraine C Backer, Stephanie K Moore, Porter Hoagland, and Henrik Enevoldsen. "Marine harmful algal blooms, human health and wellbeing: challenges and opportunities in the 21st century". In: *Journal of the Marine Biological Association of the United Kingdom* 96.1 (2016), pp. 61–91.

[11] Benedetto Bozzini, Giovanni Gambino, Diego Lacitignola, Sergio Lupo, Michele Sammartino, and Ivonne Sgura. "Weakly nonlinear analysis of Turing patterns in a morphochemical model for metal growth". In: *Acta Applicandae Mathematicae* 139.1 (2015), pp. 79–101.

[12] E.J. Buskey and C.J. Hyatt. "Effects of the Texas (USA) brown tide alga on planktonic grazers". In: *Marine Ecol. Prog. Ser.* 126 (1995), 285–292.

[13] E.J. Buskey and D.A. Stockwell. "Effects of a persistent brown tide on zooplankton population in the Laguno Madre of Southern Texas". In: *Toxic Phytoplankton Blooms in the Sea*. Amsterdam: Elsevier, 1993, 659–666.

[14] Joseph J Casciari, S V Sotirchos, and Nancy K Martin. "Variations in tumor cell growth rates and metabolism with oxygen concentration, glucose concentration, and extracellular pH". In: *Journal of Cellular Physiology* 151.2 (1992), pp. 386–394.

[15] J. Chattopadhyay, R.R. Sarkar, and A. Abdllaoui. "A delay differential equation model on harmful algal blooms in the presence of toxic substances". In: *IMA J. Math. Appl. Med. Biol.* 19 (2002), 137–161.

[16] J. Chattopadhyay, R.R. Sarkar, and S. Mandal. "Toxin producing plankton may act as a biological control for planktonic blooms: A field study and mathematical modelling". In: *J. Theoret. Biol.* 215 (2002), 333–344.

[17] J. Chattopadhyay, R.R. Sarkar, and S. Mandal. "Toxin-producing plankton may act as a biological control for planktonic blooms—field study and mathematical modelling". In: *Journal of Theoretical Biology* 215.3 (2002), 333–344.

[18] M. Cross and H. Greenside. *Pattern Formation and Dynamics in Nonequilibrium Systems*. Cambridge, UK: Cambridge University Press, 2009.

[19] G.C. Cruywagen, P.K. Maini, and J.D. Murray. "Biological pattern formation on two–dimensional spatial domains: a nonlinear bifurcation analysis". In: *SIAM J. Appl. Math.* 57 (1997), 1485–1509.

[20] Marc Dellian, Gundolf Helmlinger, Fang Yuan, and Rakesh K Jain. "Fluorescence ratio imaging of interstitial pH in solid tumors effect of glucose on spatial and temporal Gradients". In: *British Journal of Cancer* 74.8 (1996), pp. 1206–1215.

[21] Robert Dillon, PK Maini, and HG Othmer. "Pattern formation in generalized Turing systems: I. Steady-state patterns in systems with mixed boundary conditions". In: *Journal of Mathematical Biology* 32 (1994), pp. 345–393.

[22] A. M. Edwards and A. Yool. "The role of higher predation in plankton population models". In: *Journal of Plankton Research* 22.6 (2000), pp. 1085–1112.

[23] I. R. Epstein and J. A. Pojman. *An Introduction to Nonlinear Chemical Dynamics: Oscillations, Waves, Patterns, and Chaos*. Oxford University Press, 1998.

[24] Lawrence C Evans. *Partial differential equations*. Vol. 19. American Mathematical Society, 2022.

[25] Paul Falkowski. "Ocean science: the power of plankton". In: *Nature* 483.7387 (2012), S17–S20.

[26] Antonio Fasano, Anna Mancini, and Mario Primicerio. "Tumour growth modelling by cellular automata". In: *Mathematical Modelling of Tumour Growth and Treatment*. Springer, Cham, 2016, pp. 1–54.

[27] Francisco G Figueiras, Yolanda Pazos, Carolina Vall'es, Maria Fr'an Borges, Juan Padin Ter'an, and Francisco S'anchez. "Harmful algal blooms and coastal eutrophication". In: *Harmful Algal Blooms and Eutrophication in the Coastal Waters of the Galician Rias (NW Spain)*. OTAN, 2008, pp. 1–17.

[28] P. J. Franks. "NPZ models of plankton dynamics: their construction, coupling to physics, and application". In: *Journal of Oceanography* 58 (2002), pp. 379–387.

[29] G. Gambino, V. Giunta, M.C. Lombardo, and G. Rubino. "Cross-diffusion effects on stationary pattern formation in the FitzHugh-Nagumo model". In: *Discrete and Continuous Dynamical Systems-B* (2022).

[30] G Gambino, MC Lombardo, S Lupo, and M Sammartino. "Super-critical and sub-critical bifurcations in a reaction-diffusion Schnakenberg model with linear cross-diffusion". In: *Ricerche di Matematica* 65 (2016), pp. 449–467.

[31] G Gambino, MC Lombardo, and M Sammartino. "Cross-diffusion driven instability for a Lotka-Volterra competitive reaction-diffusion system". In: *Waves and Stability in Continuous Media*. World Scientific, 2008, pp. 297–302.

[32] G. Gambino, M.C. Lombardo, and M. Sammartino. "Turing instability and traveling fronts for a nonlinear reaction–diffusion system with cross-diffusion". In: *Mathematics and Computers in Simulation* 82.6 (2012), pp. 1112–1132.

[33] G Gambino, MC Lombardo, and M Sammartino. "Turing instability and traveling fronts for a nonlinear reaction–diffusion system with cross-diffusion". In: *Mathematics and Computers in Simulation* 82.6 (2013), pp. 1112–1132.

[34] G. Gambino, S. Lupo, and M. Sammartino. "Effects of cross-diffusion on turing patterns in a reaction-diffusion schnakenberg model". In: *arXiv preprint:1501.04890* (2015).

[35] Robert A Gatenby and Edward T Gawlinski. "A reaction diffusion model of cancer invasion". In: *Cancer research* 56.24 (1996), pp. 5745–5753.

[36] Robert A Gatenby and Edward T Gawlinski. "The glycolytic phenotype in carcinogenesis and tumor invasion: insights through mathematical modelling". In: *Cancer research* 63.24 (2003), pp. 3847–3854.

[37] Robert A Gatenby, Edward T Gawlinski, Arthur F Gmitro, Benjamin Kaylor, and Robert J Gillies. "Acid-mediated tumor invasion: A multidisciplinary study". In: *Cancer research* 66.1 (2006), pp. 5216–5223.

[38] Amos Gilat and Vish Subramaniam. "Numerical methods for engineers and scientists". In: *An Introduction with Applications Using MATLAB*, 20014 (2013).

[39] Valeria Giunta, Maria Carmela Lombardo, and Marco Sammartino. "Pattern formation and transition to chaos in a chemotaxis model of acute inflammation". In: *SIAM Journal on Applied Dynamical Systems* 20.4 (2021), pp. 1844–1881.

[40] Christopher J Gobler. "Climate change and harmful algal blooms: insights and perspective". In: *Harmful algae* 91 (2020), p. 101731.

[41] John Guckenheimer and Philip Holmes. *Nonlinear Oscillations, Dynamical Systems, and Bifurcations of Vector Fields*. Springer, 1983.

[42] Stanley J Guildford and Robert E Hecky. "Total nitrogen, total phosphorus, and nutrient limitation in lakes and oceans". In: *Limnology and Oceanography* 45.6 (2000), pp. 1213–1223.

[43] Mustafa Gulnihal. "DRBEM solution of acid-mediated tumor invasion model with time-dependent carrying capacity". In: *European Journal of Computational Mechanics* (2017), pp. 430–442.

[44] Gustaaf M Hallegraeff. "Ocean climate change, phytoplankton community responses, and harmful algal blooms: a formidable predictive challenge 1". In: *Journal of phycology* 46.2 (2010), pp. 220–235.

[45] Gustaaf M. Hallegraeff, Donald M. Anderson, Catherine Belin, Marie-Yasmine D. Bottein, Eileen Bresnan, Mireille Chinain, Adriana Zingone, et al. "Perceived global increase in algal blooms is attributable to intensified monitoring and emerging bloom impacts". In: *Nature Communications Earth & Environment* 2.1 (2021), pp. 1–10.

[46] B. Hansen, K. S. Tande, and U. C. Berggreen. "On the trophic fate of Phaeocystis pouchetii (Harlot). III. Functional responses in grazing demonstrated on juvenile stages of Calanus finmarchicus (Copepoda) fed diatoms and Phaeocystis". In: *Journal of Plankton Research* 12.6 (1990), pp. 1173–1187.

[47] Elizabeth L Harvey and Susanne Menden-Deuer. "Predator-induced fleeing behaviours in phytoplankton: a new mechanism for harmful algal bloom formation?" In: *Public Library of Science San Francisco, USA* (2012).

[48] Gundolf Helmlinger, Fang Yuan, and Marc Dellian. "Interstitial pH and pO2 gradients in solid tumors in vivo: high-resolution measurements reveal a lack of correlation". In: *PUBMED* 3.2 (1997), pp. 177–182.

[49] Thomas Hillen and Kevin J Painter. "A user's guide to PDE models for chemotaxis". In: *Journal of mathematical biology* 58.1 (2009), pp. 183–217.

[50] Andrew B Holder, Marianito R Rodrigo, and Miguel A Herrero. "A model for acid-mediated tumour growth with nonlinear acid production term". In: *Applied Mathematics and Computation* 227 (2014), pp. 176–198.

[51] Crawford Stanley Holling. "The functional response of predators to prey density and its role in mimicry and population regulation". In: *The Memoirs of the Entomological Society of Canada* 97.S45 (1965), pp. 5–60.

[52] Jihoon Hong, Siddhartha Talapatra, Joseph Katz, Patricia A. Tester, Randall J. Waggett, and Allen R. Place. "Algal toxins alter copepod feeding behavior". In: *PLoS One* 7.5 (2012), e36845.

[53] Xiaodong Jiang, Darcy J Lonsdale, and Christopher J Gobler. "Nutritional deficiency prolongs dormancy in post-diapause copepods from coastal waters in Bering Sea". In: *Marine Ecology Progress Series* 395 (2009), pp. 91–102.

[54] Farhan K., G. Gambino, M.C. Lombardo, and M. Sammartino. "Bifurcation analysis and pattern formation in a phytoplankton-zooplankton reaction-diffusion model with cross-diffusion and toxicity". In: *preparation* (2024).

[55] Hassan K. Khalil. *Nonlinear Systems*. 3rd. Prentice Hall, 2002.

[56] Farhan Khan, Mudassar Abbas, Jorge E Macías-Díaz, Muhammad Bilal Khan, and Safar M Alghamdi. "Computational solution of an acid-mediated tumor-growth radial model under logistic growth regimes for normal and cancer cells". In: *International Journal of Biomathematics* 16.03 (2023), p. 2250084.

[57] S. Kondo and T. Miura. "Reaction-diffusion model as a framework for understanding biological pattern formation". In: *Science* 329.5999 (2010), pp. 1616–1620.

[58] Kazumasa Kuto and Yasushi Yamada. "Multiple coexistence states for a prey-predator system with cross-diffusion". In: *Journal of Differential Equations* 197.2 (2004), pp. 315–348.

[59] Georgios Lolas. "Mathematical modelling of proteolysis and cancer cell invasion of tissue". In: *Tutorials in Mathematical Biosciences III: Cell Cycle, Proliferation, and Cancer*. Springer, 2005, pp. 77–129.

[60] Yuan Lou and Wei-Ming Ni. "Diffusion, self-diffusion and cross-diffusion". In: *Journal of Differential Equations* 131.1 (1996), pp. 79–131.

[61] Y. Lv, T. Li, Y. Pei, and R. Yuan. "A complete analysis of the global dynamics of a diffusive predator and toxic prey model". In: *Appl. Math. Comput.* 291 (2016), pp. 182–196.

[62] Anotida Madzvamuse, Hussaini S Ndakwo, and Raquel Barreira. "Cross-diffusion-driven instability for reaction-diffusion systems: analysis and simulations". In: *Journal of mathematical biology* 70.4 (2015), pp. 709–743.

[63] P. K. Maini and H. G. Othmer. *Mathematical Models for Biological Pattern Formation*. Springer, 2001.

[64] Christian Markl, Gizem Meral, and Christina Surulescu. "Mathematical analysis and numerical simulations for a system modeling acid-mediated tumor cell invasion". In: *International Journal of Analysis* (2013), pp. 1–15.

[65] James B McGillen, Eamonn A Gaffney, Nancy K Martin, and Philip K Maini. "A general reaction-diffusion model of acidity in cancer invasion". In: *Journal of Mathematical Biology* 68.1 (2014), pp. 1199–1224.

[66] A.B. Medvinsky, S.V. Petrovskii, I.A. Tikhonova, H. Malchow, and B.L. Li. "Spatiotemporal complexity of plankton and fish dynamics". In: *SIAM review* 44.3 (2002), pp. 311–370.

[67] H. Meinhardt. *Models of Biological Pattern Formation*. Academic Press, 1982.

[68] X. Meng, R. Liu, and T. Zhang. "Adaptive dynamics for a non-autonomous Lotka-Volterra model with size-selective disturbance". In: *Nonlinear Anal., Real World Appl.* 16 (2014), 202–213.

[69] François Montalant et al. *Analyse des infiniment petits, pour l'intelligence des lignes courbes*. Chez François Montalant, 1716.

[70] A. Morozov, E. Arashkevich, A. Nikishina, and K. Solovyev. "Nutrient-rich plankton communities stabilized via predator–prey interactions: revisiting the role of vertical heterogeneity". In: *Mathematical medicine and biology: a journal of the IMA* 28.2 (2011), pp. 185–215.

[71] J. D. Murray. *Mathematical Biology II: Spatial Models and Biomedical Applications*. 3rd. Springer, 2003.

[72] Ali H. Nayfeh and Balakumar Balachandran. *Applied Nonlinear Dynamics: Analytical, Computational, and Experimental Methods*. Wiley, 1995.

[73] A. Okubo and S. A. Levin. *Diffusion and Ecological Problems: Modern Perspectives*. 2nd. Springer, 2001.

[74] Hee Jeong Park, John C Lyons, T Ohtsubo, and Chang W Song. "Acidic environment causes apoptosis by increasing caspase activity". In: *British Journal of Cancer* 80.12 (1999), pp. 1892–1897.

[75] Anil A Patel, Edward T Gawlinski, Shelly K Lemieux, and Robert A Gatenby. "A cellular automaton model of early tumor growth and invasion: the effects of native tissue vascularity and increased anaerobic tumor metabolism". In: *Journal of theoretical biology* 213.3 (2001), pp. 315–331.

[76] M. Perc and A. Szolnoki. "Noise–guided evolution within cyclical interactions". In: *New J. Phys.* 9 (2007), 267–282.

[77] M. Perc, A. Szolnoki, and G. Szabo. "Cyclical interactions with alliance specific heterogeneous invasion rates". In: *Phys. Rev. E* 75 (2007), p. 052102.

[78] Lawrence Perko. *Differential Equations and Dynamical Systems*. 3rd. Springer, 2001.

[79] Ian F Robey and Nancy K Martin. "Bicarbonate and dichloroacetate: evaluating pH altering therapies in a mouse model for metastatic breast cancer". In: *BMC Cancer* 11 (2011), pp. 235–245.

[80] T. Saha and M. Bandyopadhyay. "Dynamical analysis of toxin producing phytoplankton–zooplankton interactions". In: *Nonlinear Analysis: Real World Applications* 10.1 (2009), 314–332.

[81] R.R. Sarkar and J. Chattopadhyay. "The role of environmental stochasticity in a toxic phytoplankton-non-toxic phytoplankton zooplankton system". In: *Environmetrics* 14 (2003), 775–792.

[82] William E Schiesser. *Partial Differential Equations Analysis in Biomedical Engineering: Case Studies with MATLAB*. Cambridge University Press, 2013.

[83] Patrick Schornack and Robert J Gillies. "Contributions of cell metabolism and H+ diffusion to the acidic pH of tumors". In: *PUBMED* 5.2 (2003), pp. 135–145.

[84] Erik Selander, Peter Thor, Gunilla Toth, and Henrik Pavia. "Copepods induce paralytic shellfish toxin production in marine dinoflagellates". In: *Proceedings of the Royal Society B: Biological Sciences* 273.1594 (2006), pp. 1673–1680.

[85] N. Shigesada, K. Kawasaki, and E. Teramoto. "Spatial segregation of interacting species". In: *J. Theor. Biol.* 79 (1979), 83–99.

[86] Nanako Shigesada, Kohkichi Kawasaki, and Ei Teramoto. "Spatial segregation of interacting species". In: *Journal of theoretical biology* 79.1 (1979), pp. 83–99.

[87] Jean-Jacques E. Slotine and Weiping Li. *Applied Nonlinear Control*. Prentice Hall, 1991.

[88] Kieran Smallbone, David J Gavaghan, Robert A Gatenby, and Philip K Maini. "The role of acidity in solid tumour growth and invasion". In: *Journal of theoretical biology* 235.4 (2005), pp. 476–484.

[89] Theodore J Smayda. "Complexity in the eutrophication–harmful algal bloom relationship, with comment on the importance of grazing". In: *Harmful Algae* 8.1 (2008), pp. 140–151.

[90] Steven H. Strogatz. *Nonlinear Dynamics and Chaos: With Applications to Physics, Biology, Chemistry, and Engineering*. Addison-Wesley, 1994.

[91] William G. Sunda, Edna Graneli, and Christopher J. Gobler. "Positive feedback and the development and persistence of ecosystem disruptive algal blooms". In: *Journal of Phycology* 42.5 (2006), pp. 963–974.

[92] A. Szolnoki, M. Mobilia, L.-L. Jiang, B. Szczesny, A.M. Rucklidge, and M. Perc. "Cyclic dominance in evolutionary games: a review". In: *J. R. Soc. Interface* 11 (2014), 20140735–20140755.

[93] A. Szolnoki and M. Perc. "Correlation of positive and negative reciprocity fails to confer an evolutionary advantage: phase transitions to elementary strategies". In: *Phys. Rev. X* 3 (2013), p. 041021.

[94] Youshan Tao and Michael Winkler. "A chemotaxis-haptotaxis model: the roles of nonlinear diffusion and logistic source". In: *SIAM Journal on Mathematical Analysis* 47.6 (2015), pp. 4405–4427.

[95] Bryony L Townhill, Jose F Monteiro, Shaikh Nawaf Al-Subiai, Alex Beck, Spencer Birchenough, Ester Couce, Miranda Jones, Walter JF Le Quesne, Villamor Leonardo, John K Pinnegar, et al. "Consequences of climate-induced gradients for zooplankton range extension in the Northeast Atlantic". In: *Diversity and Distributions* 24.12 (2018), pp. 1628–1642.

[96] Alan Mathison Turing. "The chemical basis of morphogenesis". In: *Bulletin of mathematical biology* 52 (1990), pp. 153–197.

[97] A.M. Turing. "The chemical basis of morphogenesis". In: *Philos. Trans. R. Soc. Lond. B* 237 (1952), 37–72.

[98] Jefferson T. Turner. "Planktonic marine copepods and harmful algae". In: *Harmful Algae* 32 (2014), pp. 81–93.

[99] V. K. Vanag and I. R. Epstein. "Cross-diffusion and pattern formation in reaction-diffusion systems". In: *Physical Chemistry Chemical Physics* 11.6 (2009), pp. 897–912.

[100] V.K. Vanag and I.R. Epstein. "Cross-diffusion and pattern formation in reaction-diffusion systems". In: *Physical Chemistry Chemical Physics* 11.6 (2009), pp. 897–912.

[101] Peter J Wangersky. "Lotka-Volterra population models". In: *Annual Review of Ecology and Systematics* 9 (1978), pp. 189–218.

[102] OTTO Warburg and F Dickens. "The metabolism of tumors, Constable & Co". In: *Ltd., London* (1930).

[103] Mark L Wells, Vera L Trainer, Theodore J Smayda, Bengt SO Karlson, Charles G Trick, Raphael M Kudela, Akira Ishikawa, Stewart Bernard, Angela Wulff, Donald M Anderson, et al. "Harmful algal blooms and climate change: Learning from the past and present to forecast the future". In: *Harmful algae* 49 (2015), pp. 68–93.

[104] Qunchao Zhang, George Petihakis, Lara Sampaio, Dion Mitropolsky, Nectarios Tsiftis, and Nektaria Stamataki. "Zooplankton community responses to increasing harmful algal blooms in a subtropical bay". In: *Chemosphere* 248 (2020), p. 126028.

[105] Chenghu Zhu and George Yin. "On competitive Lotka–Volterra model in random environments". In: *Journal of Mathematical Analysis and Applications* 357.1 (2009), pp. 154–170.